



HAL
open science

Phase transformations and microstructure evolutions in metastable beta titanium alloy Ti-B19

Hui Chang

► **To cite this version:**

Hui Chang. Phase transformations and microstructure evolutions in metastable beta titanium alloy Ti-B19. Other. Institut National Polytechnique de Lorraine, 2010. English. NNT : 2010INPL053N . tel-01749447

HAL Id: tel-01749447

<https://hal.univ-lorraine.fr/tel-01749447>

Submitted on 29 Mar 2018

HAL is a multi-disciplinary open access archive for the deposit and dissemination of scientific research documents, whether they are published or not. The documents may come from teaching and research institutions in France or abroad, or from public or private research centers.

L'archive ouverte pluridisciplinaire **HAL**, est destinée au dépôt et à la diffusion de documents scientifiques de niveau recherche, publiés ou non, émanant des établissements d'enseignement et de recherche français ou étrangers, des laboratoires publics ou privés.



AVERTISSEMENT

Ce document est le fruit d'un long travail approuvé par le jury de soutenance et mis à disposition de l'ensemble de la communauté universitaire élargie.

Il est soumis à la propriété intellectuelle de l'auteur. Ceci implique une obligation de citation et de référencement lors de l'utilisation de ce document.

D'autre part, toute contrefaçon, plagiat, reproduction illicite encourt une poursuite pénale.

Contact : ddoc-theses-contact@univ-lorraine.fr

LIENS

Code de la Propriété Intellectuelle. articles L 122. 4

Code de la Propriété Intellectuelle. articles L 335.2- L 335.10

http://www.cfcopies.com/V2/leg/leg_droi.php

<http://www.culture.gouv.fr/culture/infos-pratiques/droits/protection.htm>

Institut National Polytechnique de Lorraine – Nancy
Ecole Doctorale EMMA
Northwestern Polytechnical University – Xi'an

PhD THESIS

To obtain the grades of
Doctor of the Institut National Polytechnique de Lorraine,
Spécialité Science et Ingénierie des Matériaux, Métallurgie
Doctor of the Northwestern Polytechnical University

Presented by

Hui CHANG

**Phase transformations and microstructure evolutions in
metastable beta titanium alloy Ti-B19**

October 28, 2010

Jury :

Joël DOUIN	Research Professor CNRS	Rapporteur
Xianghong LIU	Professor at NIN	Rapporteur
Benoit APPOLAIRE	Docteur, Ingénieur de recherches ONERA	Examinator
Rui HU	Professor at NPU	Examinator
Elisabeth GAUTIER	Professor at CNRS	Supervisor
Lian ZHOU	Professor at NPU	Supervisor

PhD thesis prepared at SI2M UMR CNRS 7198 Ecole des Mines, Nancy, France
and at Northwestern Polytechnical University (NPU), Xi'an, China
in the framework of the PRA program

ACKNOWLEDGEMENTS

The present work would have been impossible without the support of the Sino-French Doctoral College Program and the PRA program (MX05-01).

Here, first of all, I would like to express my great gratitude to my supervisors, Prof. Lian ZHOU and Prof. Elisabeth GAUTIER, from the deep of my heart due to their much more attention paid on my whole Ph.D works. It was through their encouragement and understanding that I could continue to finish my works till today. Special thanks also go to Prof. Gautier for her kindly revision of all the documents and the instructive discussions in skype-meeting during the past days in spite of her column sickness. When I was in Nancy for the doctoral work, she gave me a lot of cares not only in the work but also in life. From all the doctoral process, I have learned a lot of intensive knowledge about titanium and titanium alloys even though I have already worked in this field for many years. Thank you very much for all that you have done for me.

My work would not have been possible without the collaboration and assistance from many individuals. I owe lots of love to all of my colleagues and friends in China and France. Prof. Jinshan LI, Prof. Xiangyi XUE, Prof. Rui HU Mr. Yichuan WANG and Dr. Hongchao KOU have given me great support not only from minds but also from actions, especially, allowing me more free time so that I could write the thesis. A special note of thanks also goes to Dr. Fabien Bruneseaux, who helped me to finish the analysis of the X-ray diffraction results to get the correct data. Here, I would like to thank Dr. Benoît Appolaire for the instructive discussion on the phase theory. The thanks should also be given to Madam Martine Tailleur as well as other colleagues in LSG2M Nancy. During writing the thesis, Dr. Bin TANG and

Guoqiang SHANG as well as Xiangbo DAI also give me helpful support. Thanks for Prof. Weimin BIAN who helps to do the TEM observations.

Finally, I would like to express my deepest gratitude to my mother, farther in law, and mother in law, they give me strong support during those past days wherever I was. Great thanks should also be given to my wife Ms. Liang FENG and my lovely daughter Miss Shuwen CHANG for their unconditional love and encouragement, which makes me possible to finish all the work and I would like to share all of these with them.

CONTENTS

ACKNOWLEDGEMENTS	1
CONTENTS	3
I. INTRODUCTION.....	6
<i>I.1. Brief introduction of titanium alloys</i>	<i>6</i>
<i>I.2. Phase transformation in titanium alloys</i>	<i>9</i>
I.2.1. Main phase transformations in titanium alloys	9
I.2.2. Martensitic phase transformation	11
I.2.3. Phase transformation	13
I.2.4. Decomposition of metastable β phase	16
<i>I.3. The phase transformation kinetics of titanium alloys.....</i>	<i>20</i>
<i>I.4. The aim of the present research work.....</i>	<i>22</i>
II. RESEARCH SCHEME AND EXPERIMENTAL PROCEDURE.....	24
<i>II.1. Research contents</i>	<i>24</i>
<i>II.2. Researching routes.....</i>	<i>25</i>
II.2.1. Study of isothermal phase transformation kinetics	26
II.2.2. Study of the influence of heating on isothermal phase transformation	27
II.2.3. Study of the phase transformation kinetics during continuous cooling.	28
II.2.4. Influence of plastic deformation of the beta metastable phase on isothermal phase transformation kinetics during aging.....	29
<i>II.3. Experimental materials.....</i>	<i>29</i>
II.3.1. Brief introduction of Ti-B19 alloy	29
II.3.2. Preparation of materials and samples.....	30
<i>II.4. Experiment methods and devices</i>	<i>32</i>
II.4.1. In-situ resistivity measurement method and device	32
II.4.2. High energy synchrotron X-ray diffraction.....	35
II.4.3. Other research methods.....	37
III. ISOTHERMAL PHASE TRANSFORMATION KINETICS AND MICROSTRUCTURE EVOLUTIONS OF TI-B19 ALLOY	38
<i>III.1. Variations of electrical resistivity with time and further analysis method.....</i>	<i>39</i>
III.1.1. Variation of electrical resistivity with time generally	39
III.1.2. Variations of electrical resistivity with time during isothermal treatment	41

III.1.3. Method to obtained phase transformation kinetics from in-situ resistivity variations	43
III.2. Isothermal phase transformation kinetics.....	46
III.3. Microstructure observations.....	51
III.3.1. Initial state	51
III.3.2. Structure and microstructure evolutions for aging at 300~ 350°C.....	52
III.3.3. Structure and microstructure evolutions for aging at 400~ 450°C.....	58
III.3.4. Structure and microstructure evolutions for aging at 500 ~ 550°C.....	63
III.3.5. Structure and microstructure evolutions for aging at 600°C and 700°C.....	68
III.4. The design of TTT diagram for Ti-B19 alloy	73
III.5. Summary.....	77
IV. INFLUENCE OF HEATING RATE ON ISOTHERMAL PHASE TRANSFORMATION IN TI-B19 ALLOY	80
IV.1. Evolutions during the heating.	82
IV.1.1. Variation of resistivity with temperature (time) during the heating process	82
IV.1.2. Variation of structure and microstructure during the heating for a heating rate of 0.1°C/s.	83
IV.2. Evolutions during the holding step.....	88
IV.2.1. Evolutions of electrical resistivity variations.	88
IV.2.2. Microstructures and structure obtained after isothermal holding.....	89
IV.3. Brief summary and discussion.....	91
V. EFFECT OF PLASTIC DEFORMATION ON PHASE TRANSFORMATION OF TI-B19 ALLOY DURING AGING.....	95
V.1. Resistivity variation during heating and aging processes	95
V.1.1. Resistivity variation in the heating range	95
V.1.2. Resistivity variations during holding at 500°C.	100
V.2. Isothermal phase transformation kinetics.....	104
V.3. Influence of deformation on microstructure evolutions.	105
V.4. Brief Summary.....	114
VI. PHASE TRANSFORMATION OF TI-B19 ALLOY DURING CONTINUOUS COOLING.....	116
VI.1. Influence of the cooling rate on the microstructure evolution in Ti-B19 alloy.....	117
VI.2. Resistivity variations during continuous cooling.....	118
VI.3. Establishment of phase transformation kinetics functions.....	123
VI.4. Brief summary.....	129

Contents

VII. RELATIONSHIPS BETWEEN MICROSTRUCTURE AND MECHANICAL PROPERTIES OF TI-B19 ALLOY	130
<i>VII.1. Mechanical characteristics of Ti-B19 alloy after solution aging</i>	<i>130</i>
<i>VII.2. Influences of volume fraction of precipitated phases on mechanical characteristics of Ti-B19 alloy.</i>	<i>135</i>
<i>VII.3. Summary.....</i>	<i>140</i>
CONCLUSIONS.....	142
APPENDIX	146
REFERENCES	151
RESUME.....	161

I. INTRODUCTION

I.1. Brief introduction of titanium alloys

As an important structural and functional family of material, titanium and titanium alloys have been widely used in many fields such as aerospace, chemical industry, biomechanical applications etc due to the low density, high strength, good corrosion resistance as well as high temperature performances^[1~6]. Generally, titanium and titanium alloys can be divided into three different classes, such as α , β and $\alpha+\beta$ according to the phases present at room temperature. With the development of titanium alloys, a more detailed classification has been made with 5 different classes corresponding to α , near α , $\alpha+\beta$, metastable β as well as stable β titanium alloys as shown on a pseudo binary phase diagram in Figure 1-1^[2, 5, 14].

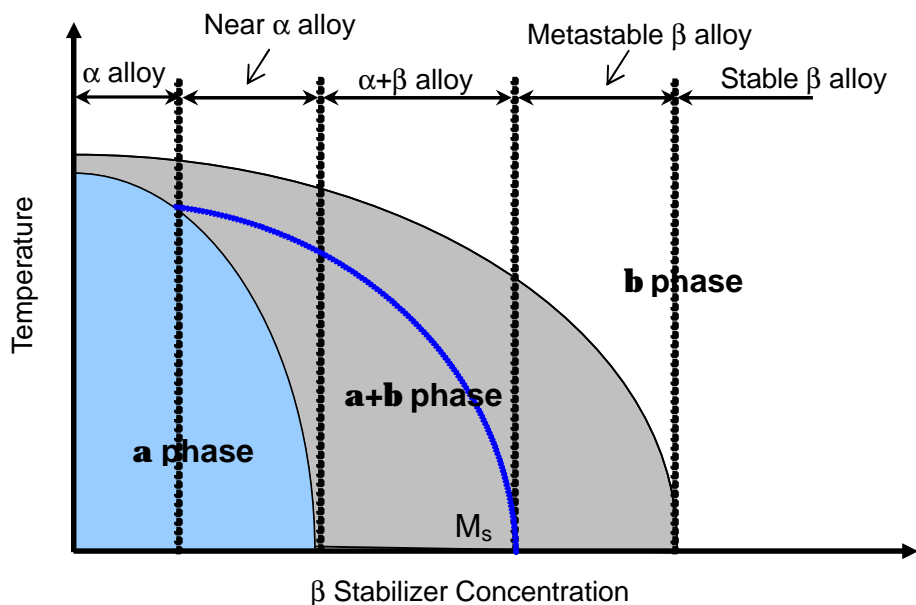
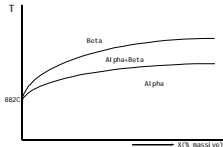
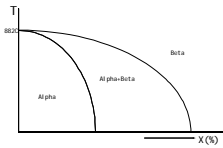
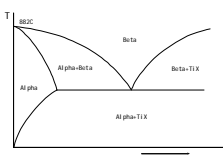
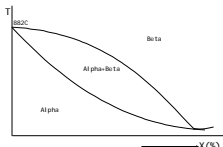


Figure 1-1 The pseudo binary phase diagram of Ti alloys and different classes of Ti Alloys.

The alloying elements of titanium are classified as α -stabilizers, β -stabilizers and

neutral according to their influence on the β transformation temperature (T_β). The α -stabilizers addition stabilizes the α phase and increases the β transformation temperature, while the β -stabilizers stabilize the β phase and decrease the β transformation temperature^[2,5,6]. Table 1-1 shows the alloying elements and their function in titanium alloys.

Table 1-1 Classification and effect of alloying elements in Titanium alloys^[4]

Alloying elements category	Phase diagram	Interstitial elements	Main elements
α -stabilizers		O,N,B,C	Al
Isomorphous elements			Mo, V, Nb, Ta
β -stabilizers		H	Mn, Fe, Cr, Co, W, Ni,Cu, Au, Ag, Si
Neutral			Sn, Zr

In order to compare the alloys, and the relationships between the chemical composition, the phases present and the mechanical properties in titanium alloys, the aluminum-equivalent (expressed as $[Al]_{Eq.}$) and molybdenum-equivalent (expressed as $[Mo]_{Eq.}$) have been used to describe the stability and strengthen ability of an alloy^[1~4, 6], and can be calculated with the following formulations:

$$[Al]_{Eq} = Al\% + 1/3Sn\% + 1/6Zr\% + 10O_2\%$$

$$[Mo]_{Eq} = Mo\% + 1/1.5V\% + 1/0.6Cr\% + 1/0.35Fe\% + 1/1.3Cu\% + 1/3.6Nb\%$$

By now, more than 100 different titanium alloys are known, in which only 20~30 alloys have been used as commercial alloys [3, 5, 6, 15]. According to the performances, different kinds of alloys have been developed for different application fields. For the α and near α alloys, the microstructure at room temperature is mainly composed of only α phase or a mixture of $\alpha+\beta$ phases with very low β phase amount (normally not exceeding 15%). Those kinds of alloys can be used for high temperature parts due to its combination of suitable strength, good weldability, good creep properties as well as thermal stability, such as IMI834 alloy [3, 15]. Meanwhile, some of those alloys can be used in the lower temperature ranges for their nice low temperature properties, for example Ti-5Al-2.5Sn [6]. The $\alpha+\beta$ class alloy contains α phase and β phase at room temperature, and normally the α phase volume fraction exceeds 50%, and the alloys are one of the structural material with excellent mechanical properties. This class can be strengthened by heat treatment and even the strength can be adjusted through the heat treatment. Ti-6Al-4V is a typical $\alpha+\beta$ alloy which has been developed in the 1950s [6, 15-26], and now it is most widely used, as a structural material. Metastable and stable β titanium alloys contain more β stabilizer elements. For metastable titanium alloys, the amount of β stabilizer is sufficient to avoid any diffusive or displacive (martensitic) transformation during quenching. The martensitic transformation temperature is lower than the room temperature, and the high temperature β phase can be remained at room temperature by quenching from solution temperature. Such kinds of alloys have good cold deformability, and can be strengthened by heat treatment by precipitation of α phase from metastable β phase. So these alloys can be used for high strength structural parts, such as Ti-1023 alloy [10, 12, 13, 27-29].

I.2. Phase transformation in titanium alloys

I.2.1. Main phase transformations in titanium alloys

As for other metallic alloys ^[30~34], different solid/solid phase transformations may occur during the thermal treatments in titanium alloy controlling the microstructure and in consequence the properties of the alloy. The study of the solid phase transformations during heat treatments have thus been a necessary research field for the material scientists ^[29, 34, 35]. In titanium alloy, the basic phase transformation is the $\alpha \leftrightarrow \beta$ transformation. The crystal structures of α and β phases are shown in Figure 1-2 a and b, respectively. The α phase has a hexagonal close packed (HCP) lattice structure; there are two atoms in each cell with 12 near neighbor atoms.

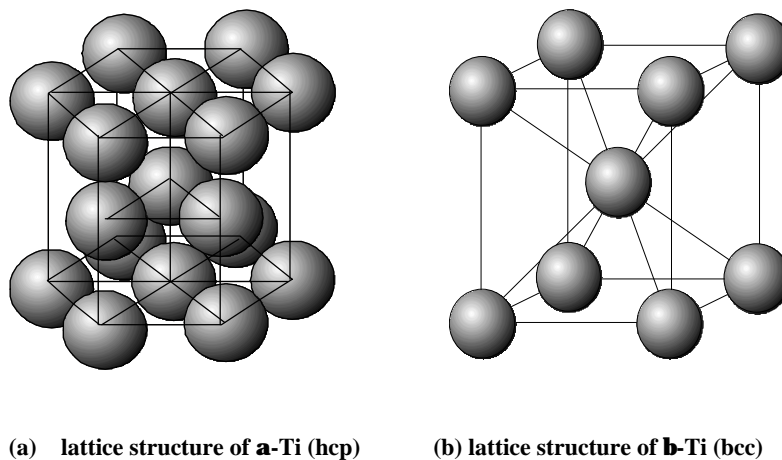


Figure 1-2 Crystal structure of α -Ti (a) and β -Ti (b).

The lattice parameters of α are $a = b = 2.95 \text{ \AA}$ and $c = 4.68 \text{ \AA}$, giving the c/a ratio of 1.587, that is a little smaller than that of the ideal HCP lattice ($c/a = 1.633$). The β phase has a body-centered cubic (BCC) structure and there are also 2 atoms in each cell, surrounded by 8 near neighbor atoms. The lattice parameter of bcc β phase is $a = b = c = 3.206 \text{ \AA}$. In titanium alloys, the solid phase transformations can be classified into different kinds and Tingjie Zhang has summarized it as show in Table 1-2 ^[30].

Table 1-2 The main phase transformations in titanium alloys

Phase transformation	Transformation processing
1 Decomposition of β phase during cooling	1) $\mathbf{b} \rightarrow \mathbf{a} + \mathbf{b}_{remains}$. 2) Martensite: $\mathbf{b} \rightarrow \mathbf{a}' + \mathbf{a}'$ 3) $\mathbf{b} \rightarrow \mathbf{w}_{an-iso} + \mathbf{b}_{remains}$
2 Decomposition of β phase during isothermal processing	1) $\mathbf{b}_{metastable} \rightarrow \mathbf{a} + \mathbf{b}_{remain}$, $\mathbf{b}_{remains} \rightarrow \mathbf{a} + \mathbf{b}_{transformed}$ 2) $\mathbf{b}(\mathbf{b} + \mathbf{a}) \rightarrow \mathbf{a}'(\mathbf{a}'_{rich} + \mathbf{a}'_{poor})$, β' , β_{rich} , β_{poor} , 1α , 2α 3) $\mathbf{b} \rightarrow \mathbf{w}_{iso} + \mathbf{b}_{transformed}$ 4) $\mathbf{b}_{remains} \rightarrow \mathbf{b}_{remains} + \mathbf{b}_{transformed}$ 5) $\mathbf{b}_{remains} \rightarrow \mathbf{a}_2 + \mathbf{b}$ 6) Isothermal martensite transformation
3 α phase formed via transition phases	$\mathbf{b}_{Metastab / remains} \rightarrow \mathbf{w} \rightarrow \mathbf{a} + \mathbf{b}_{transformed}$, $\mathbf{b}_{Metastab / remains} \rightarrow \mathbf{b}' \rightarrow \mathbf{a} + \mathbf{b}_{transformed}$
4 Decomposition of martensite	1) $\alpha' \rightarrow \mathbf{a} + \mathbf{b}_{transformed}$, $\alpha' \rightarrow \mathbf{a} + \text{compounds}$ 2) $\alpha''(Ms \gg T_{room}) \rightarrow \mathbf{a} + \mathbf{b}_{transformed}$, $\alpha''(Ms \leq T_{room}) \rightarrow \mathbf{b}_{transformed}$
5 Eutectoid decomposition	1) Active eutectoid: pearlite type microstructure 2) No-active eutectoid: mass type microstructure
6 Decompose of α solid solution	Compounds, ordered α_2 phase
7 Interface phase	α/β interface phase forming at a lower cooling rate.

All these transformations are not observed in all titanium alloys. As the research is mainly focused on β -metastable alloys, the transformations occurring in those alloys will be detailed in the following. At first we will detail the transformations occurring at the lower temperatures.

I.2.2. Martensitic phase transformation

Martensitic phase transformation is an important solid phase transformation in titanium alloys; it is a first order, non diffusive phase transformation, and the growth is controlled by the movement of the interface. The martensitic phase transformation has an important influence on the mechanical properties and it results in complex microstructure changes. Thus more and more researchers have paid more attention in this field [2, 5, 6, 30, 34, 36-48].

Martensitic phase transformation in titanium alloy can be classified into three different types according to its formation conditions, which includes quenching martensite, isothermal martensite as well as stress induced martensite^[30, 34, 48]. Quenching martensite is formed during the cooling from high temperature with an enough quick cooling rate avoiding diffusion of solute elements, isothermal martensite is formed during an isothermal period. Stress induced martensite may be formed for example during tensile tests of a metastable beta phase; martensitic transformation is assisted by stresses including outside loading stress as well as internal stress.

According to the crystal structure, martensite can be classified into four different types^[30]: they are {334} hexagonal martensite, {344} hexagonal martensite, orthorhombic martensite as well as FCC martensite. But anyway, the hexagonal Martensite (α') and orthorhombic martensite (α'') are familiar in industrial titanium alloys. Normally, α' martensite exists in the alloys that contain the lower amounts of alloying elements; its crystal structure is HCP. The martensite morphology is plate shaped without internal twins and with a habit plane of $\{334\}_b$, meanwhile the orientation relationships with the β matrix is: $(111)_M // (110)_b$, $\left[\begin{matrix} 11\bar{2}0 \\ \end{matrix} \right]_M // [111]_b$.

The orthorhombic martensite α'' , is observed in the alloys with higher amounts of alloying elements. Their morphology is needle-like. In those morphologies, there are

possible internal twins, and the orientation relationships with the β matrix is: $(111)_M // (110)_b$, $[110]_M // [111]_b$. During further heat treatments, the martensite will decompose into stable α phase due to its metastable state. The α' martensite decomposes directly into stable α phase. However, for α'' martensite, the decomposition process is a little more complex; the α' martensite will be formed first followed by the stable α phase.

The martensite formation conditions in titanium alloy are dependent on the alloy chemical composition (the category and amount of alloying elements) as well as the heat treatment conditions, especially the cooling rate when the alloy is cooled from the high temperature. The influence of the elements position in the periodic table on the martensitic transformation temperature (M_s) have been investigated by A.V. Dobromyslov et al.^[40] using more than 150 different binary titanium alloys which content different amount of alloying elements such as V? Cr? Mn? Fe? Co? Ni? Cu? Nb? Mo? Ru? Rh? Pd? Ta? W? Re? Os? Ir? Pt etc.. The results indicated that the alloying elements above mentioned should be added within the critical lowest amounts in order to retain the metastable phase during quenching from high temperature. For the binary alloys for which the added elements have a BCC crystal structure, the M_s point of the alloy will be greatly elevated, and the M_s point increased with the family position of the added element increase in the element periodic table. When the crystal structure of the added elements is FCC, the M_s point of the alloy will be elevated with the family position of the added element decrease in element periodic table.

The research results of Ti-35Nb-7Zr-5Ta alloy by J.I. Qazi et al.^[41] shows that α'' phase forming conditions are nearly related with the alloy chemical composition as well as the cooling rate. The α'' phase will be formed in the alloy at the water cooling condition, but it will not be formed at the air cooling condition. Meanwhile,

the volume fraction of α'' phase decreased with the addition amount of Nb+Ta increase, and the formation of α'' phase will be inhibited completely when the addition amount of Zr element is between 4.1~ 4.6%. However the addition of the interstitial elements will counteract such effects of Zr addition.

The results of research on the kinetics of martensite formation in Ti-6Al-4V alloy containing hydrogen reveal that the Ms point of the alloy will be decreased with the addition of hydrogen^[41], and the Ms point will be lower than 500°C when the additional amount of hydrogen is 30at%. It is also shown that the volume fraction of α'' formed during quenching changes from 0% to 80% when the hydrogen addition amount change from 0at% to 30at%, and the temperature “nose” for the martensitic transformation decreased from 800°C to 625°C during the following aging treatment processing. In another point, the starting time of α'' martensite decomposition is lagged from 6 seconds to 10 minutes when 10at% hydrogen is added in the alloy.

I.2.3. ω Phase transformation

The ω phase is a transition phase in titanium alloy, and often appears in the metastable beta titanium alloys that contain high amounts of beta stabilizing elements. Two different sorts of ω phase are reported in the literature, one is the quenching or an-isothermal ω phase, and the other one is the isothermal ω phase. The forming mechanism of an-isothermal ω phase can well be explained by the theory model of $\{111\}_\beta$ plane collapse^[31,39,49~53]. It is said that the crystal lattice of ω phase is formed by one $\{111\}_\beta$ plane in the β matrix that collapses to the middle and while the neighbor $\{111\}_\beta$ planes keeps the original position. The isothermal ω phase is formed during isothermal treatment at low temperatures (300-350°C) and is controlled by diffusion.

However, those two kinds of ω phase have in general a similar crystal structure, but

for the detailed crystal structure, there are three different comments. Some researchers consider it is BCC structure^[31], and some of them think it is a HCP structure^[31]. There are also some authors that take it for a “triangle” structure which is a kind of aberrant HCP structure and normally appears in the alloy which contain high volume fraction of alloying elements^[31]. By now, most researchers are apt to consider the crystal structure as HCP^[49~55]. The two kinds of ω phase show differences in the diffraction patterns, and there are dispersion stripes appearing for an-isothermal ω phase, but not for the isothermal ω phase.

Normally, an-isothermal ω phase shows particle-like shape^[27,34,49], and precipitates are dispersed in the β matrix. For the isothermal ω phase, the shape of the precipitates is ellipsoidal with a size of a few nanometers. Precipitates are dispersed in the β matrix. Moreover, an ω phase with lamellar-like shape has been reported by Japanese researchers when investigating martensite transformation during quenching in shape memory alloy of Ti-30Nb-3Pd(wt%)^[35]. The crystal structure of this ω phase is HCP and the precipitate size is of a few nanometers. The orientation relationships between the lamellar-like ω phase and the β matrix is the same as for the particle-like ω phase. The different morphologies of the ω phase are shown in Figure 1-3a,b^[43,46].

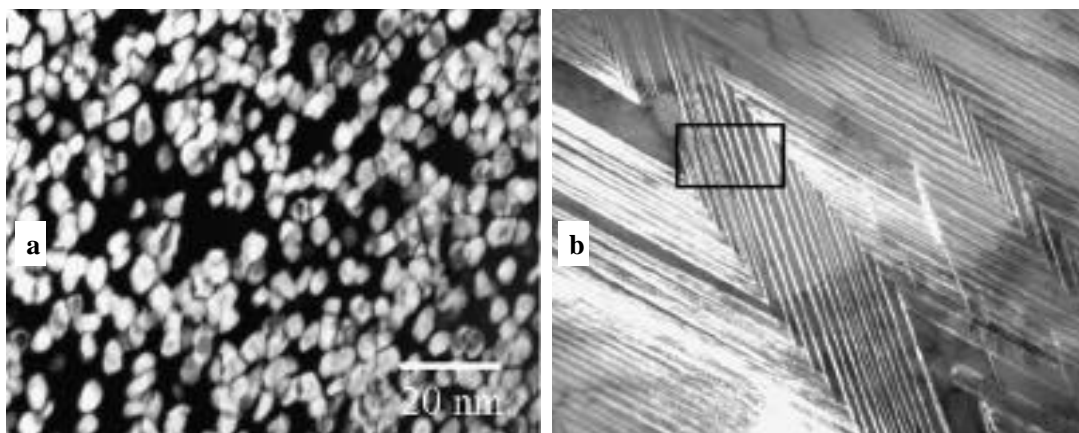


Figure 1-3 Dark field TEM image of ω phase for ellipsoidal-shaped (a) and lamellar-shaped (b).

D.H. Ping^[35] et al., have related the formation mechanism of lamellar-like ω phase.

The interface of the lamellar-liked ω phase and β matrix are very plain observed in the experiment, and the habit plane is close to $\{112\}_\beta$ crystal plane where phase transformed due to shear stress occurred along (111) crystal orientation.

The ω phase is a transition phase and is not stable, so it will disappear or transform when the alloy is reheated at higher temperatures. The role of the ω phase on the formation of the α phase has been studied in detail [49,51]. In the different studies, the authors have reported that the ω phase favors the nucleation of the α phase. Three different explanations have been proposed. At first [51], it has been proposed that α phase nucleates in the β matrix, at some distance from the ω/β interface, enriched in Al. For other authors [51] the α phase nucleates at the ω/β interface, and grows in β and ω phases consuming the ω phase. During this period, the three different phases keep the orientation relationship as: $(\bar{1}100)_\omega // (10\bar{1}0)_\alpha // (211)_\beta$, $(\bar{1}\bar{1}20)_\omega // (0001)_\alpha // (0\bar{1}1)_\beta$, $(0001)_\omega // (\bar{1}2\bar{1}0)_\alpha // (\bar{1}11)_\beta$. At last, Prima et al [46] have proposed that α nucleates in the ω phase keeping the following orientation relationships: $(\bar{2}\bar{1}0)_\omega // (002)_\alpha$, $[001]_\omega // [110]_\alpha$. Their schematic model is shown in Figure 1-4.

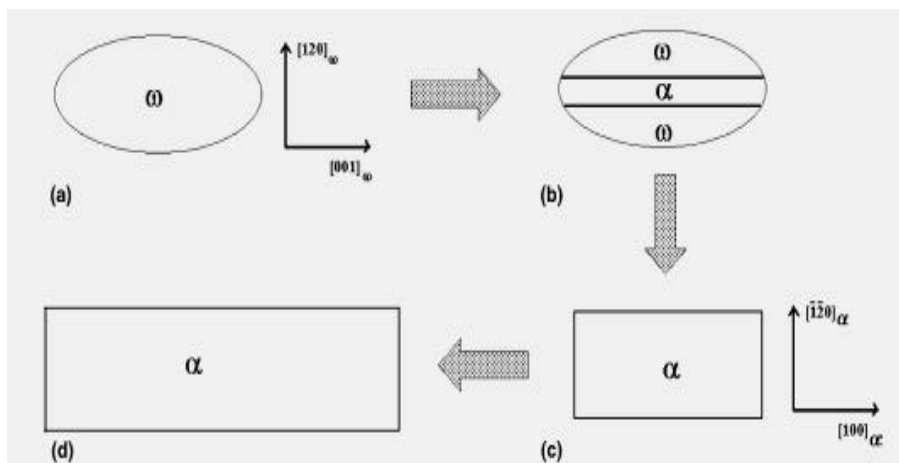


Figure 1-4 Nucleation and growth model of a phase in inner ω phase [46].

(a) ω phase act as nuclear site for a phase; (b) a growth in inner ω phase by consuming ω phase; (c) ω phase disappear; (d) a phase growth with the ω phase exhaust.

Anyway, the detail about isothermal ω phase formation mechanisms and phase transformation kinetics is still in research and related experimental data as well as models are still lacking. Uniform answers are not yet obtained. Nevertheless, in order to gain a fine and dispersed distribution of α phase, the processing route with a low aging temperature leading to ω precipitation followed by high temperature treatment leading to α formation has been used to reduce the size of α precipitates.

I.2.4. Decomposition of metastable β phase

Depending on the chemical composition of the alloys, the decomposition of the β phase may occur during the cooling from the high temperature β phase range, or for β -metastable alloys during reheating processes after high temperature solution treatment as well as during isothermal aging treatments. Different authors have paid attention to the formation of α phase during isothermal aging to understand its mechanism of nucleation and growth, and the related kinetics and crystallography of the phases. Some progresses focused on those aspects will be presented considering at first the transformation on heating and further aging of mainly beta metastable alloys, and in a second part the transformation on cooling of different titanium alloys.

Transformation on heating and aging of beta metastable alloys.

The decomposition of the β phase on aging can lead to the formation of different phases: β' , ω , martensite as well as α . β' , ω , and martensite are not stable phases, and they will further decompose or transform into stable α phase during the following thermal process^[5,32,56-84]. The transformation of β' and α phases will be introduced in detail. Martensite and ω phase transformation have been introduced above.

The β' phase normally appears in the initial stages of aging at lower

temperature(200~500°C) in titanium alloy which is rich in β stabilizer elements (such as Ti-15-3)^[51,65]. The β' phase has the same crystal structure as the parent phase, and also takes coherent structure with the β phase, but has a lower concentration of alloying elements as compared with the parent phase. The morphology of β' phase is very fine (several nanometers) and with short bar-shape or crescent-shape. The stability and transformation kinetics of β' phase are strongly dependent on the chemical composition of the alloy, and it will be decomposed with the aging time prolongation until the stable α phase formed. It is very hard to distinguish the β' phase and β phase by the X-ray diffraction technology because the difference in lattice parameter is very little, so the film TEM technology should be used to observe the precipitated β' phase in titanium alloy.

For the direct formation of α phase from the metastable β phase during isothermal aging, the transformation mechanisms, precipitates distributions, volume fraction, appearance as well as the transforming kinetics are strongly influenced by the chemical composition of the alloy, the transformation temperature, the grain size of the parent β phase and the heating rate to the aging temperature^[64,65,79,82].

The isothermal phase transformation in Ti-15-3 alloy has been investigated in detail by Guiqin SHEN^[51]. The results related that, when aging at 700°C for 4 hours (the heating rate to 700°C is not reported), the α phase is first formed at grain boundaries. After 12 hours holding at 700°C, intragranular α precipitates are observed and the transformation is completed after nearly 48 hours. The final α volume fraction is about 22%. Decreasing the aging temperature, the $\beta \rightarrow \alpha$ transformation kinetics is accelerated. At 600°C, the α phase begins to precipitate after 15 minutes holding, and is finished after 24 hours holding, and the final volume fraction of α phase is about 41%. Meanwhile, at 550 and 500 °C, the beginning of the transformation is respectively observed after 30 seconds and 1 minute, and the transformation is

finished after 12 hours. The volume fractions of α phase are 50% and 62% (measured by X-ray diffraction), respectively. TEM observations have been performed for a Ti-15-3 alloy by Furuhashi^[79]. The observations revealed that the α phase formed during aging at temperatures above 450°C (Figure 1-5) has a lath morphology. For an aging temperature of 300°C (3600s), α is present and has an aggregated morphology, composed with thin twinned laths (Figure 1-5).

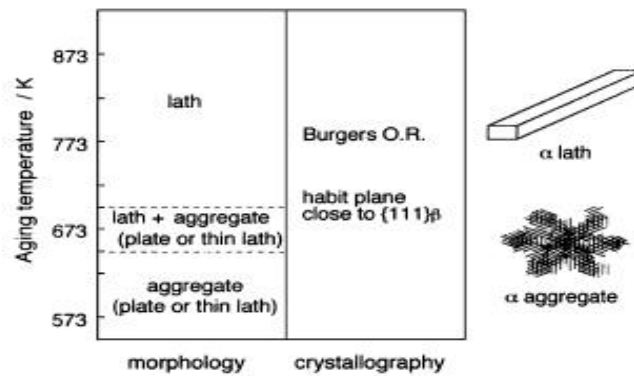


Figure 1-5 Variations of a phase morphology and crystallography with aging temperature in Ti-15-3^[79].

Different studies report the existence of alpha phases presenting two different orientation relationships. THOMAS J. et al.^[31] have observed these two different kinds of α phase formed in Ti-38644 alloy during aging treatment at 350°C~400°C and above 450°C, respectively, named 1α and 2α . The orientation relationships between 1α and β are the Burgers one, i.e.: $\{\bar{1}\bar{1}0\}_b // \{0001\}_a$; $[111]_b // [11\bar{2}0]_a$. 1α morphology is lens-liked and is twinned with a habit plane of $\{01\bar{1}\}$. 2α and the matrix do not obey to the Burgers orientation relationships; the morphology of 2α shows raft-liked shape. 2α presents also a twinned structure and the twin plane is the same as for 1α phase. C.G. Rhodes and J.C. Williams^[47] considered that there are no difference in crystal structure between the two kinds of α phase, but the 2α is more stable than 1α and during its growth it consumes 1α . Moreover, they proposed that there are two possible different mechanisms for the formation of 2α : one mechanism is that 2α is obtained by mechanical twinning of 1α , and the second one is the

formation of 2α by nucleation and growth. R. Jeffrey et al^[24] have also reported the formation of 1α and 2α in Ti-10-2-3 alloy. 1α has been observed in the alloy during aging at temperature above 550°C , while for aging at temperature lower than 550°C , 1α phase and 2α can be observed after decomposition of β .

Isothermal Transformation during cooling from the high β temperature range.

Characterizations of transformation have also been performed during isothermal treatments after direct cooling from the stable beta temperature range. Studying metastable alloys such as β_{CEZ} or Ti17^[80-82] three different morphologies of α phase have been identified depending on their nucleation sites, and the condition of transformation. The first called α_{GB} morphology is formed at first at the β grain boundaries; the second one defined as α_{WGB} morphology grows from α_{GB} and is observed as colonies of lamellae with a same crystallographic orientation^[80]. The last one called α_{WI} or α_{WM} precipitates in the β grains and present a Widmanstätten morphology; the precipitates arrangement look as a basketweave. For β_{CEZ} and Ti17, the results indicate that α_{GB} and α_{WGB} are mainly formed at temperatures above 750°C ; the average width of α_{GB} is about $2.3\mu\text{m}$, the maximal length of α_{WGB} phase is about $40\mu\text{m}$ ^[109]; when the isothermal temperature is 700°C , the three kinds of morphologies are observed, that is to say α_{GB} , α_{WGB} and α_{WI} phase. At that transformation temperature, the average width of α_{GB} phase is about $1.3\mu\text{m}$, the length of α_{WGB} phase is less than $0.5\mu\text{m}$; when the isothermal temperature is 600°C , and the average width of α_{GB} is about $0.2\mu\text{m}$.

The authors also consider that the β phase between the α_{WGB} lamellae is enriched in β stabilizer elements, while its chemical composition ahead of the lamellae tip is modified on a shorter distance. The length of the α_{WGB} lamellae is decreased with the decrease of the transformation temperature for example, it is $10\sim 20\mu\text{m}$ when the isothermal temperature is 790°C and less than $7\mu\text{m}$ when the temperature is down to

750°C. A numerical model describing the formation sequences of the α phase at high isothermal temperatures has been proposed according to the experimental observations, and has been schematized as the sequence shown in Figure 1-6.

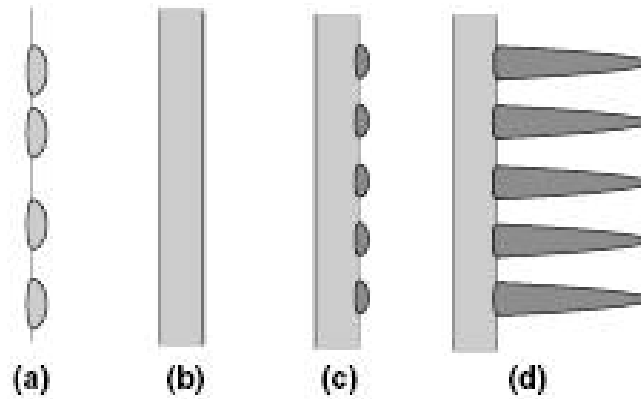


Figure 1-6 Sequence of the phase transformation modeling established based on b_{CEZ} alloy at high temperature isothermal treatment ^[101].

(a) nucleation of α_{GB} , (b) growth of α_{GB} , (c) appearance of α_{WGB} , (d) growth of α_{WGB} .

Studies performed by S.Malinov et al^[84,85] on Ti-6-4, Ti-811 and Ti-6242 alloys have led to similar observations but at different temperature ranges. Above 900°C the α phase is first formed at the β grain boundaries and the lamellar α phase nucleates and grows in the β grain; at lower temperatures, lamellar α grains nucleate and grow uniformly in the β grains.

I.3. The phase transformation kinetics of titanium alloys

The solid phase transformation kinetics in alloys can be established by a continuous characterization of changes of physical properties which are sensitive to the structural evolutions leading to a relationship of the relative change of property with temperature and time^[86-90]. These properties can be expansion coefficient, volume, hardness, electrical resistivity as well as enthalpy changes etc.. Assuming a linear relationship between those relative properties and the relative structural change, the

equation between the phase transforming degree (f) and those changes of physical parameters can be given as:

$$f = \frac{P - P_0}{P_1 - P_0}, \quad 0 \leq f \leq 1 \quad (1-1)$$

where, P is the value of the measured physical parameters at time t ; P_1 and P_0 are the values of the measured physical parameters at the beginning and at the end of the phase transformation, respectively.

The isothermal kinetics of the transformation will be expressed as $f = f(t)$. For diffusive transformations, the transformation kinetics often presents a sigmoid shape that is expressed by JMAK law (Equation 1-2).

$$f = \frac{P - P_0}{P_1 - P_0} = f_{\max} (1 - \exp(-k(t - t_b)^n)) \quad (1-2)$$

Here, k means the temperature coefficient which is sensitive to the variation of temperature; n is the Avrami exponent; t is time at transformation temperature and t_b is the beginning time for the transformation. The Avrami coefficient is dependant on the nucleation and growth mechanisms.

In order to model the transformation during cooling, different models have been established. Considering additive characters for both the incubation time and the progress of the transformation, the an-isothermal processing can be treated as series of different very short isothermal steps ^[91,95]. The beginning of the transformation will be calculated according to Scheil law:

$$\int_0^t \frac{dt}{t_b(T)} = 1 \quad (1-3)$$

Here, $t_b(T)$ is the time at which transformations begins at the isothermal temperature T , and t is the time. The JMAK equation can be expressed as formula 1-4 for the an-isothermal processing:

$$f(t) = 1 - \exp \left\{ - \left[\int_0^t k(T) dt + \ln \left(\frac{1}{1-f_0} \right)^{1/m} \right]^m \right\} \quad (1-4)$$

Here, f_0 is the volume fraction of new formed phase at the phase transformation start, and m is the Avrami exponent for an-isothermal treatment.

Then the relationship between phase transformation degree and time or temperature can be calculated for the isothermal and an-isothermal processing according to JMAK law based on the experimental results. Generally, the an-isothermal phase transformation kinetics can be investigated and calculated based on the research or calculated results of isothermal ones [4, 91-95]. For the titanium alloy, research and calculation on the phase transformation kinetics in Beta CEZ, Ti-17, Ti-6-4, Ti-6242, Ti-811, Ti-1023 as well as Beta21s have been done by E. Laude, J. Da Costa Teixeira and S. Malinov etc. [84,85,91,102,109], and the research results indicated that the JMAK equation can be used to describe the isothermal phase transformation kinetics in titanium alloy.

I.4. The aim of the present research work

Excellent combination of mechanical properties can be obtained in titanium alloys by controlling the heat treatment process. So it is very important to understand in detail the phase transformations occurring during the process in order to improve the mechanical properties by controlling the microstructure formation and design the deformation and heat treatment. Anyway, it is also an important guide to design and

develop new alloys.

Ti-B19 is a kind of new metastable beta titanium alloy developed by China. Remarkable combination of mechanical properties as strength, ductility and toughness can be obtained by appropriate heat treatments. The microstructure of the alloy is strongly depended on the parameters of the heat treatment, that is to say the difference of temperature, time and the rate of heating and cooling will lead to differences in volume fraction, shape, size as well as distribution of the formed phase, which introduce differences in mechanical properties. So the aim of the present work is to study the phase transformation kinetics in Ti-B19 alloy during heating and cooling as well as isothermal periods, and to understand the phase transformation behaviors. The results of this work will provide some important data to understand the microstructure evolution as well as some guides to design the processing route (deformation and heat treatment) for a new composition of titanium alloys.

II. RESEARCH SCHEME AND EXPERIMENTAL PROCEDURE

II.1. Research contents

The phase transformation kinetics during isothermal and an-isothermal processing (continuous cooling) in the metastable beta titanium alloy Ti-B19 have been investigated systematically considering the influence of several processing parameters. The nature of the formed phase is analyzed as well as the microstructure evolutions. According to the results, the TTT diagram has been determined for the Ti-B19 titanium alloy for transformation of beta metastable phase during aging. Additional results have been obtained for precipitation during cooling allowing establishing a part of the CCT diagram. These results are a basic work for establishing the relationships between mechanical properties, heat treatment and microstructure. All the work was performed on TiB19 alloy. Our research focused on the following points:

- (1) The isothermal phase transformation kinetics during aging for temperatures in the range of 300~700°C.
- (2) The structure and microstructure evolutions for the given temperatures.
- (3) The influence of heating rate on the phase transformation kinetics and microstructure evolutions.
- (4) The an-isothermal phase transformation kinetics and microstructure evolution during continuous cooling from the beta temperature range.
- (5) The influence of plastic deformation on isothermal phase transformation kinetics and microstructure evolution during aging.
- (6) The relationships between mechanical properties, microstructure evolution and heat treatment.

II.2. Researching routes

The researching routes of the present work are designed as Fig.2-1. Firstly, in-situ electrical resistivity measurements have been used to get the relationships between kinetics of resistivity variations and treatment temperature, time and processing parameters. Then the phase transformation kinetics has been analyzed, considering a global modeling approach as the JMAK law, and the TTT diagram has been designed. Meanwhile, the nature of the phases, the nucleation and growth of the phases as well as microstructure evolutions have been investigated through synchrotron high energy X-ray diffraction, optical microscopy (OM), electron microscopy (SEM and TEM). Finally, the relationships between mechanical properties, aging temperature and microstructure parameters have been analyzed.

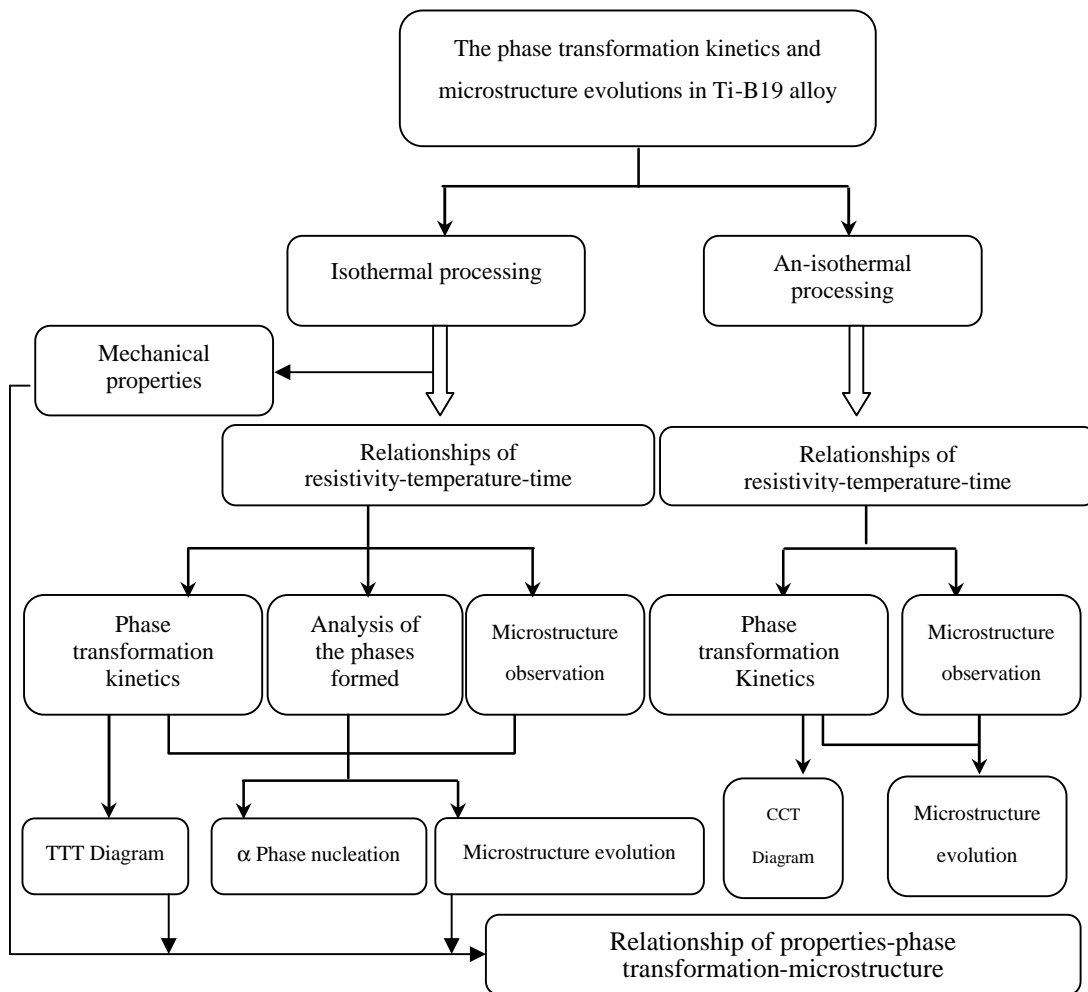


Figure 2-1 Scheme for research route of the present works

Based on the designed research routes and results, the research plan of isothermal kinetics, influence of heating rate and plastic deformation on isothermal phase transformation kinetics and phase transformation process during continuous cooling have been designed and described as following, respectively.

II.2.1. Study of isothermal phase transformation kinetics

In order to investigate systematically the isothermal decomposition of β metastable phase in Ti-B19 alloy a wide range of temperature has been selected. The temperature is ranging from 300°C to 700°C. The holding time at the transformation temperature is varying, depending on the end of the transformation time. The treatment applied to the specimens is schematized in Figure 2-2. For all specimens, a first solution treatment in the β temperature range is realized to control the initial state and the β grain size. The heating rate is 5°C/s, the temperature is 900°C, with 10 minutes holding time and a cooling rate of 20°C/s is used to freeze the microstructure obtained after the solution treatment at high temperature and keep a metastable β state.

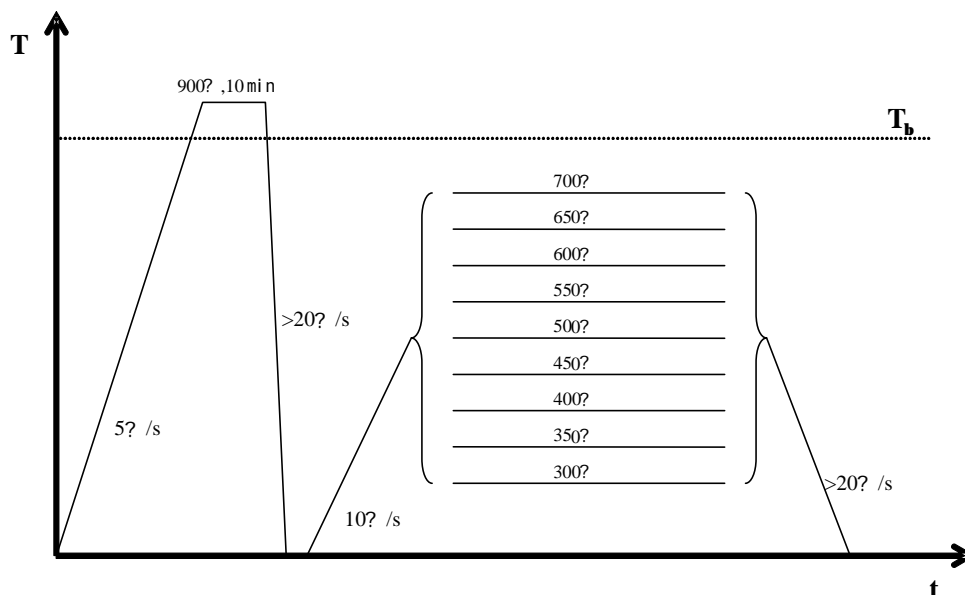


Figure 2-2 Program for isothermal phase transformation behaviors investigation

As transformation kinetics is obtained during aging, and in order to avoid or limit any transformation on heating before the isothermal decomposition of the β phase, a heating rate of 10°C/s has been applied.

After isothermal transformation during the aging treatment, specimens have been quenched at a rate higher than 20°C/s , avoiding thus a further precipitation and allowing freezing the microstructure obtained after transformation during aging. The microstructure observations and synchrotron X-ray diffraction analysis have been performed after those treatments. In order to analyze the isothermal phase transformation sequences, samples have been quenched at different holding time during isothermal treatment at 400°C , 500°C , and 600°C , according to the transformation kinetics obtained by electrical resistivity. For the sample transformed at 400°C , specimens have been quenched after 11,000s and 21,000s, holding time; for the sample treated at 500°C , the holding times have been 1,000s and 2,000s; while for the sample treated at 600°C , the holding times have been 2,500s, 6,000s and 10,800s.

II.2.2. Study of the influence of heating on isothermal phase transformation

Heating rate may influence the isothermal phase transformation kinetics and microstructure evolution remarkably. So the influence of heating rate on isothermal phase transformation behaviors have been studied as schematically shown in Fig.2-3. The first solution treatment in the beta temperature range is the same as previously leading to a similar beta metastable state. A single aging temperature is selected as 500°C and the holding time for all conditions is four hours. Three heating rates have been applied 10°C/s , 1°C/s and 0.1°C/s , respectively. After transformation, a rapid cooling rate is applied to freeze the microstructure formed during aging. The cooling rate was more than 20°C/s .

Moreover, according to the variation of resistivity obtained during heating at 0.1°C/s ,

samples were quenched from 350°C, 450°C and 500°C, respectively, in order to analyze the structure and microstructure evolutions.

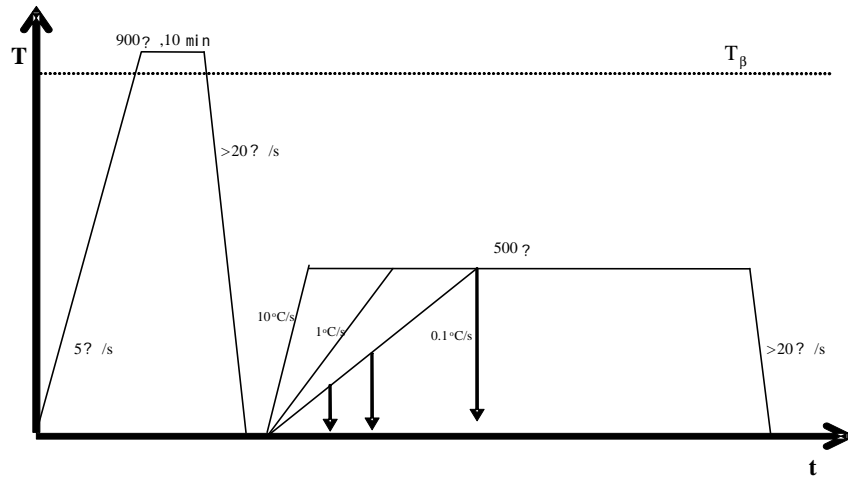


Figure 2-3 Applied treatments to study the influence of heating rate on the isothermal phase transformation

II.2.3. Study of the phase transformation kinetics during continuous cooling.

For the previous conditions, we applied a cooling rate from the beta temperature range leading to a beta metastable state. However, during cooling processes phase transformation may occur depending on the local cooling rate in the material. So the phase transformation kinetics and microstructure evolutions have been studied in Ti-B19 alloy during cooling from 900°C to room temperature according to the programs showed in Fig.2-4. The solution temperature of all samples are 900°C and holding time was 10 minutes with a heating rate of 5°C/s. The cooling rates considered were the following: 1°C/s, 0.2°C/s, 0.1°C/s, 0.06°C/s and 0.03°C/s, respectively.

II.2.4. Influence of plastic deformation of the beta metastable phase on isothermal phase transformation kinetics during aging.

At last, we analyzed the influence of plastic deformation of the beta metastable phase on isothermal phase transformation during aging. The aging temperature considered was 500°C. Two levels of pre deformation of 43% and 52% were considered.

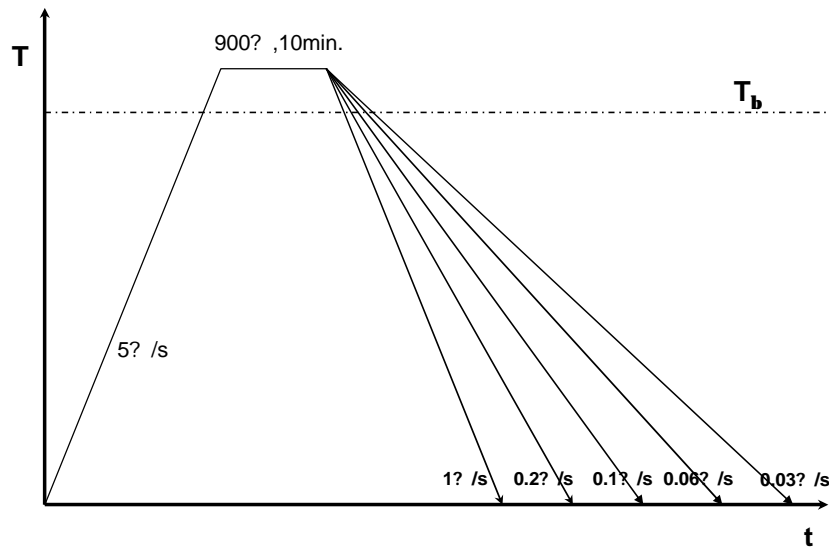


Figure 2-4 Applied cooling rates to study the phase transformation during continuous cooling.

II.3. Experimental materials

II.3.1. Brief introduction of Ti-B19 alloy

Ti-B19 is a metastable beta titanium alloy developed by China, with a good combination of properties: high strength, high toughness and reasonable ductility as well as a good stress corrosion resistance^[102]. The nominal chemical composition of Ti-B19 is Ti-3Al-5Mo-5V-4Cr-2Zr (wt%), and the typical physical properties are listed in Table 2-1. The T_{β} temperature is 790°C.

Previous studies have shown that^[103] Ti-B19 alloy is a kind of alloy which integrates the α/β Ti alloys and β Ti alloys. The molybdenum equivalent of the alloy is $[Mo]_{eq}=15$ and the alloy presents enhanced heat treatments capacities. Ti-B19 alloy

forging can be realized in the β and metastable β temperature range, and further aging treatments in the $\alpha+\beta$ range may lead to tensile strength higher than 1250MPa; the elongation can be maintained at a level higher than 6% with K_{1C} higher than $70\text{MPa}\cdot\text{m}^{1/2}$; more favorable matching among strength-plasticity-tenacity can be gained in metastable alloy.

Table 2-1: Some physical properties of Ti-B19 alloy

Phase transformation point($^{\circ}\text{C}$)	Density g/cm^3	Thermal expansion coefficient $\times 10^{-6}\cdot?$	Coefficient of thermal conductivity $\text{W}/\text{m}\cdot\text{k}$	Thermal diffusion coefficient $\times 10^{-6}\text{m}^2/\text{s}$
790 \pm 5	4.77	8.2~8.9 (100~300?)	6.9~11.8 (25~300?)	2.78~4.09 (25~300?)

II.3.2. Preparation of materials and samples

The Ti-B19 alloy used for this thesis comes from finely forged bars sized in $\Phi 20\text{mm}$. The alloy is obtained by a triple VAR process. The preparation and manufacturing processes are the following: sponge-structured Ti and master alloy are combined according to the nominal composition of the alloy and prepared to make an electrode; then, the material is made into ingot ($\Phi 296\text{mm}$) through Vacuum Arc Remelting process. The chemical composition of the alloy is given in Table 2-2.

Table 2-2 Chemical composition of Ti-B19 alloy used in present work. (wt.%)

Elements	Al	Mo	V	Cr	Zr	C	N	H	O	Fe	Si	Ti
Content	3.3	4.7	5.1	4.0	1.92	0.01	0.08	0.01	0.01	0.08	<0.04	Balance

The ingot is further forged in the β -phase range to breakdown the solidification microstructure and its size is reduced to a forged billet of 60mm in diameter; finally, the billet is transformed into bars of 20 mm diameter on KF-16 precision forger.

Cylindrical samples, 4 mm in diameter and 30 mm length as shown in Figure 2-5, are machined from the bar by linear cutting. No heat treatment has been done on the specimens.

The β transus temperature of the Ti-B19 alloy is $760\pm 5^\circ\text{C}$. This value has been obtained by metallographic observations as well as by differential thermal analysis. The wrought microstructure of the alloy is typical of a deformed microstructure, as shown in Figure 2-6. A certain amount of α -phase is present.

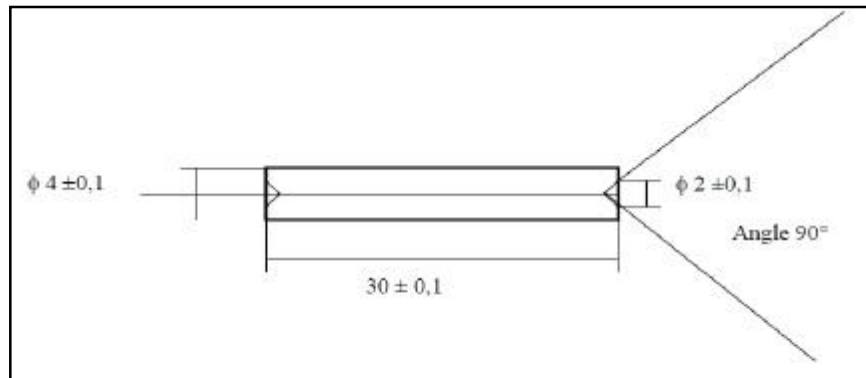


Figure 2-5 Size of the Ti-B19 alloy sample used in the present work (mm)

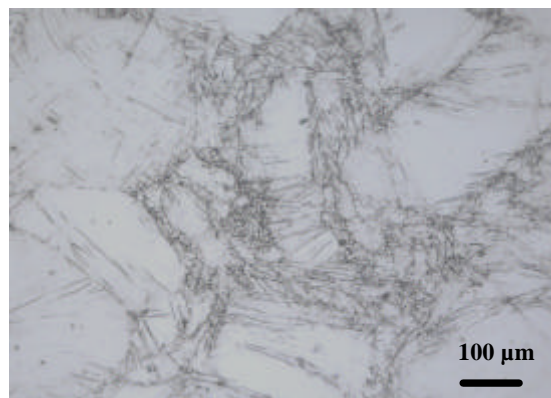


Figure 2-6 The microstructure of Ti-B19 alloy after forging

II.4. Experiment methods and devices

II.4.1. In-situ resistivity measurement method and device

The tests have been performed at LSG2M (Institut National Polytechnique de Lorraine Nancy) on an in house dilatometer able to characterize simultaneously the electrical resistivity changes.

The phase transformation kinetics is analyzed thanks to electrical resistivity measurements. The basic principle of the resistivity measurement is as follows: during phase transformations in the alloy different changes will occur (variations in the lattice structure, nature, density of interfaces, differences in chemical compositions of the phases) resulting in changes in the electrical resistivity^[84,101]. Therefore, it is possible to determine the dynamical changes by measuring the variation of the resistivity of the material in the thermal-mechanical process, so as to determine the kinetics of the structure evolutions.

Figure 2-7 is the diagram of the resistivity measurement method used. The samples used are usually cylindrical shape sized (diameter of $\Phi 3\sim 4$ mm and the length of 30~40mm); moreover, sheet-shaped samples are also often utilized in the dimensions of $(0.5\sim 0.8) \times (3\sim 4) \times (20\sim 30)$ mm. To reach changes in electrical resistivity, the most frequent way is to apply constant current on the sample and to measure the voltage variations. The calculation formula for the resistivity r is as follows:

$$r = (U/I) \times (A/L) \quad (2-1)$$

Wherein, A is the sectional area (m^2) of the sample; L is the distance (m) between the two voltage measurement points; I is the loading current (A), which is a constant value; U is the voltage (V) measured during the experiment.

The tension and temperature variations are continuously recorded during the overall

treatment process as a function of time. A further analysis of the obtained data will lead to a dynamical description of the phase transformation kinetics. Test equipment is shown in Figure 2-8. The system mainly includes the following parts:

- ? A sample heating chamber. This unit is connected with a vacuum system and the dynamic vacuum is as high as 10^{-5} Pa.
- ? A heating furnace. This unit comprises four infra-red lamps mounted inside the heating chamber. The power applied to the lamps is computer controlled; the heating rates may vary in the range $0.001\sim 100^{\circ}\text{C/s}$; the temperature difference between interior and exterior of the sample is $\pm 2^{\circ}\text{C}$.
- ? A sample cooling system. It utilizes a computer to control the flow rate of inert gas, so as to control the cooling rate ($0.001\sim 150^{\circ}\text{C/s}$) of the sample.
- ? An acquisition and treatment system for the experimental data. It includes sample temperature measurements using thermocouples (Pt/Pt-10%Rh), resistivity variation data acquisition (platinum wire), computer hardware and software for all system control and data process. An electronic treatment is realized to amplify (9000x) the electrical tension variations in order to gain in sensitivity.

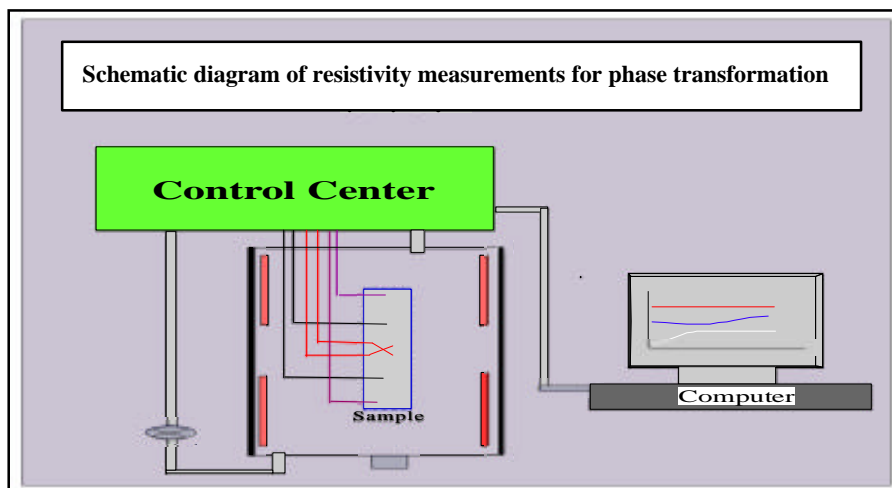


Figure 2-7 The schematic diagram of resistivity measurements for phase transformation

To lower oxidation of the sample during the heat treatment, the sample chamber

should be under vacuum during the whole process.

For our experiments, the current applied to the sample is constant, with a value of 2A supplied by an external battery; the connection wires are made of Pt with a diameter of 0.4mm. The voltage variation of the sample during the treatment is measured with two Pt wires (or Pt/Rt-Rh) 0.2mm in diameter.

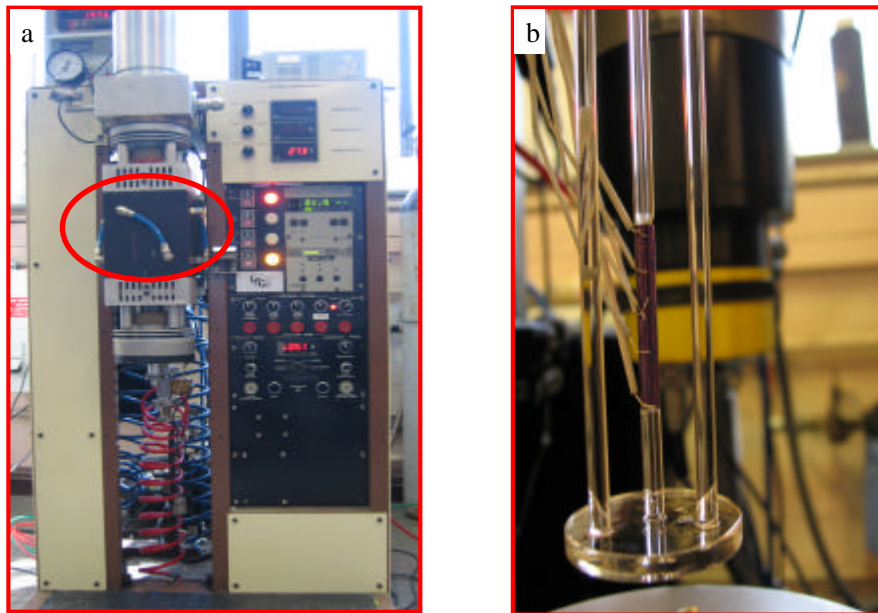
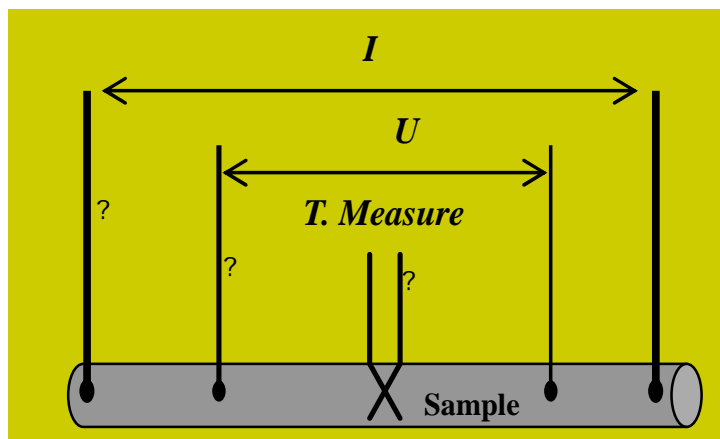


Figure 2-8 Test equipment (a) and sample connection (b) for the phase transformation study with the resistivity /expansion method



(① current wire, ② voltage measuring wire, ③ temperature measuring wire)

Figure 2-9 Sketch map of wires connection on the sample in resistivity /expansion method.

The connection of all wires is shown as Figure 2-9. All the wires are spot welded on the sample surface; the thermocouple is welded on the sample mid length; the current wires are welded on both ends of the sample; the voltage measurement wires are welded between the thermocouple and the current leads. It is necessary to record the following data prior to the test: The distance l between the welding points of the two voltage test wires; the starting voltage value U_1 after amplification through the amplifier, as well as the starting voltage value U_2 without amplification through the amplifier; the current I applied on the sample and the diameter D of the sample. All these parameters are used to calculate the resistivity r_t during the test and the calculation formula is as follows:

$$r_t = \left\{ \rho \cdot \left(\frac{D}{2} \right)^2 \div (l \times I) \times ((U_t - U_1) / 9000 + U_2) \right\} \div 1000 \quad (2-2)$$

Wherein, U_t is the voltage value that is measured during the test; all the parameter units are international standard units, and the resistivity unit that is gained as Ohm.m

II.4.2. High energy synchrotron X-ray diffraction

The synchrotron X-ray refers to a synchronous radiation X-ray source emitted from electronic accelerators or storage links; the X-ray is a bremsstrahlung created by high-speed moving electrons through field deflection acceleration; wherein, the wavelength electromagnetic radiation on the X-ray wave band is used as an effective X-ray source^[106]. The synchrotron X-ray has the following main characteristics: ① Flux rate – It is approximately 3~4 orders of magnitude higher than the flux rate of common X-ray; ② Perfect collimation – The energy resolution can reach 10^{-4} ; ③ Wide radiation spectrum – It can be used to record absorption edges of K series and L series of most of elements; ④ Specific time structure – The synchrotron X-ray is a pulse source and the pulse duration is about 10~1ns, and especially adapts to the analysis on instant spectrums or structure; ⑤ Excellent polarity – It is basically

100% linear polarization on the electronic track plane for convenience in the polarization X-ray research and anisotropic measurement for objects; ⑥ Pure spectrum – The synchrotron X-ray is the pure continuous wave spectrum without influence of stray radiation; ⑦ Accurate calculation for the wave spectrum characteristics – calculation required light sources according to a few parameters. Therefore, the synchrotron X-ray diffraction technology is considered as the most effective measure of accurate analysis on material structure and phase transformation at present [78,102].

High energy synchrotron X-ray diffraction has been used to determine the structure of the phases, the crystal parameters, the amount of each of phase in the samples. The tests were performed on ID15B beam line at ESRF (Grenoble) using transmission X-Ray diffraction. Unfortunately, no time resolved experiments could be done. The principle is shown in Figure 2-10. The incident X-ray energy is $E=89.283\text{KeV}$; the wavelength is $\lambda=0.13893\text{nm}$ and the radiation time is 5~15s. The samples (3 or 4 mm in diameter) are placed on a rotating sample holder. The high energy allows collecting the transmitted diffraction X-ray with a CCD detector to obtain Debye diffraction patterns. A circular integration leads to more usual (I-2 θ) diffraction data. These data are further analyzed using Fullprof software, so as to obtain phase types in the samples, their volume amounts and their lattice parameters.

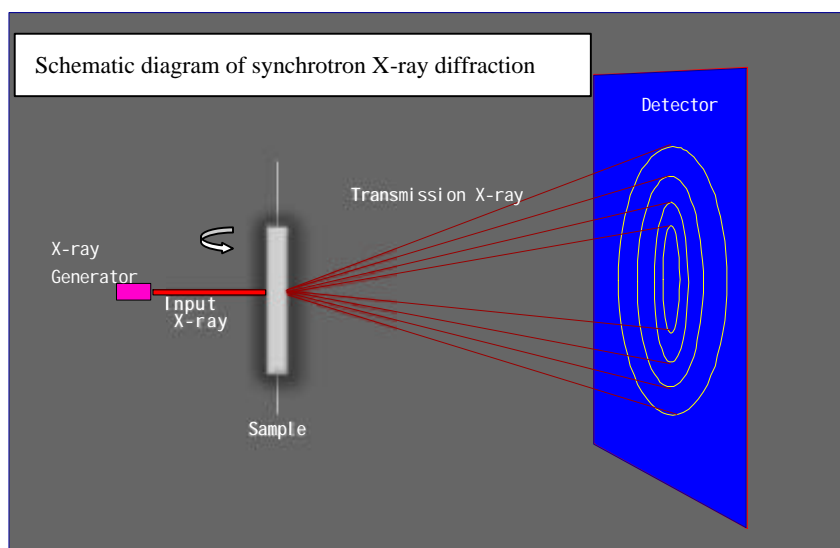


Figure 2-10 Schematic diagram of synchrotron X-ray diffraction

The samples analyzed are the ones for which the transformation kinetics were characterized by electrical resistivity measurements. Additional X-Ray characterizations were realized using laboratory SIEMENS X-Ray, and using the Cobalt anode ($\lambda = 1.78897 \text{ \AA}$), 35 kV, 20 mA. The diffraction peaks of the α and β phases were analyzed in a 2θ range of $[35^\circ, 110^\circ]$.

II.4.3. Other research methods

Microstructure observations for the samples have been performed with PHILIPS optical microscopes, PHILIPS XL30S-FEG scanning electronic microscope (SEM) and TECNAI G²20 transmission electronic microscope (TEM) (with a camera length of 1.73nm·mm). The sample preparation for SEM observations is the same as for the OM observations involving standard procedures. The TEM samples are thin foils, which are prepared by cutting to pieces with a thickness of 1mm from heating treated specimen and handle polished to about 0.1mm thickness and final thinning was performed by jet polishing at 223K in a solution of 99ml butyl alcohol, 186ml methyl alcohol and 15ml perchloric acid.

Hardness measurements were performed with Emco · TEST M4U025 with a load of 10g. Mechanical properties were realized with an INSTRON 5581 testing machine.

III. ISOTHERMAL PHASE TRANSFORMATION KINETICS AND MICROSTRUCTURE EVOLUTIONS OF TI-B19 ALLOY

Ti-B19 alloy is a metastable β titanium alloy, whose metastable β phase can be maintained at room temperature in air-cooled conditions after solid solution treatment. This metastable β phase will decompose into stable α phase or other metastable phases. Previous studies have demonstrated that the precipitation of α phase increase significantly the mechanical properties of Ti-B19 alloy^[88,97,98]. Thus, the aim of the study is to get the relationships between thermal treatments and microstructure in order to control the precipitation of α phase and adjust the microstructure to optimize the properties concerning strength and ductility. The microstructure of the alloy is characterized by different parameters: the nature of the phase, their amount, shape and distribution. These parameters are strongly dependant on the alloy phase transformation kinetics.

In this chapter, we report the study of the isothermal transformation kinetics using in-situ resistivity measurements. We recall that the initial microstructure is a beta metastable phase obtained after solution treatment in the beta phase temperature range and quenched to room temperature. The isothermal transformation temperatures are ranging from 300°C to 700°C and in all cases the heating rate to the holding temperature is 10°C/s.

III.1. Variations of electrical resistivity with time and further analysis method

III.1.1. Variation of electrical resistivity with time generally

Before analyzing the transformation kinetics during isothermal treatments, we present the variations of electrical resistivity measured on heating and further holding at constant temperature. As an example, the variations obtained during heating and the beginnings of the holding at 700°C are shown in Figure 3-1. A first decrease in electrical resistivity is observed during heating from room temperature to 400-450°C, followed by an increase in resistivity. During the holding at 700°C, the electrical resistivity is nearly constant for the time considered in Figure 3-1.

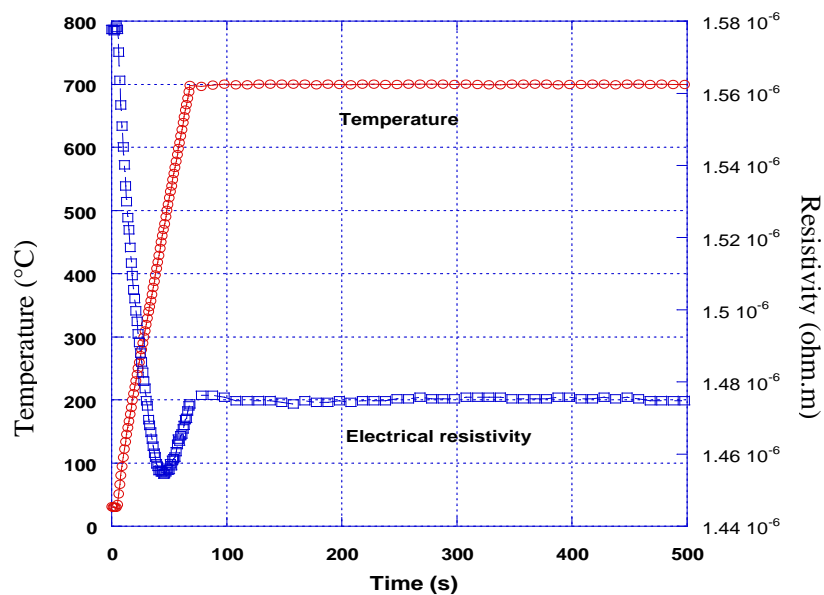


Figure 3-1 Variations of electrical resistivity and temperature versus time during heating to and holding at 700°C with 10°C/S heating rate

The electrical resistivity variations with time during heating is quite complex. From room temperature to nearly 400°C, a negative dependence of electrical resistivity with temperature is measured, commonly observed for different beta-metastable alloys^[80,82,95,99]. At higher temperature the electrical resistivity raises with the

increase of temperature.

In Figure 3-2 we compare the variations in electrical resistivity measured during rapid cooling from beta temperature range to the variations in electrical resistivity measured during heating up to 700°C. The variations on cooling present a first decrease as temperature decreases from 900°C to 500°C. At lower temperature the electrical resistivity increases. During cooling, no major transformation happens. Formation of an isothermal β' phase cannot be excluded. Thus these variations are considered as a base line for the resistivity behavior on cooling without transformation. The comparison of the variations on cooling and heating leads to similar evolution between 20°C and 200°C. At higher temperature, we do not have a clear superposition for the two evolutions, but the global evolutions are similar. It is difficult to establish a clear correspondence of the observed variations with structural changes in the alloy. Changes in the vacancies density can for example lead to differences in the resistivity variations. In the present case, as the resistivity on heating behaves nearly similarly to the previous one on cooling we consider that the precipitation is negligible for the considered heating rate of 10°C/s. The occurrence of precipitation during heating is further discussed in Chapter 4

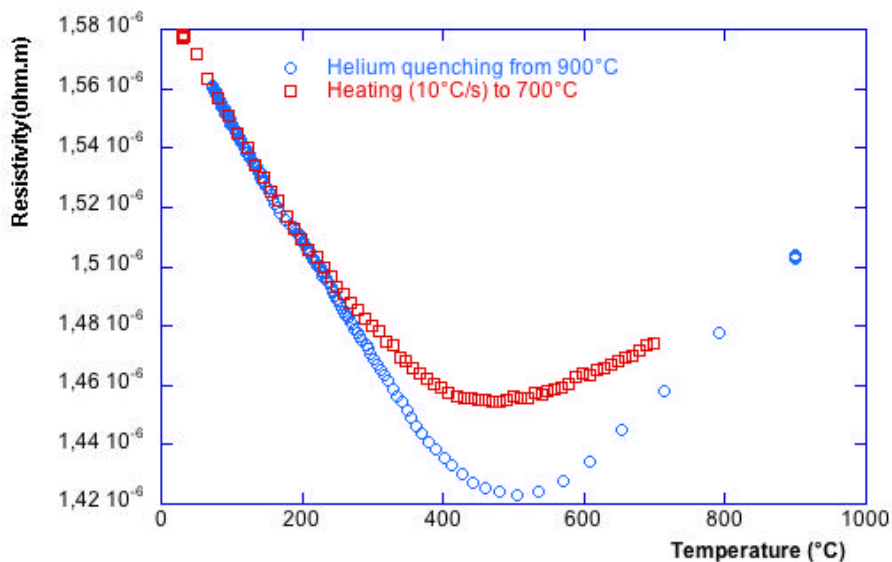
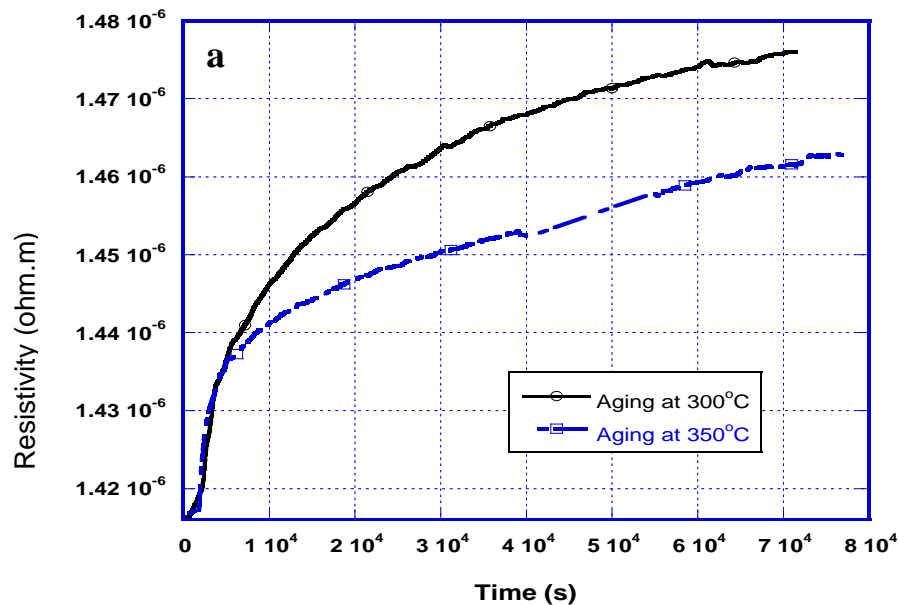


Figure 3-2 Variations in electrical resistivity measured on cooling from beta temperature range and on heating up to 700°C.

III.1.2. Variations of electrical resistivity with time during isothermal treatment

Figure 3-3 shows the variations of electrical resistivity versus time during aging treatment for different temperatures ranging from 300°C to 700°C. It can be found from the figure that:

- (1) For each temperature, the resistivity increases with the duration of the aging time until it reaches the maximum value and maintains constant (excepting 300°C and 350°C), which means that the phase transformation process is completed for the corresponding isothermal aging treatment condition.
- (2) For temperature varying from 650°C to 400°C, the curve has a nearly sigmoid shape. It can be divided into different stages. The first stage is the beginning of the phase transformation. When the isothermal treatment temperature is below 550°C, the resistivity increases slowly with time while above 550°C (including 550°C) the resistivity increases at a higher rate. The required time for finishing the beginning stage of phase transformation varies with the isothermal temperature, with a minimum of about 500s (500~550°C) and a maximum about 15000s (400°C).



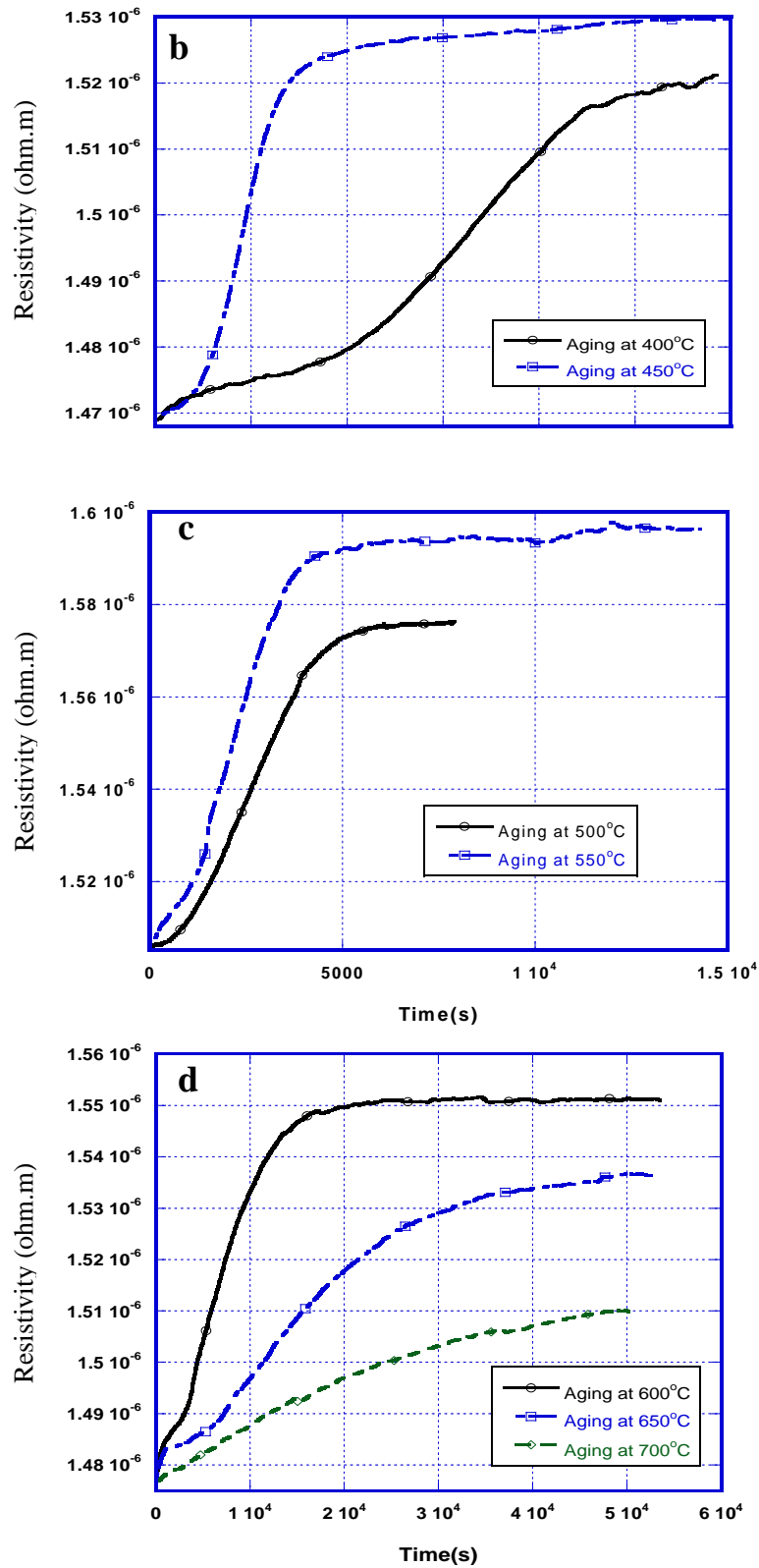


Figure 3-3 Variations of resistivity with time during aging at different temperatures: 300- 350°C(a), 400- 450°C(b), 500- 550°C(c), 600- 700°C(d), respectively.

In the second stage the electrical resistivity increases rapidly with time. The third stage is the ending stage of phase transformation during which the phase transformation is nearly finished and the trend that resistivity increases with time slows down and holds after reaching a maximum value. For the lower (300~350°C) and higher (650°C~700°C) temperatures, the variations of resistivity with time have more a parabolic shape.

- (3) The time required to reach the maximum value for the resistivity change is dependant on the temperature: the shortest time to reach the maximum is for 550°C; the duration of the transformation increases for transformation temperatures above 550°C as well as below 550°C.

III.1.3. Method to obtained phase transformation kinetics from in-situ resistivity variations

Resistance is a physical property of materials, which has close relation with the chemical elements and microstructure, etc. The variation trend of resistivity evolution with time corresponds to the phase transformation kinetics of the alloy during isothermal process. Previous results obtained for several titanium alloys by Laude, Bein, Malinov, Gautier and Bruneseaux^[83,100-102] for isothermal transformation on cooling from beta range indicated a linear relationship between the variation of resistivity (relative change of resistivity) and the relative amount of α phase. This was clearly established by Bruneseaux et al comparing in-situ electrical resistivity variations with amount of alpha phase obtained by in-situ high energy X-ray diffraction^[103]. A link can thus be established between the relative changes in electrical resistivity and the transformation kinetics. It is thus considered that the progress of the transformation during the isothermal process is proportional to the measured relative resistivity, and a higher increase of electrical resistivity corresponds to a higher amount of alpha phase.

The variations of electrical resistivity with time are further analyzed using the

method shown in Figure 3-4. The relative resistivity change (here R) is symbolized by $\Delta R_t / R_{\min}$, $\Delta R_t = R_t - R_{\min}$, and R_t stands for the resistivity measured during the isothermal aging treatment at time t ; R_{\min} stands for the sample's resistivity when reaching the isothermal transformation temperature, i.e., the minimum value of the resistivity curve at the beginning of the transformation; R_{\max} corresponds to the resistivity at the end of the phase transformation, i.e., the maximum value of resistivity on the variation curve with time. The maximal increase in electrical resistivity during isothermal aging treatment can be calculated by ΔR_{\max} , $\Delta R_{\max} = R_{\max} - R_{\min}$. The variations of $\Delta R_t / \Delta R_{\max}$ (corresponding to the variations of phase transformation progress with time) can be generated in this way, and these results can be used to describe the phase transformation kinetics of the alloy during the isothermal aging treatment.

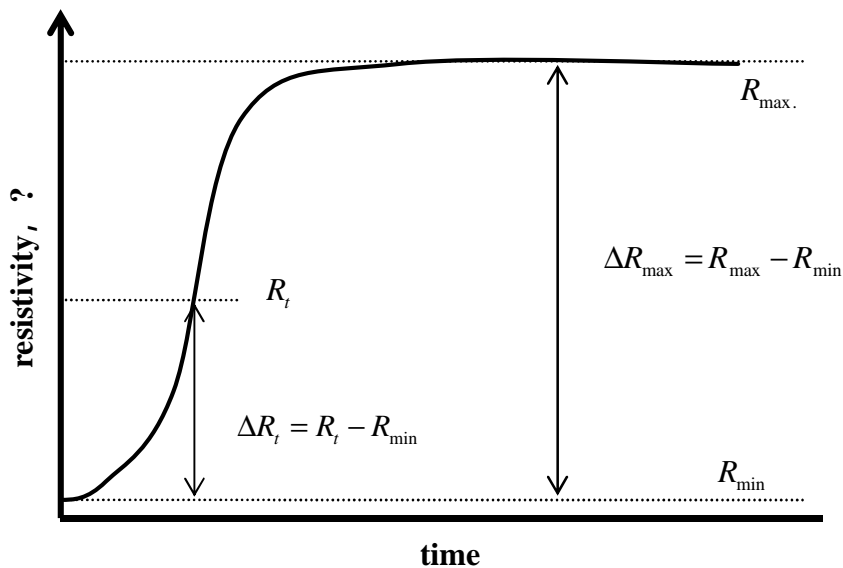


Figure 3-4 The analysis method for the resistivity curve.

In a second step, these variations can be further studied in order to describe the kinetics with the Johnson-Mehl-Avrami-Kolmogorov equation (JMAK equation in short). The JMAK equation is often used to link the phase transformation progress and the time for diffusive phase transformations controlled by nucleation and growth. It integrates the different mechanisms of the phase transformation and describes the

phase transformation process broadly in isothermal conditions. The equation has been widely applied for different isothermal phase transformation kinetics in different alloys. The equation can be written as follows ^[99~101]:

$$y = y_{\max} (1 - \exp(-Kt^n)) \quad (3-1)$$

In this equation, y stands for the transformation amount of the new phase at the time of t , y_{\max} is the maximal amount of phase formed at the given temperature, K stands for temperature constant which is related to nucleation and growth rates and is sensitive to temperature, and n is Avrami exponent which is used for describing the nucleation and growth mechanisms and has no relation with temperature to a large extent for a given transformation mechanism.

During the isothermal phase transformation of Ti-B19 alloy, the equilibrium amounts of α and β phases are dependent on the transformation temperature. To obtain the transformation progress, the JMAK equation can be rewritten as follows:

$$\frac{y(t)}{y_{\max}} = f = 1 - \exp(-Kt^n) \quad (3-2)$$

In this equation, $y(t)$ stands for the transformation amount of α phase at the isothermal time of t , is proportional to ΔR_t (Fig.3-4), y_{\max} is the equilibrium volume fraction of α phase at the transformation temperature, and is proportional to ΔR_{\max} in Figure 3-4. So the equation (3-2) can be rewritten as follows:

$$\frac{\Delta R_t}{\Delta R_{\max}} = \frac{R_t - R_{\min}}{R_{\max} - R_{\min}} = f = 1 - \exp(-Kt^n) \quad (3-3)$$

After transposition, the equation (3-3) can be written as follows:

$$1 - f = \exp(-Kt^n) \quad (3-4)$$

After calculating the logarithm \ln , the equation can be written as follows:

$$\ln\left(\ln\left(\frac{1}{1-f}\right)\right) = \ln(K) + n \ln(t) \quad (3-5)$$

From equation (3-5), it can be seen that if we draw a diagram for $\ln\left(\ln\left(\frac{1}{1-f}\right)\right)$ and $\ln(t)$, there would be a linear relation between them and the slope of the straight line is n and the intercept is $\ln(K)$, so the Avrami exponent n and temperature constant K can be obtained.

In addition, considering a same transformation mechanism in a given temperature range, the relationship between temperature constant K and temperature in equation (3-1) can be demonstrated by ^[101]

$$K = K_0 \exp\left(-\frac{E}{RT}\right) \quad (3-6)$$

In this equation, K_0 is the frequency constant; E is the phase transformation activation energy value whose unit is Joule; T is the temperature of phase transformation whose unit is K; R is the perfect air constant. After calculating the logarithm \ln for both sides, the equation is as follows:

$$\ln K = \ln K_0 - \frac{E}{RT} \quad (3-7)$$

Thus, if we draw a diagram for $\ln(K) - 1/T$, we would have a linear evolution with a slope equal to $-E/R$, so that the phase transformation activation energy E during the process of isothermal phase transformation can be obtained as 417.4 KJ/mol.

III.2. Isothermal phase transformation kinetics

Using the method presented in the above section, we obtain the phase transformation kinetics curve of Ti-B19 alloy for each temperature (Figure 3-5). The X axes

coordinate in the figure is time and the Y axes coordinate is the degree of phase transformation (or transformation progress) that varies from 0 to 1, and is given by:

$$f = \frac{R_t - R_{\min}}{R_{\max} - R_{\min}} \quad (3-8)$$

In all cases, we have assumed that the transformation kinetics is completed.

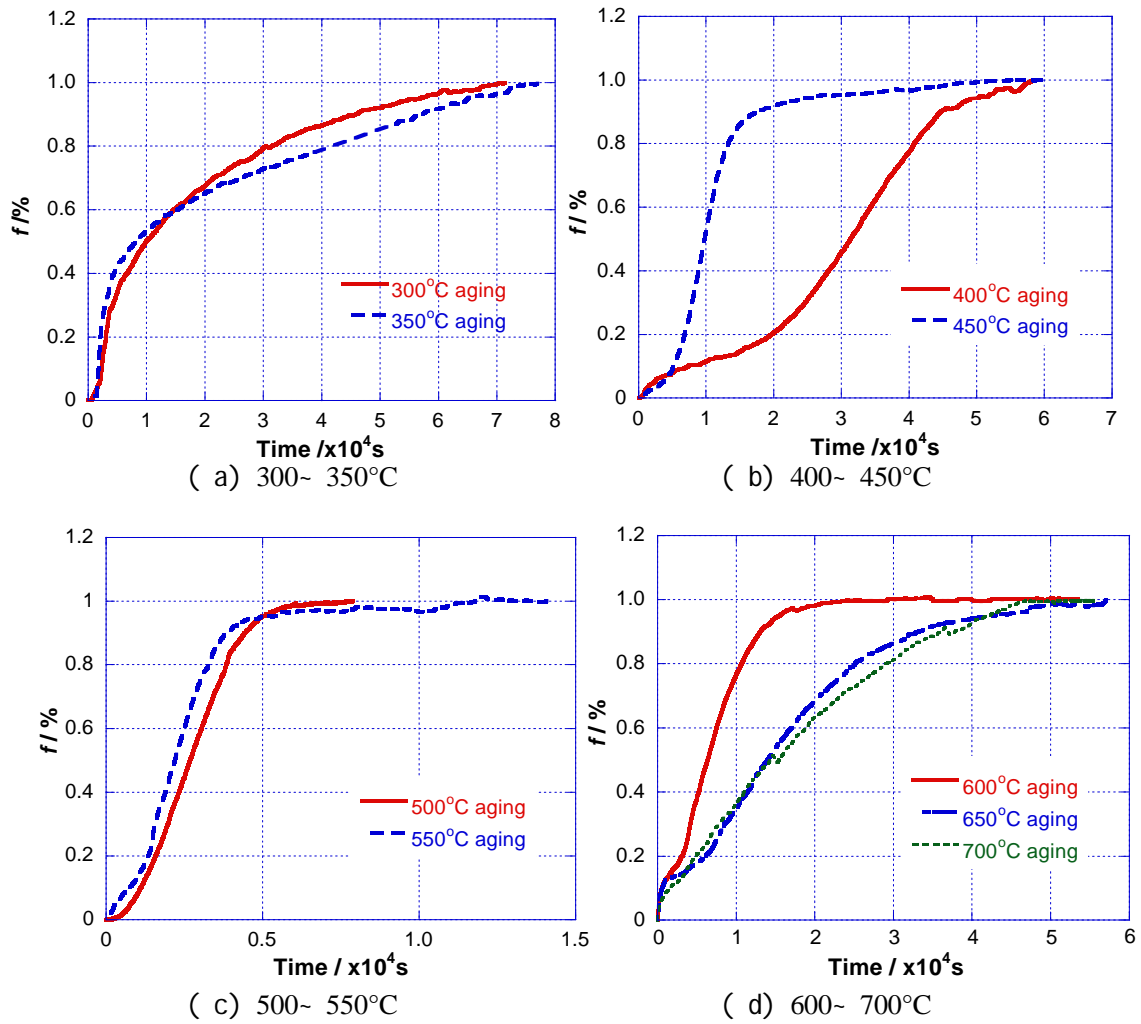


Figure 3-5 The phase transformation kinetics curves for Ti-B19 alloy isothermal treated at

300~ 350°C(a), 400~ 450°C(b), 500~ 550°C(c) and 600~ 700°C(d) respectively

It can be seen that temperature affects significantly the phase transformation kinetics of Ti-B19 alloy. These have the same shape as the resistivity variations with time, but they reflect more exactly the relationship between the isothermal time and the degree of phase transformation. For the lower temperature, the kinetics presents a parabolic shape (Figure 3-5a). The transformation rate is low at the beginning stage (first stage); the incubation time is about 500s at 300°C and 1500s at 350°C. Thereafter, the phase transformation comes to a stable stage (the second stage) and the transformation rate increases obviously. 30~40% of the transformation is reached within 3000~4000s. Then, at the end of the phase transformation (the third stage), the phase transformation rate reduces from 60~70% to the end of the recording (about 19 hours (68400s)).

In the temperature range 400~ 700°C, the kinetics presents a sigmoid shape, but show different features that can be divided into three types according to different aging temperatures. The first type corresponds 400~450°C isothermal transformation (Figure 3-5b). For those temperatures, we have a beginning stage (the first stage), with a quite low transformation rate. The duration of this stage increases when the temperature reduces, about 15000s at 400°C and 500s at 450°C. This stage corresponds to about 5~ 10% of the phase transformation progress. In the second stage, the phase transformation rate increases until 90% of the phase transformation finished. The time required to finish the transformation varies with the aging temperature. At 400°C, the time needed is about 30000s, and at 450°C, the time is about 10000s. In other words, in the second stage, the rate of phase transformation progress at 450°C is three times higher than that at 400°C. The time need for 100% of phase transformation at 400°C and 450°C is 58000s and 53000s respectively.

The second type is 500~ 550°C isothermal transformation (Figure 3-5c). This type is characterized by a high transformation rate. The beginning stage (the first stage) is short (about 500s), as well as the transformation duration. 90% of the phase transformation is finished in only 4000s, and 100% of the phase transformations

finished in about 6000s and 8000s at 500°C and 550°C respectively.

At aging temperature ranging from 600 to 700°C (Figure 3-5d), the phase transformation rate in the first stage is also high. Over 10% of the transformation occurs within 1500~ 2000s. Then the transformation rate reduces gradually and comes to a stable status (the second stage). 90% of the transformation is finished in 15000~ 37000s, and the time needed for finishing 100% of the phase transformation varies with temperature: the time is about 26000s at the temperature of 600°C and 47000s at the temperatures of 650°C and 700°C.

From the transformation kinetics presented in Figure 3-5, we can use equation (3-3)~(3-5) to obtain the relationship between $\ln(\ln(1/(1-f)))$ and $\ln(t)$. The results are shown in Figure 3-6. The obtained diagrams show that a near linear relation is observed during the second stage of the isothermal phase transformation, i.e. between 10% and 90% of transformation progress, and that the slope is changing for some transformation temperatures. The values of n and K in JMAK equation have been determined in each temperature and are given in Table 3-1.

From the results we can define several groups of temperature for which we obtain same values of n .

- At 300°C and 350°C, the value of n is lower to 1 (0.76 and 0.49 respectively)
- At 400°C and 450°C, the value of n is near 3 (3.08 and 3.1 respectively)
- At 500°C and 550°C, n values are near 2, respectively 2.17 and 2.04
- At 600°C, n is equal to 1.8, this is between the values obtained at 500°C and at higher temperatures
- Above 600°C, n is more near 1 (1.1 for 700°C and 1.3 for 650°C)

The differences in n values can be attributed to differences in the phase transformation mechanisms involved, depending on the transformation temperature.

Different values of n are reported in the literature. For Ti-6Al-4V and Ti-6Al-2Sn-4Zr-2Mo-0.08Si, Malinov et al.^[85] obtained n value equal to 1.15 for higher temperatures (900~930°C); for this given case, the value corresponds to grain boundary α phase and colonies of α -plates nucleated and grown from the grain boundary. For lower temperatures 750~850°C, n value is increased (1.48) and was corresponding to colonies of α -plates nucleated and grown from the grain boundary and to α phase nucleation within the parent beta grain. A similar study conducted on β 21s alloy^[99], lead to an n value of about 1.8 at isothermal temperature 650~750°C. At last, in the study of Da Costa Teixeira^[95] for Ti-17 alloy, the reported n value is of 1.3 for the formation of alpha colonies ($T > 700^\circ\text{C}$) and an n value is of 1.6 for the formation of alpha on intragranular sites. The values that we obtained in the temperature range between 700°C and 600°C are consistent with the previous results.

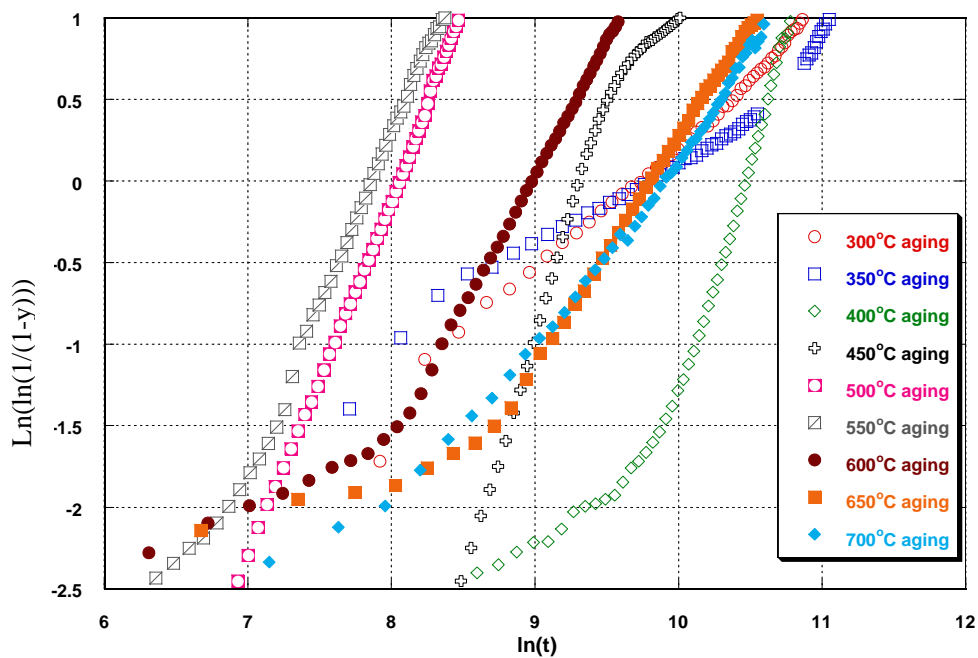


Figure 3-6 Plot of $\ln(\ln(1/(1-f))) - \ln(t)$ for the aging treatment at different temperature for Ti-B19 alloy.

Table 3-1 The n and K values of JMA equation for Ti-B19 alloy during aging treatment.

T/°C	300	350	400	450	500	550	600	650	700
n	0.76	0.49	3.08	3.1	2.17	2.04	1.8	1.3	1.1
K	6.23	8.31	1.02	3.1	2.78	1.13	1.13	2.05	1.85
	$\times 10^{-4}$	$\times 10^{-3}$	$\times 10^{-14}$	$\times 10^{-13}$	$\times 10^{-8}$	$\times 10^{-7}$	$\times 10^{-7}$	$\times 10^{-6}$	$\times 10^{-5}$

III.3. Microstructure observations

III.3.1. Initial state

The microstructure obtained after 900°C/10min solution treatment and quenching to room temperature at the cooling rate of 20°C/s is shown in Figure 3-7. The OM observations as well as the SEM ones reveal beta grains, which mean size is about 100µm, with clean intragranular structure and clear grain boundaries.

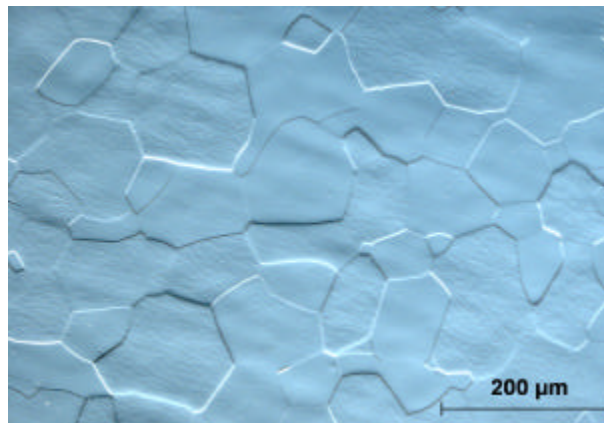


Figure 3-7 The microstructure (OM) of Ti-B19 alloy after 900°C/10min solution treatment and quenched with a cooling rate of 20°C/s

The XRD pattern obtained (Figure 3-8) reveals only the presence of beta phase, which implies that the alloy is in a full beta metastable state. No TEM observations

were made on this state that could reveal a possible precipitation of athermal ω phase. This beta phase is a supersaturated solid solution in which transformation is able to proceed in the isothermal aging process.

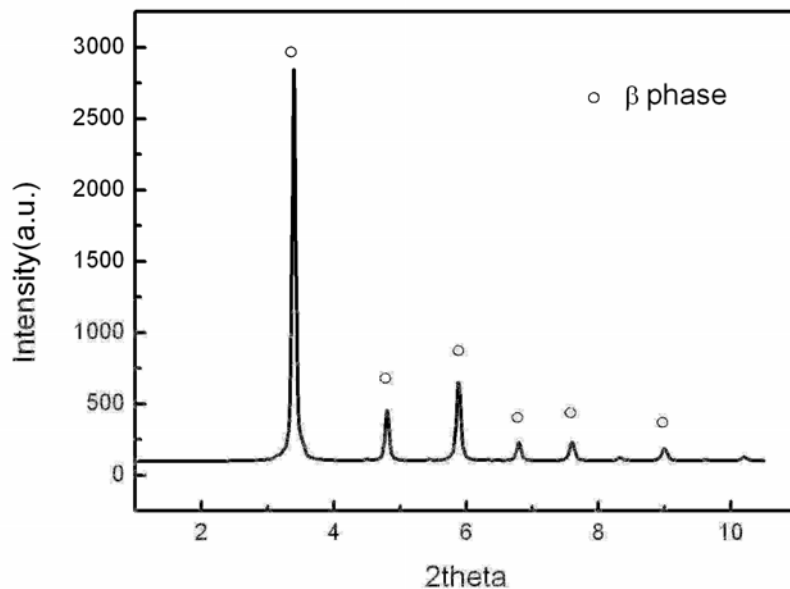


Figure 3-8 XRD pattern for specimen after 900°C/10min solution treatment and quenched at 1°C/s

III.3.2. Structure and microstructure evolutions for aging at 300~ 350°C

Figure 3-9 and Figure 3-10 show respectively OM images and synchrotron XRD diffraction pattern after isothermal aging 20h at 300°C and 350°C. At the OM scale, and compared with the microstructure after solution treatment (Fig.3-7), no obvious change is observed for the microstructure of Ti-B19 alloy after aging at 300°C for 20h (Figure 3-9a). However, the XRD analysis (Figure 3-10) shows that metastable ω phase has been formed in the alloy. In order to observe the microstructure changes, TEM observation have been realized, Figure 3-11 shows a TEM dark field image and diffraction pattern of Ti-B19 alloy after aging for 20h at 300°C, the size of precipitates is a few nanometers appears uniformly distributed in the parent phase. The electron diffraction pattern confirms that the structure of the precipitates is the hexagonal one of ω phase.

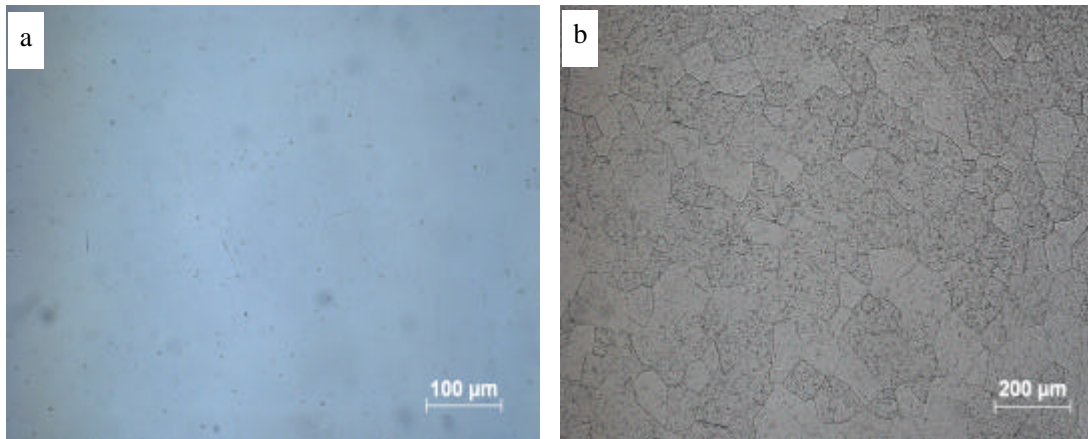


Figure 3-9 OM images of Ti-B19 alloy after isothermal aging 20h at 300°C(a) and 350°C(b).

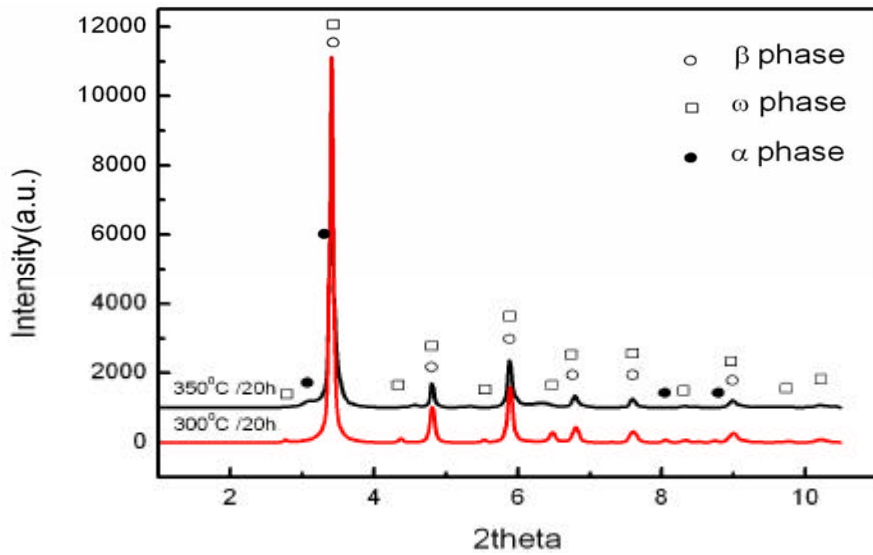


Figure 3-10 Synchrotron XRD patterns after isothermal aging 20h at 300°C and 350°C.

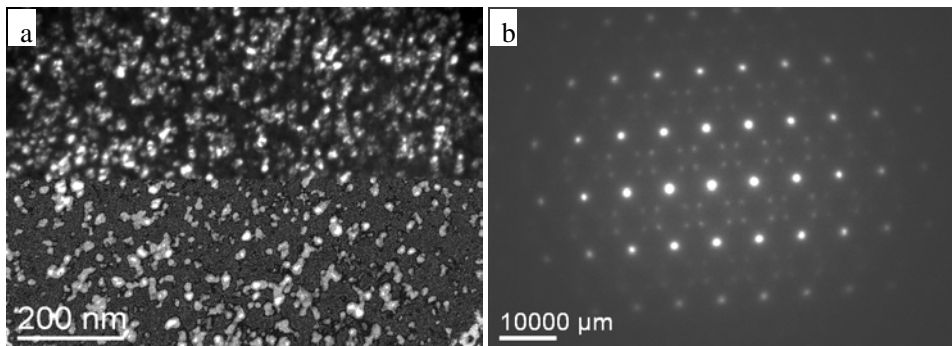


Figure 3-11 TEM dark field image (a) and diffraction pattern (b) after aging 20h at 300°C.

The quantitative analysis of the XR diffraction pattern leads to a mixture with 27 vol.% of ω phase and 73 vol.% of β phase after 20h aging at 300°C. Crystal lattice parameters of ω phase in Ti-B19 alloy after treated at this condition are as follows: $a = b = 4.689\text{\AA}$, $c = 2.879\text{\AA}$, $c/a = 0.614$. At last, through scaling the diffraction pattern shown in Fig.3-11b, the orientation relationships between ω phase and beta phase can be gained as following:

$$[110]_b // [2\bar{1}\bar{1}0]_v, [1\bar{1}0]_b // [0\bar{1}1\bar{1}]_v$$

We can thus consider that at this aging temperature, that transformation involved is the decomposition of β (or $\beta + ?_{iso}$) into $\beta + ?_{iso}$.

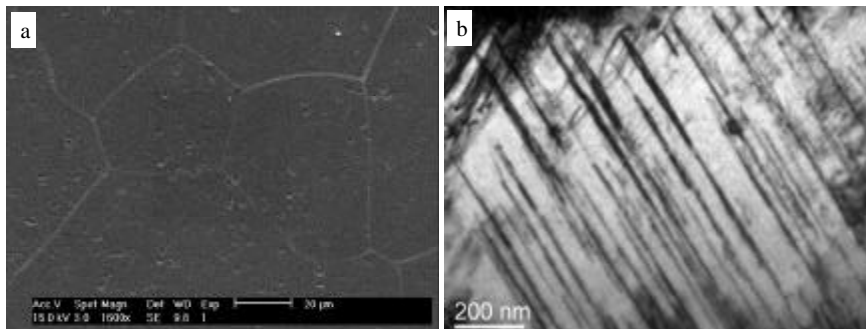


Figure 3-12 SEM (a) and TEM (b) images after aging treated at 350°C for 20h.

Considering aging at 350°C, OM observations in Figure 3-9 shows differences between the microstructure after 20h aging at 300°C and 20h aging at 350°C. The synchrotron XRD analysis results shown in Figure 3-10 leads to three present phases: ω , α and β with the following content in volume percent 5%, 14% and 81% respectively. Compared with aging at 300°C, the quantity of ω phase is considerably decreased but α phase is present. Figure 3-12 provides additional SEM and TEM micrographs. The β grain boundaries are rather distinct, and fine acicular α phase is uniformly formed within β intragranular grains. It is thought through the analysis here above that the decomposition mode of metastable β phase of Ti-B19 alloy at 350°C is $\beta \rightarrow \alpha + \omega + \beta \rightarrow \alpha + \beta$.

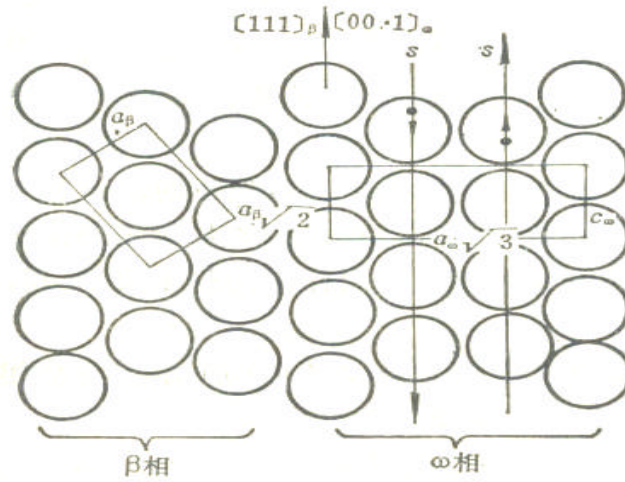


Figure 3-13 Schematic diagram of the atom movement by shear lattice deformation in $(111)_\beta$ plane during $\beta \rightarrow \omega$ transformation.

In metastable β titanium alloys with more β stabilizer elements, β phase does not directly transform into stable α phase at low aging temperatures, but transforms through an intermediate transition process, with namely the formation of γ [1,2]. This is confirmed in the present results. It is usually considered that γ phase in titanium alloys includes the γ phase formed during quenching and that formed during isothermal aging. For the nucleation mechanism of the quenched γ phase, most people agree with the dislocation mechanism^[27]. However, the research on nucleation mechanism of isothermal γ phase is not so sufficient to research agreements^[27,35,48]. The isothermal γ phase has a hexagonal structure. It is generally thought that γ nucleation in the isothermal process is non-diffusive; i.e. the hexagonal structure is formed from the body-centered structure by a shear lattice deformation mode. Figure 3-13 schematizes the atom movement in $(110)_\beta$ plane β phase is transformed into ω . Its growth process is considered as controlled by the diffusion of solute atoms.

The kinetics obtained at 300°C, and even at 350°C, corresponds thus to that of γ

phase formation (Fig.3-5a). The transformation rate is quite low at the beginning stage (the first stage). The incubation period is about 500s at 300°C and 1500s at 350°C. Thereafter, transformation rate increases obviously until 3000~4000s aging. At the end of the experiment, the transformation rate reduces. Accordingly, it can be considered that after the incubation period, the transformation rate of $\beta \rightarrow \alpha + \beta$ is mainly controlled by the homogeneous nucleation rate of β . When the nucleation sites are nearly full, the phase transformation rate reduces and tends to be controlled mainly by the growth rate of the new phase. The global β transformation kinetics for isothermal aging at 300°C is a parabola, which is a typical uniform nucleation phase transformation kinetics curve^[27]. That is to say, in our test conditions, the β nucleation process is uniform, i.e. precipitates are distributed in a uniform dispersed way in the β matrix that is consistent with TEM observations (Fig.3-11a). Fig.3-14 recalls the logarithmic relationship of β phase transformation extent with time for aging at 300°C. In the transformation conditions, and considering that the transformation is completed, the kinetics considering $\ln(\ln(1-(1-f)))$ against $\ln(t)$ present a linear variation with a single slope. That means the β phase transformation mechanism is unique for the given alloy and the given transformation conditions (isothermal process at 300°C), without a main variation of the phase transformation mechanism; the Avrami index is equal to 0.67. For the present test, the aging time was 20 hours. Luo Yuanyuan^[104] has realized aging treatments for the same alloy, but longer aging times. Her results suggest that β has been formed after 10h aging at 300°C, and when the aging time is extended to 50h, β phase quantity is increased and α phase appears. For aging time extended to 100h, a quite high quantity of β is transformed into α . For the experiment and test conditions reported here, the precipitation of β occurs at earlier aging times. However, it can be noticed that the resistivity curve does not show a clear end of transformation. It may be possible that the transformation is not completed after 20h aging as suggested by Luo Yuanyuan results. Thus the n value could change considering a final ending time for the

transformation. Additional experiments should be realized in order to characterize the amount, density and size of the precipitates at different transformation time in order to precise the transformation mechanisms.

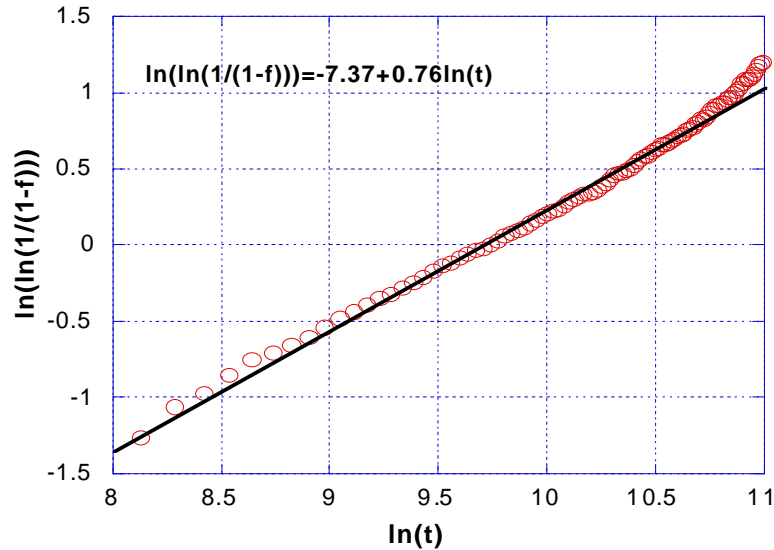


Figure 3-14 Plot of $\ln(\ln(1/(1-f)))$ versus $\ln(t)$ for isothermal aging at 300°C

The literature reports that the β phase is not a stable phase and will finally turn into stable α ^[27]. In our aging conditions (300°C, 20h) the microstructure at room temperature is still β plus α . However, according to Luo Yuanyuan's results, we can consider that the decomposition mode of metastable β phase of Ti-B19 alloy in the isothermal aging process at 300°C is $\beta \rightarrow \omega + \beta \rightarrow \omega + \alpha + \beta \rightarrow \alpha + \beta$.

Therefore, we can consider that in low aging temperature, the beta metastable phase of Ti-B19 alloy transforms into $\omega + \beta$ or $\omega + \alpha + \beta$. Particle shape precipitates, which size is a few nanometers, are formed. They are rather difficult to identify under OM, only TEM can provide a clear observation. These ω precipitates are uniformly distributed in the β matrix; the α precipitates have a fine acicular shape and are rather dispersed within the β grain.

III.3.3. Structure and microstructure evolutions for aging at 400~ 450°C

The XRD patterns obtained for specimens aged at 400 and 450°C are given Figure 3-15. The microstructures observed by OM and SEM are shown in Figure 3-16. For these temperatures, the XRD patterns reveal that the presence of two phases identified as α and β . The α phase volume fraction is dependant on the aging temperature; the amount is 51% at 400°C and 57% at 450°C. These values are considerably increased

Table 3-2 Cell parameters measured by XRD at aging temperature of 400°C and 450°C.

Aging temperature	Parameters of α phase(nm)		Parameters of β phase(nm)
	a_α	c_α	a_β
400°C	0.3010	0.4729	0.3291
450°C	0.3006	0.4762	0.3279

in comparison with that obtained after isothermal aging at 350°C. The cell parameters of α and β phase in these aging temperatures were determined from XRD patterns and are given in Table 3-2.

The microstructure of the α phase formed at 400°C appears in fine acicular shapes and is distributed within β grains; the β grain boundary does not present large transformation amounts. However, when aged at 450°C, α phase appears with an obvious acicular morphology; meanwhile, the dimensions are also greatly changed, mainly by an increase in the length direction (about 6~10 μ m) but no considerable changes are noticed for the precipitates width. This acicular α precipitates cross the grain and some of them are tightly arranged in certain directions to form “tire” patterns; meanwhile, the α acicular elements appears in an angle of 60°.

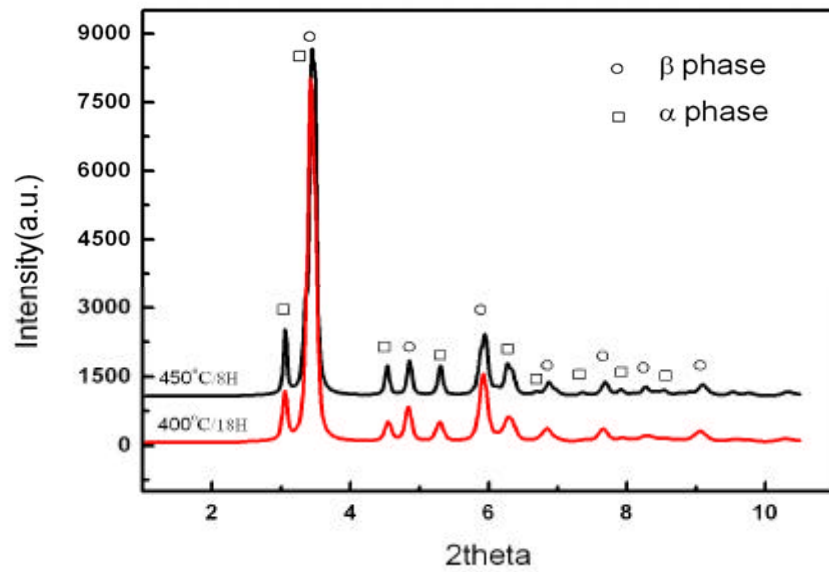


Figure 3-15 The synchrotron XRD patterns for Ti-B19 alloy after isothermal aging at 400°C/18h and 450°C/8h respectively.

To understand the arrangement and nucleation and growth processes of α phase during the transformation progress, microstructure observations have been done for samples quenched at different aging time at 400°C according to the variations of phase transformation kinetics.

Figure 3-17 provides the phase transformation kinetics for aging at 400°C, and Figure 3-18 shows the microstructure characteristics observed for specimens after 11000s and 21000s aging; wherein, 11000s correspond to Point A of the first stage in kinetics curve; 21000s correspond to a point shortly after start of the second stage of the kinetics (Point B).

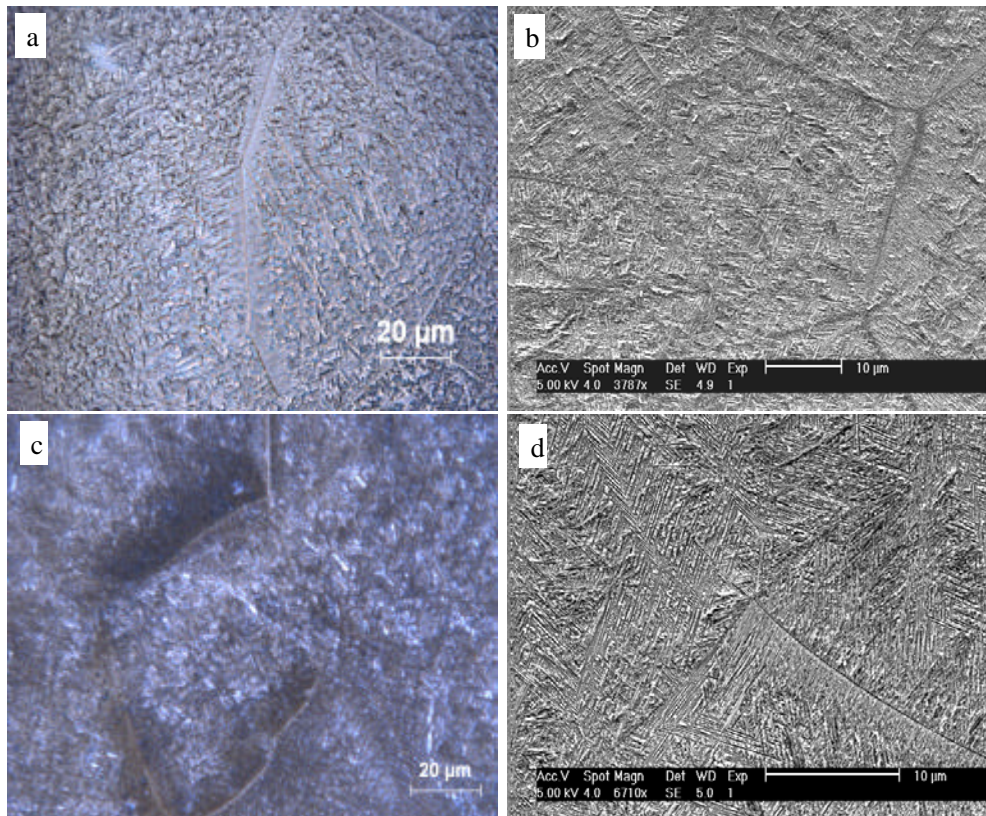


Figure 3-16 micrographs of Ti-B19 alloy after isothermal aging at 400°C(18h) and 450°C(8h).

(a) OM-400°C/18h, (b) SEM-400°C/18h, (c) OM-450°C/8h, (d) SEM-450°C/8h

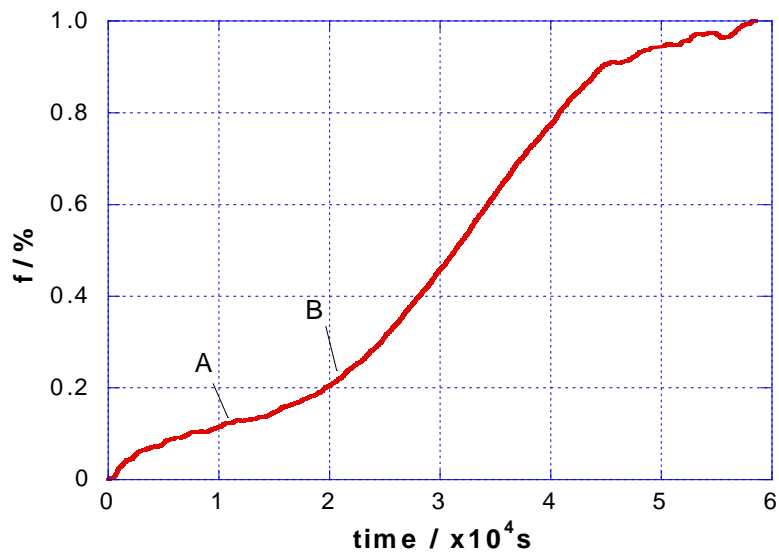
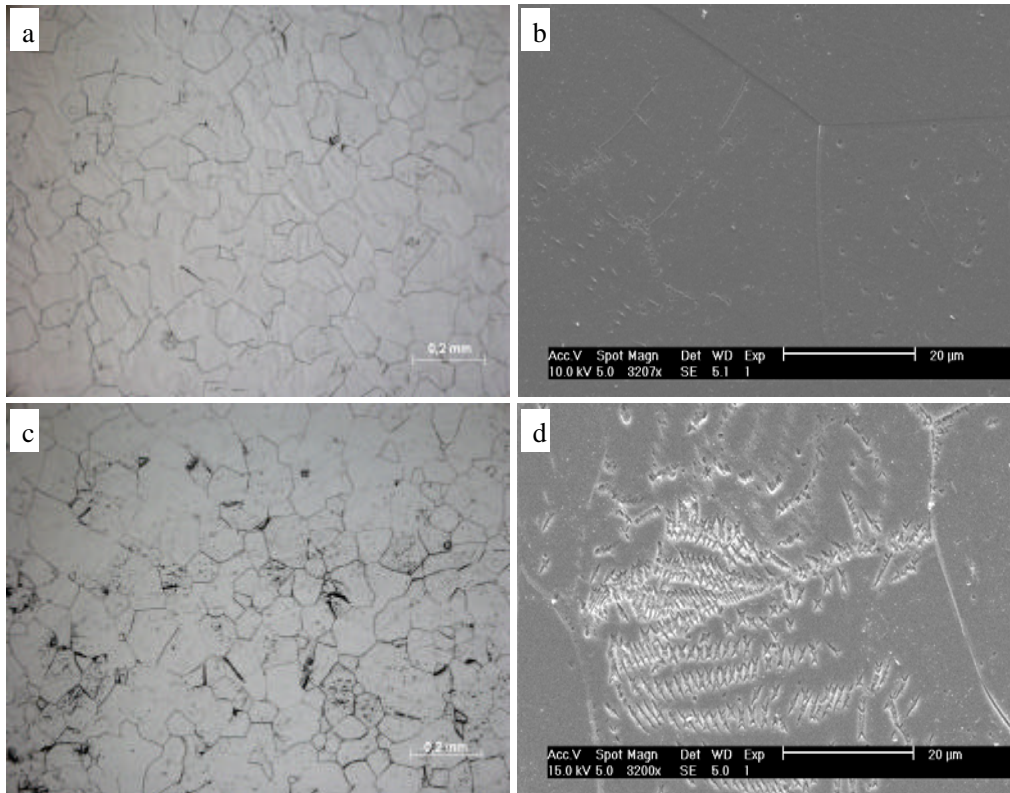


Figure 3-17 Transformation kinetics for isothermal aging treatment at 400°C.



(a) OM-11000s, (b) SEM-11000s, (c) OM-21000s, (d) SEM-21000s

Figure 3-18 Micrographs of Ti-B19 alloy isothermal aged at 400°C for different times.

After 11000s at 400°C, a small amount of precipitation is observed. Some β grain boundaries are more contrasted and intragranular α phase is clearly observed with a non-uniform distribution. The α phase is fine acicular shape.

Increasing the aging time, additional nucleation of α starts at β grain boundaries; meanwhile, intragranular α phase amount increases by growth and further nucleation, and transformation area is gradually extended towards the grain boundaries. The nucleation and growth modes for α might be maintained until the phase transformation progress reaches a rather high value (over 80%) according to the kinetics of Figure 3-17; at the longer aging time, the phase transformation should mainly include α phase growth.

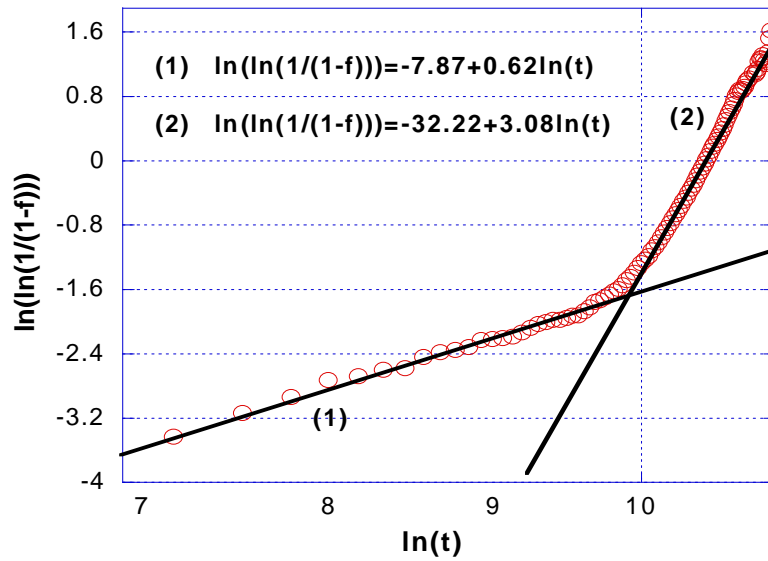


Figure 3-19 Plot of $\ln(\ln(1/(1-f))) - \ln(t)$ of Ti-B19 alloy during the isothermal aging at 400°C.

Figure 3-19 shows the logarithmic relationship between phase transformation progress against time in the isothermal phase transformation process at this temperature, which is the $\ln(\ln(1/(1-f)))$ versus $\ln(t)$ plot. Two straight lines with different slopes can describe the obtained evolutions. One could thus consider that the phase transformations for the Ti-B19 alloy present two regimes in the isothermal aging process at 400°C. The slope of the first straight line, which Avrami index is $n = 0.62$ in the JMAK function, corresponds to the stage from the beginning to the transformation progress of around 20%, and the time is about 18000s; the slope of the second straight line, which Avrami index is $n = 3.08$ in the JMAK function, corresponds to the remaining 80% phase transformation process, and the time is about 40000s.

It is thought that for the first straight line in Figure 3-19, phase transformation occurs mainly by nucleation and growth of the intragranular acicular α , and α nucleates on the dislocation lines; the second straight line in Figure 3-17 corresponds to the second and third stages in the phase transformation process, and the phenomena involved, include the nucleation and growth of intragranular α phase as well as

precipitation of boundary α phase.

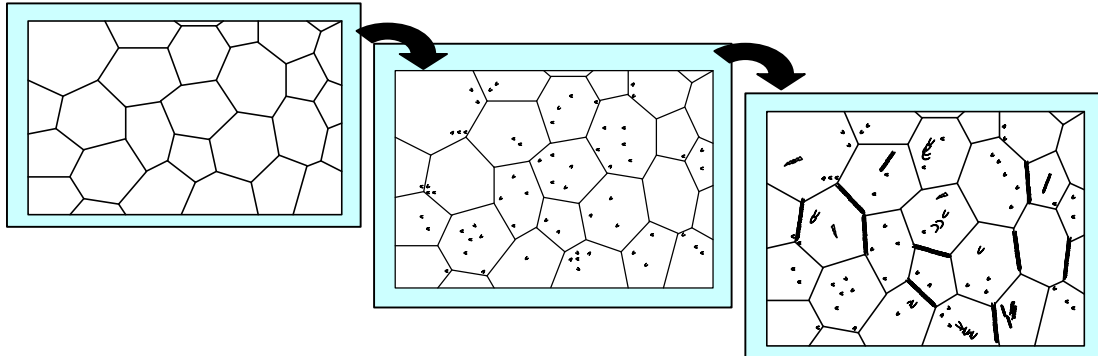


Figure 3-20 The isothermal microstructure evolutions of Ti-B19 alloy at 400~ 450°C.

The α phase nucleation rate is decreased with increasing the aging time, and the diffusion controlled growth of acicular α phase plays an important role in the phase transformation process at this temperature aging. According to the above analysis, the decomposition sequence of the metastable β phase in Ti-B19 alloy is $b \rightarrow a + b$ when aged at the temperature range of 400~450°C. The schematized microstructure evolutions are shown in Figure 3-20.

III.3.4. Structure and microstructure evolutions for aging at 500 ~ 550°C

The transformation kinetics gained from electrical resistivity measurements evidenced a third type at 500~550°C (Figure 3-3c) characterized by rapid phase evolution. Figure 3-21 provides the synchrotron XRD patterns after aging for 4h at 500°C and 550°C, Figure 3-22 shows the microstructures observed in the above-mentioned test conditions. For these two aging temperatures and 4h after aging, the microstructure of Ti-B19 alloy is composed of α and β phase has been proven by the XRD pattern.

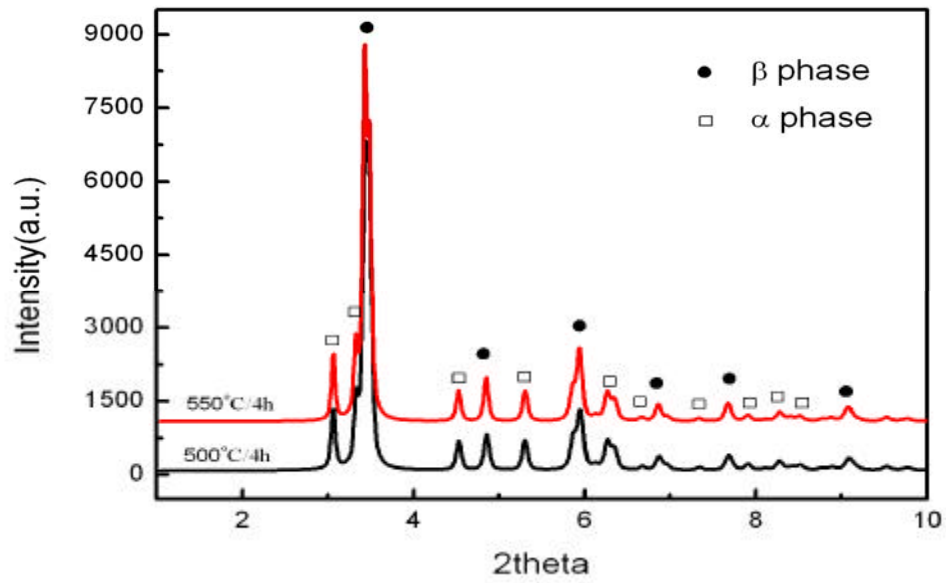
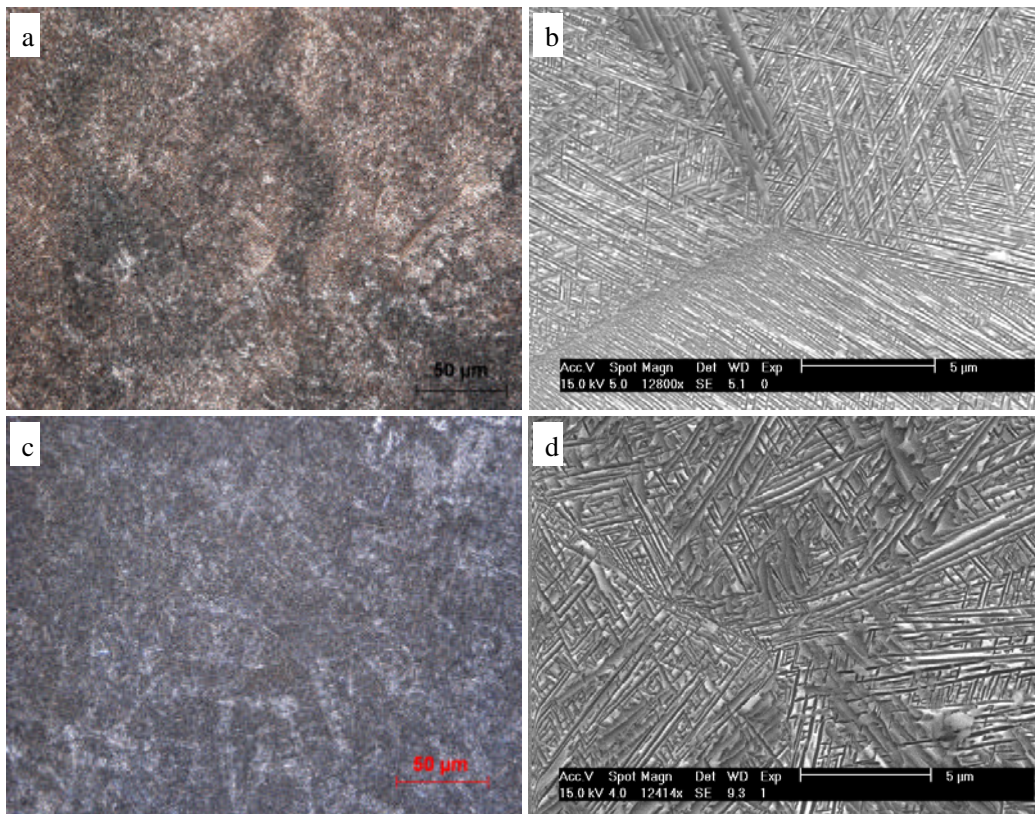


Figure 3-21 Synchrotron XRD patterns after isothermal aging treated at 500°C and 550°C.



(a) OM-500°C, (b) SEM-500°C, (c) OM-550°C, (d) SEM-550°C

Figure 3-22 Microstructure after 4h isothermal aging treated at 500°C and 550°C.

The quantitative analysis of the patterns leads to a volume fraction of the α phase equal to 58% at 500°C and 55% at 550°C. The cell parameters at room temperature for each phase are given in Table 3-3.

Table 3-3 Cell parameters obtained by XRD at aging temperature of 500°C and 550°C

Aging temperature	Parameters of a phase(nm)		Parameters of b phase(nm)
	a_{α}	c_{α}	a_{β}
500°C	0.3003	0.4775	0.3279
550°C	0.3002	0.4783	0.3284

The cell parameters of the α phase formed at 500°C and 550°C are slightly different. When increasing the aging temperature, the a value is decreased while c is increased. Considering the morphology of the α phase, its shape is acicular and α is distributed in crossed shape within the β grain and arranged in parallel way or in crossed way at the grain boundaries. Compared with aging at 500°C/4h, α phase formed after aging at 550°C/4h has a slightly larger width.

The above observation and results suggest that α phase transformation mechanisms of Ti-B19 alloy at 500~550°C are somewhat different from those in isothermal aging at 400~450°C. Therefore, additional experiments have been performed at the same aging temperature (500°C), but samples have been quenched after 1000s and 2000s aging respectively. Figure 3-23 recalls the phase transformation kinetics curve of Ti-B19 alloy for isothermal aging temperature of 500°C. Figure 3-24 shows the microstructure observation after 1000s aging (Point A in Figure 3-23) and 2000s aging (Point B in Figure 3-23).

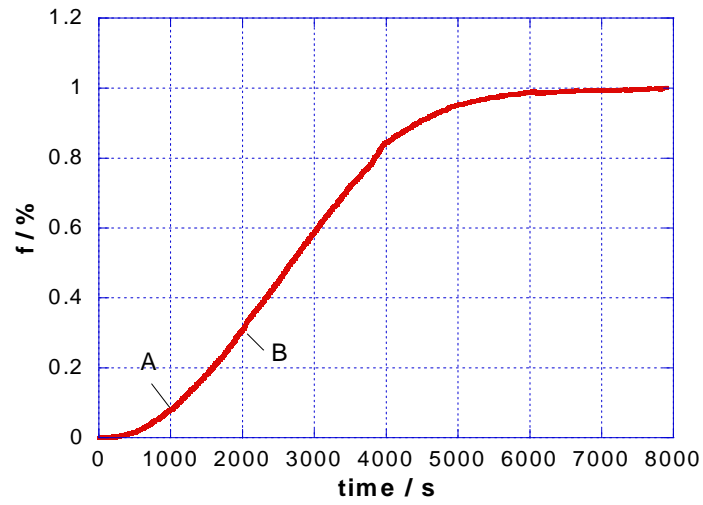
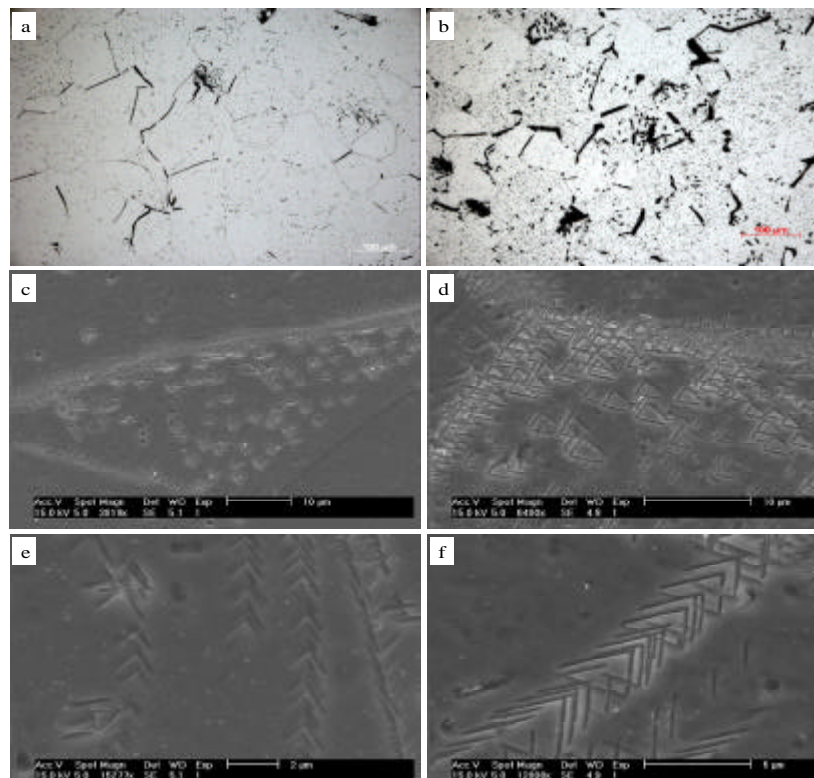


Figure 3-23 Phase transformation kinetics for isothermal aging at 500°C.



(a) OM-1000s, (b) OM-2000s, (c) and (e) SEM-1000s, (d) and (f) SEM-2000s

Figure 3-24 Microstructure after isothermal aging at 500°C for 1000s and 2000s respectively.

After 1000s aging at 500°C, the α phase is present, but in limited amount. The different micrographs show that nucleation occurs at grain boundaries as well as within the parent β grains without any difference in the sequence. For the optical micrographs (Figure 3-24a and b), α phase appears in rather dispersed “dotted formation” in the β grain, while it is a more “linear formation” at grain boundaries. Further SEM observations (Figure 3-24c~f) suggest that these intragranular α precipitates in dotted formations are composed of quite fine “short acicular precipitates” forming an angle of 60°. The morphology of α precipitates that grew from grain boundaries phase is acicular and parallel distributed.

In some β grain, the “V-shape” morphology of the α phase with the angle of 60° shows nucleation along a certain “line track”, and this might be related to α phase nucleation along dislocation lines. After 1000s the mounts of acicular α precipitates is limited, and mean length is about 1 μ m. After 2000s aging, the amount of acicular α phase is increased, and the mean length is increased to about 5 μ m; the arrangement of acicular α is still observed. Moreover, the precipitates are observed along a third direction as can be evidenced at the higher magnification, and the amount of β grain boundaries with the presence of the α phase is increased as seen on Figure 3-24c and 3-24d.

Figure 3-25 recalls the $\ln(\ln(1/(1-f))) - \ln(t)$ plot of Ti-B19 alloy for isothermal aging at 500°C. The logarithmic relationship can be well described with a straight line, and Avrami index in JMAK function is $n = 2.17$. Considering a constant n value, the hypothesis can be made that no change happens in the α phase transformation mechanism at this temperature. Simultaneous nucleation and growth of α phase happens in the β intragranular area and at the grain boundaries. The growth process is controlled by diffusion of the solute atoms; as the width is poorly modified, the growth results mainly in lengthening of the precipitates; as transformation progresses,

the nucleation rate is decreased. The decomposition mode of metastable β phase is $b \rightarrow a + b$.

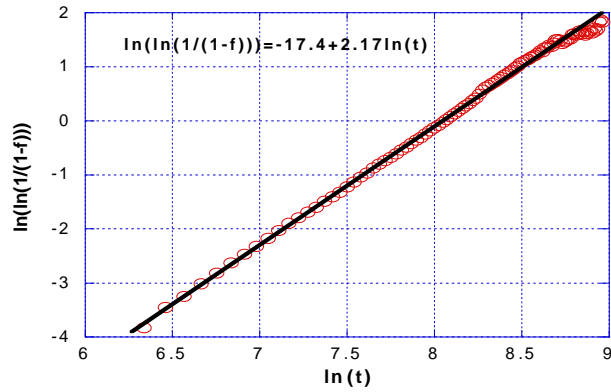


Figure 3-25 Plot of $\ln(\ln(1/(1-f)))$ versus $\ln(t)$ for isothermal aging at 500°C

Thus, α phase nucleation and growth; the evolution of precipitation processes and transformation sequence are schematized in Figure3-26.

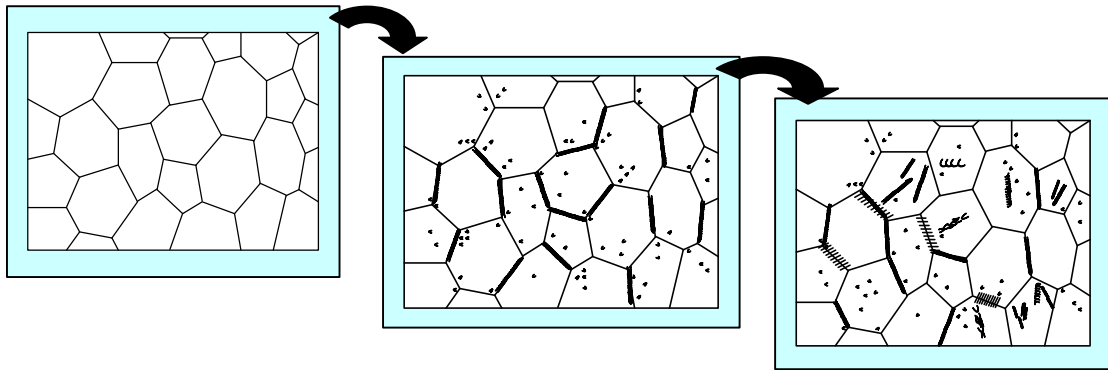


Figure 3-26 Isothermal phase transformation sequence at 500- 550°C

III.3.5. Structure and microstructure evolutions for aging at 600°C and 700°C

The third group of transformation kinetics was the one corresponding to aging at 600~700°C (Figure 3-3d).

The XRD patterns for the specimens aged for 15h, 16h and 18h at 600°C, 650°C and 700°C are given in Figure 3-27. The corresponding optical micrographs are given in Figure 3-28. For the three aging temperature, the final structure is a mixture of α and β phases. From the XRD patterns we have determined the amount of α and β phase after aging, as well as the cell parameters for each phase. Values are given in Table 3-4.

Table 3-4 Amount and cell parameters of α and β phase after aging at 600~700°C.

Aging Temperature(oC)	Amount of α phase (Vol.%)	Parameters of α phase (nm)		Parameters of β phase(nm)
		a	c	
600	47	0.2999	0.4787	0.3292
650	38	0.2999	0.4792	0.3230
700	26	0.2996	0.4798	0.3307

A significant decrease in the amount of α phase can be observed as the aging temperature increases. This tendency is the one expected while in this temperature range, the volume fraction of the α phase at equilibrium is decreased with rising the aging temperature. Some changes are also observed for the cell parameters. A decrease in a cell parameter of the α phase is clearly noticed while the c parameter increases.

Considering the microstructures, at 600°C, the α phase morphology is fine and acicular; the precipitates mean length is about 20 μ m; parallel distributed precipitates are observed at grain boundaries; within the β grain, the α precipitates arrangement is rather fussy. For aging temperatures of 650°C and 700°C, the precipitated α phase appears also with an acicular morphology except that the width is considerably increased to 2~3 μ m, compared with that of α phase after aging at 600°C. The length is also increased to about 30~40 μ m. Moreover, continuous α layer is formed on β grain boundaries with a thickness of about 2 μ m; most of the acicular α phase is within the parent grain and grows up from β grain boundaries. Additional

observations and analysis have been performed in order to analyze the nucleation and growth of the α phase in this temperature range.

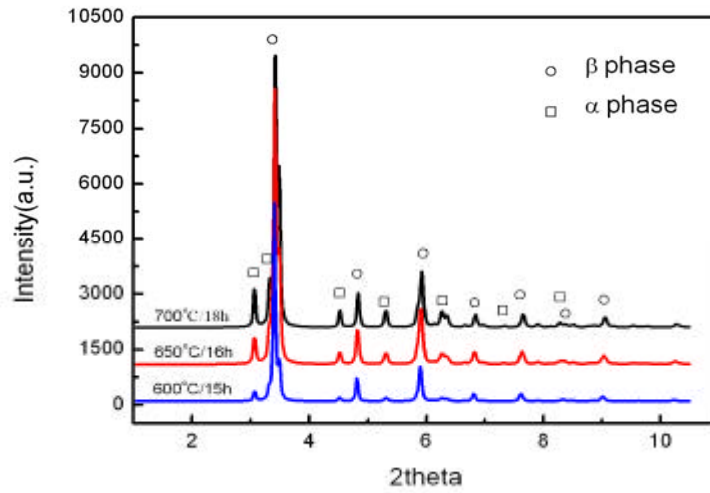
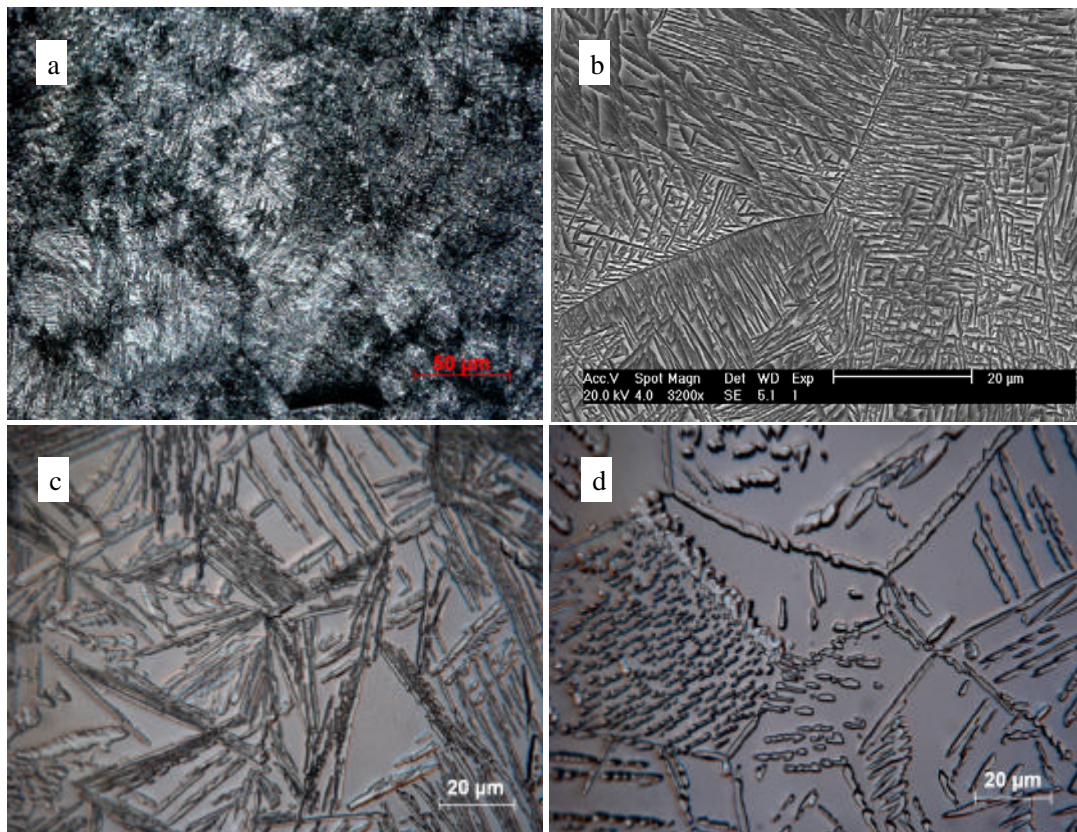


Figure 3-27 Synchrotron XRD patterns for Ti-B19 alloy after 600°C/15h, 650°C/16h and 700°C/18h isothermal aging respectively.



(a) OM-600°C, (b) SEM-600°C, (c) SEM-650°C, (d) SEM-700°C

Figure 3-28 Microstructure of Ti-B19 alloy specimens after aging at different temperatures:

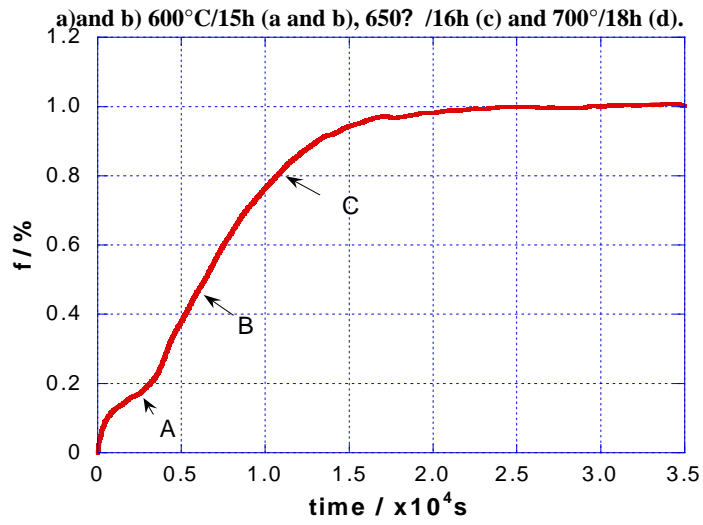
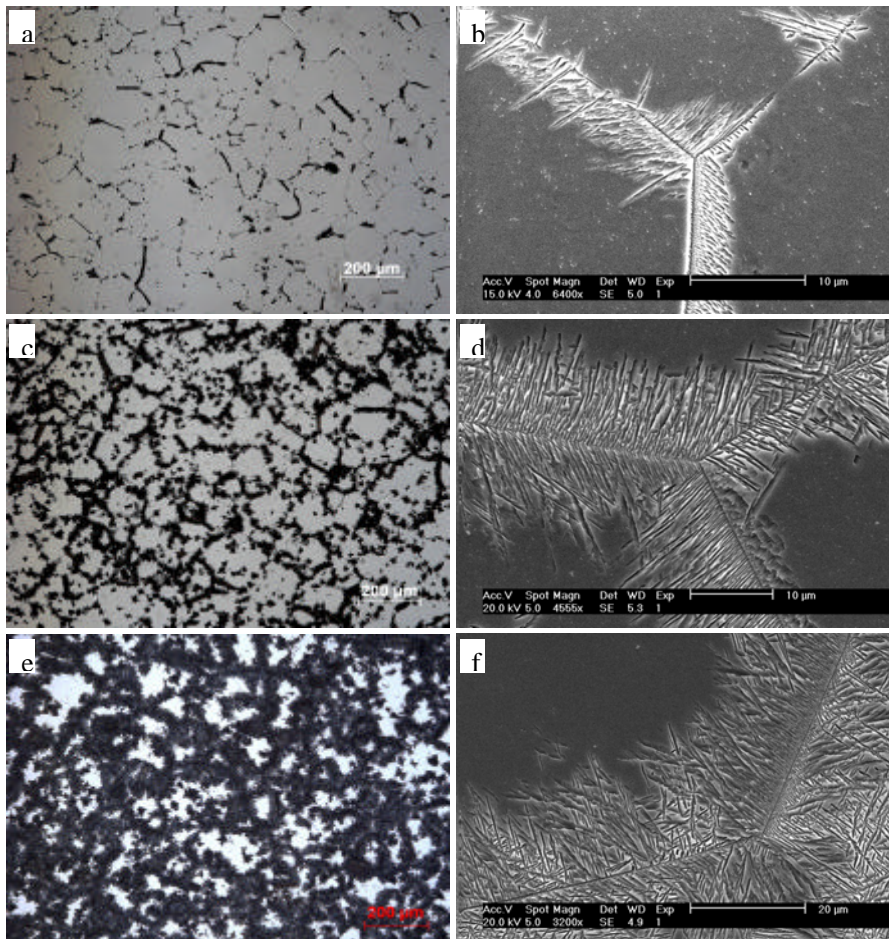


Figure 3-29 Transformation kinetics for Ti-B19 alloy isothermal aged at 600°C



(a) OM-2500s, (b) SEM-2500s, (c) OM-6000s,

(d) SEM-6000s, (e) OM-10800s, (f) SEM-10800s

Figure 3-30 Microstructure of Ti-B19 alloy after isothermal aging treated at 600°C

for 2500s, 6000s and 10800s, respectively.

Samples have respectively been aged for 2500s, 6000s and 10800s at 600°C, corresponding to point A, B and C on the transformation kinetics curve recalled Figure 3-29. Figure 3-30 shows the optical and SEM micrographs obtained. In the early stage of the transformation (2500s), α nucleation happens first on β grain boundaries. At higher magnification, acicular parallel α precipitates are observed growing from α formed on the grain boundaries. These parallel precipitates grow within the β grain, increasing their length. Simultaneously, small volumes of acicular α phase start to form within the β grain; increasing the aging time, leads to an increase in the occupancy of α phase at the grain boundaries and an increase in the length of the parallel precipitates. When the phase transformation is finished, the acicular α phase is made up into cross reticulation structure in the β grains.

Figure 3-31 provides $\ln(\ln(1/(1-f)))$ versus $\ln(t)$ plot for isothermal aging at 600°C. At this temperature, the logarithmic relationship of phase transformation degree versus time can be described with two straight lines; that is to say, two ranges exist in the phase transformation process. The slope of the first straight line, leads to an Avrami index n equal to 0.4 in JMAK function. This period spends about 3000s and corresponds to a transformation progress from beginning to about 18%. A main process in this period is the nucleation of α at the β grain boundaries and its growth until the formation of the acicular parallel α precipitates.

The slope of the second straight line, with an Avrami index $n=1.8$ in JMAK Function, describes the remaining phase transformation process at values up to about 80%. In this stage, the transformation includes growth of α at β grain boundaries, growth of acicular parallel α (α colonies) as well as nucleation and growth of acicular α phase within the β grains. In this stage, the nucleation rate of α decreases as the aging time increases. All in all, the α phase nucleation and growth processes involved for

Ti-B19 alloy in the temperature range of 600- 700°C can be schematized in Figure 3-32.

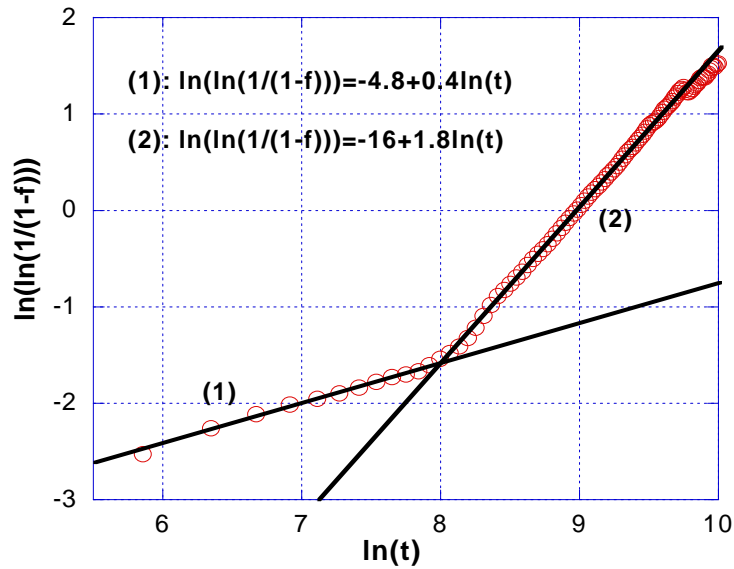


Figure 3-31 Plot of $\ln(\ln(1/(1-f))) - \ln(t)$ of Ti-B19 alloy during the isothermal aging at 600°C

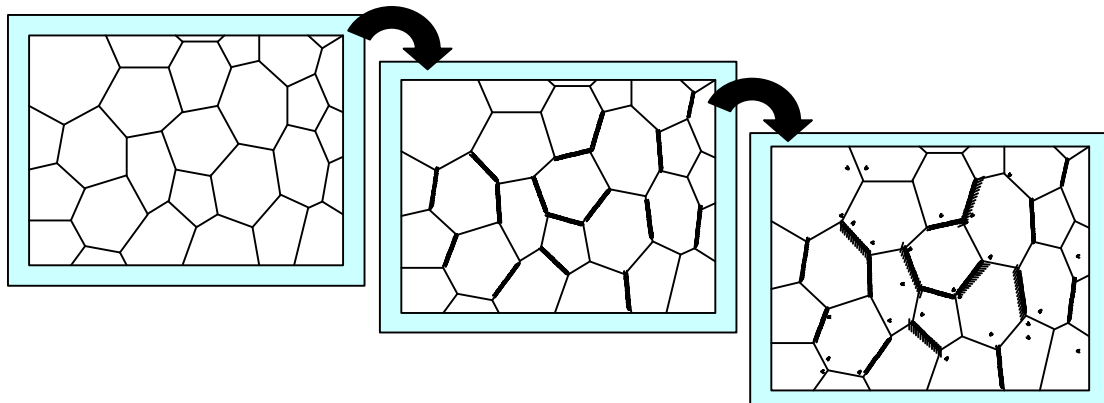


Figure 3-32 Isothermal phase transformation sequence for of Ti-B19 alloy during aging at 600- 700°C.

III.4. The design of TTT diagram for Ti-B19 alloy

Time-temperature-transformation diagram (TTT diagram for short) permits to describe the kinetics of isothermal phase transformation of the alloy in the

transformation temperature range of interest. It has three parameters: time, temperature and degree of phase transformation. This section shows the TTT diagrams of Ti-B19 alloy according to the obtained results. Because enough data have been obtained, we have plotted the different times necessary to obtain five equal transformation progress quantities for the each transformation temperature analyzed: t_s (0% degree of phase transformation), $t_{10\%}$ (10% degree of phase transformation), $t_{50\%}$ (50% degree of phase transformation), $t_{90\%}$ (90% degree of phase transformation) and $t_{100\%}$ (100% degree of phase transformation). These values are obtained according to the kinetics of phase transformation at each isothermal temperature, after being taken the common logarithm of time. Point t_s is the intersection of the tangent of the beeline part of the curve. The rest of the curve is divided into ten equal parts. Then the four points at every temperature treatment are obtained: $t_{10\%}$, $t_{50\%}$, $t_{90\%}$ and $t_{100\%}$, which are linked together to form the TTT diagram for this alloy (Figure 3-33).

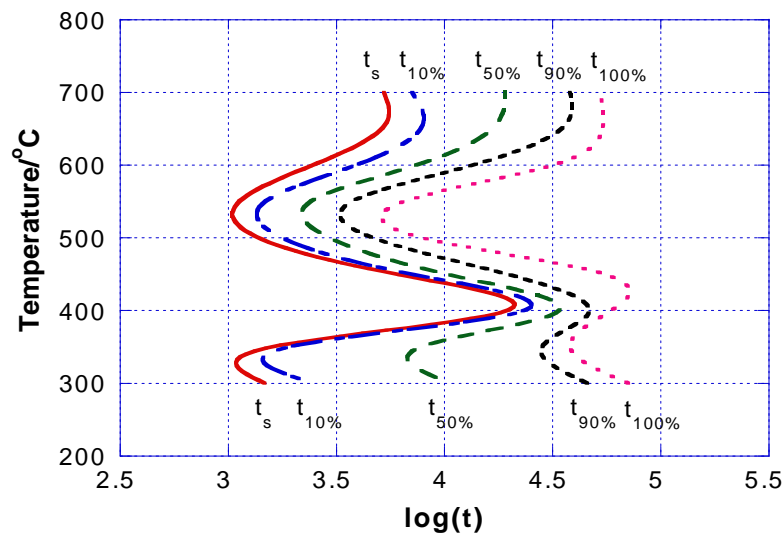


Figure 3-33 Experimental TTT diagram of Ti-B19 alloy

Seen from Figure 3-33, TTT diagram of Ti-19 alloy can be divided into two parts by the boundary of 400°C, forming two “C-shape” curves. The first “C-shape” curve is above 400°C and describes mainly the transformation process of precipitation of a

phase from metastable β phase. The second “C-shape” curve is below 400°C and describes the transformation process of precipitation of α' phase from metastable β phase. We also can see from Figure 3-33 that the velocity of a phase transformation is the highest in the temperature range of 500~ 550°C, that is known as the “nose” temperature of the “C-shape” curve. For titanium alloy, the velocity of the isothermal phase transformation is closely related to the degree of supercooling^[99].

For the higher temperatures, transformation temperature approaches the phase transformation (α' β) point of the alloy (760°C); the diffusion of solute atoms is favored, but the overcooled extent is not considerable, and thus the driving force is small. The necessary time to complete the phase transformation is longer than that in medium temperature aging. Therefore, the quantity of the new phase is also decreased accordingly.

The transformation kinetics is determined by both the transformation driving force and by the diffusion rate of solute atoms. In the high temperature aging treatment (for instance 700°C), the nucleation and growth rates are affected by the low value of the driving force. Although the diffusion rate of solute atoms is high, the driving force still dominates the process. One can mention that the low driving force allows mainly nucleation at grain boundaries, while intra granular nucleation is poor. In the low temperature aging treatment (for instance 400°C), the phase transformation rate is slowed down by the low diffusion rate of solute atoms although the driving force is strong. At those temperatures intra granular nucleation is observed, and transformation progresses mainly by nucleation of new precipitates. In the middle temperature range, at 500~550°C aging treatment, the driving force of phase transformation leads to nucleation at grain boundaries and within the grain and the diffusion rate of solute atoms can occur. In consequence, the phase transformation rate reaches a peak value leading to the “nose temperature” in the TTT diagram.

These results are in good agreement with other studies on titanium alloy [84,99]. Some differences can be mentioned. Indeed, for transformations from the beta temperature range in Ti-17 alloy, Da Costa Teixeira^[95] mentions three different noses in the temperature range 850°C and 400°C. The first and second noses are associated with the formation of a phase, but with different morphologies. The first one near 750°C is associated with the formation of $a_{GB} + a_{WGB}$, the second nose at 650°C corresponds to formation of a_{WI} . The structure change occurring at the third nose at 450°C, was clearly identified by synchrotron XRD analysis^[103] that confirmed the formation of a β'' phase. Ti-B19 contains more β stabilizers elements as Ti-17, reducing the transformation point (T_{β}) and delaying the transformation kinetics. The formation of a at temperatures near the phase transformation point is very slow, and this domain may not be really covered by our experiments. For the transformation at lower temperatures, our XRD characterizations were mainly done after long aging times. The amount of precipitated phase is large, and the obtained data cannot allow to precise if a'' or a is formed at 400 and 450°C. However, one can mention that a cell parameters measured at those temperatures are near the one obtained for an orthorhombic phase formed during the aging treatment at lower heating rates (chapter 4).

TTT diagram can also be obtained using JMAK equation and values of n and K gained from experiments. Equation (3-4) can be changed to:

$$-Kt^n = \ln(1-f) \quad (3-12)$$

Thus, equal transformation quantity point t_f for each isothermal temperature can be described as follows:

$$t_f = \left(\frac{\ln(1-f)}{-K} \right)^{1/n} \quad (3-13)$$

Combining K and n values given in Table 3-1), the value of $t_{10\%}$, $t_{50\%}$, $t_{90\%}$ at each isothermal temperature can be calculated by employing equation (3-13) (Due to mathematical reasons, the value of t_s and $t_{100\%}$ can not be given), so that the “theoretical” TTT diagram of Ti-B19 alloy is obtained (Figure 3-34).

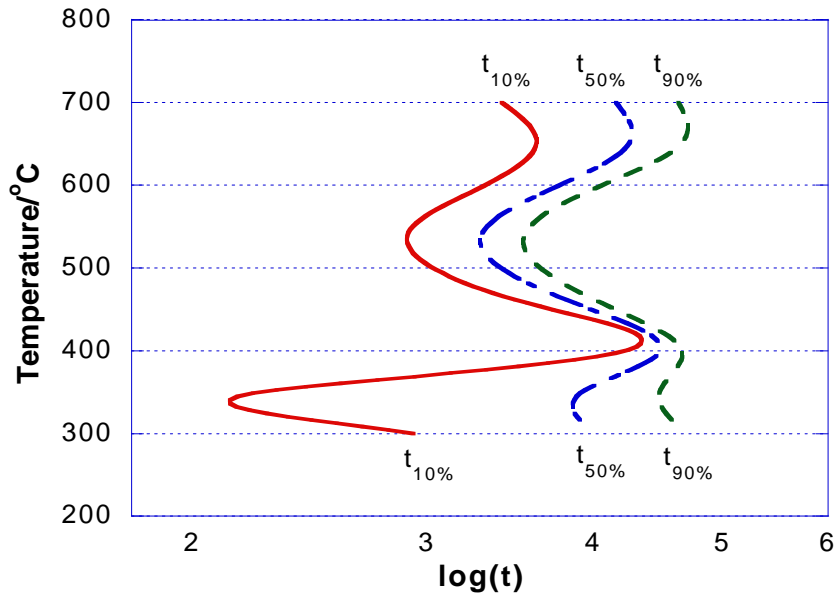


Figure 3-34 Calculated TTT diagram of Ti-B19 alloy

The two diagrams presented Figure 3-33 and Figure 3-34, are quite similar. The small deviations from the JMAK laws considered here and detailed in 3.3 do not lead to large deviations for the reconstructed TTT diagram.

III.5. Summary

Employing the in-situ electric resistivity measurement, a systematic study on the isothermal phase transformation kinetics and microstructure observations is carried out in Ti-B19 alloy at the aging treatment temperature 300~700°C, and the result shows that:

- Only β phase transformation occurs after 20h aging at 300°C, with a volume fraction of β of 27%. Additional experiments on the alloy for longer aging times show that α may be formed. The metastable β phase decomposition mode is $\beta \rightarrow \omega + \beta \rightarrow \omega + \beta + \alpha \rightarrow \alpha + \beta$. After 20h aging at 350°C, formation of β and α occurred, with a volume fraction of 5% and 14%, respectively. The metastable β phase decomposition mode is $\beta \rightarrow \omega + \beta + \alpha \rightarrow \alpha + \beta$.
 - When the alloy is aged at 400°C and 450°C, the final structure is identified as α phase and the volume fraction is of 51% and 57%. We consider that the decomposition sequence of the metastable β phase is $\beta \rightarrow \alpha + \beta$. In this temperature range, the precipitated α phase appears in fine acicular shapes and forms at first within β grain; precipitates are arranged in certain directions to form “tire” patterns with an included angle of 60° between each acicular α phase. The phase transformation may include two different steps; the first one is nucleation and growth of the intragranular acicular α phase, and α precipitates on the dislocation line; the second one is a mixed mechanism, which includes the nucleation and growth of intragranular α phase as well as the grain boundary α phase, and the diffusion controlled growth of acicular α phase plays an important role in the phase transformation process, and corresponding to the second stage of phase transformation.
 - For the isothermal aging at 500°C and 550°C, the identified transformation product is α . The volume fraction of α phase is respectively 58% and 55%. Nucleation occurs simultaneously at the β grain boundaries and within the β grains. The shape of the intra granular α is fine acicular, and some precipitates appear forming an angle of 60° and follow certain “linear tracks”; the grain boundary α phase forms in parallel acicular structure and grow into the β grain.
 - For the isothermal aging at 600°C ~ 700°C, the α phase is also directly formed,
-

but the nucleation site is the β grain boundary. Intra granular nucleation happens in the later phase transformation process. At the end of the transformation, the volume fraction of α is 47%, 38% and 26% when the aging temperatures are 600°C, 650°C and 700°C respectively. This decrease in α phase amount is associated with the variations of equilibrium α phase amount with temperature. Meanwhile, the width of α precipitates is increased as aging temperature is increased (as diffusion is enhanced).

- The phase transformation kinetics have been analyzed using JMAK equation, and the values of Avrami index n , temperature constant K and the phase transformation activation energy E of Ti-B19 alloy have also been gained. Through experimental data and calculated results, the TTT diagram of Ti-B19 alloy in isothermal phase transformation have been established respectively, and the results show that the highest phase transformation rate ---“nose temperature” is in the temperature range of 500~ 550°C. This is mainly due to the driving force of phase transformation and the diffusion speed of solute atoms cooperate ideally in this temperature range.

IV. INFLUENCE OF HEATING RATE ON ISOTHERMAL PHASE TRANSFORMATION IN TI-B19 ALLOY

In addition to the isothermal temperature and the aging time, the heating rate from room temperature to the isothermal temperature is a factor ^[86, 107] that may affect the transformation kinetics and the final microstructure. In order to analyze the effect of this parameter on transformation kinetics and resulting microstructure, aging treatments were realized at 500°C, with heating rates of 10°C/s, 1°C/s and 0.1°C/s. The normalized resistivity variations ($R/R_{20^\circ\text{C}}$) versus time are given Figure 4-1 for the three different heating rates. The time corresponds to the whole duration of the experiments (heating to 500°C, and holding).

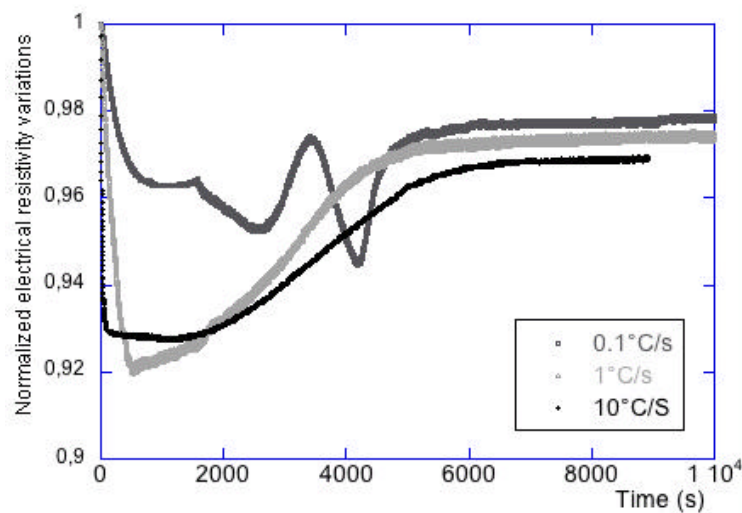


Figure 4-1 Normalized electrical resistivity variations as a function of time.

The comparison of resistivity variations reveals a different behavior for the three different rates, namely a strong difference between 0.1°C/s and the two other heating

rates of 1°C/s and 10°C/s. Keeping in mind that 500°C is reached after 4800s for heating at 0.1°C/s, 480s for heating at 1°C/s and 4.8s for 10°C/s, most changes in resistivity occur during the heating stage for 0.1°C/s, while a strong variation is measured during the holding stage for heating at 1°C/s and 10°C/s. The effect of the heating rate on the final microstructure obtained after 4h holding at 500°C is shown in Fig.4-2 to 4-3. After being heated to 500°C with a heating rate of 10°C/s (Fig. 4-2), a large amount of precipitates has been formed. The precipitates in the parent β grain present an acicular morphology. Their observation by optical microscopy is rather difficult (Fig. 4-2a). Scanning electronic microscopy (Fig. 4-2b) shows that the acicular character of the α phase with a length of the precipitates of about 10 μ m.

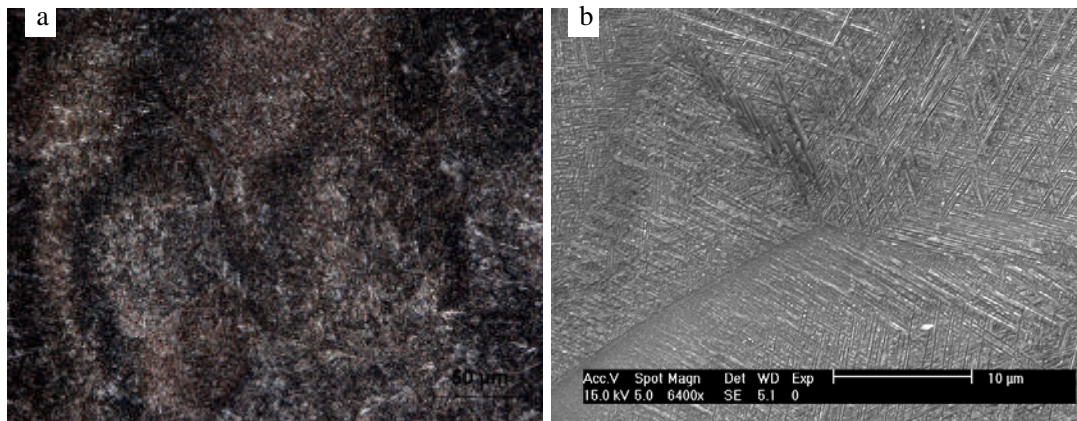


Figure 4-2 Microstructures of Ti-B19 alloy after 500°C/4h aging treatment with a heating rate of 10°C/s

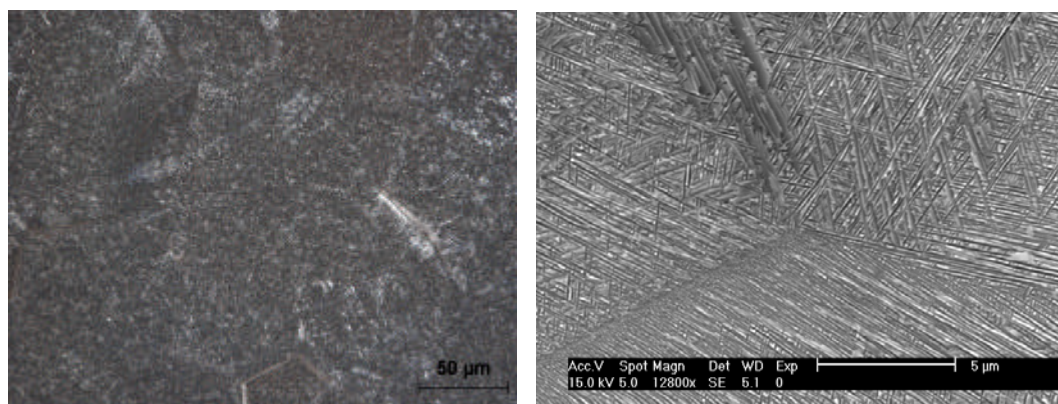


Figure 4-3 Microstructure after 500°C/4h aging treated with a heating rate of 1°C/s

The optical micrograph of the microstructure obtained after heating at 1°C/s is shown in Figure 4-3. The microstructure obtained is very similar to that obtained when heating at 10°C/s . Therefore, no deep analysis is performed for the microstructure in this condition.

At last, the microstructure obtained for the lowest heating rate of 0.1°C/s is very thin and difficult to observe even by SEM. TEM investigations will be shown in the following paragraph.

These first results show that the heating rate has a strong effect on the electrical resistivity variations as well as on the final microstructure. In the following we further analyze these evolutions, considering at first the heating step and further the holding period.

IV.1. Evolutions during the heating.

IV.1.1. Variation of resistivity with temperature (time) during the heating process

In Figure 4-4 we have reported the variations of resistivity versus temperature measured during the heating stage. For all heating rates investigated, a negative dependence with temperature (NTD) is observed at the beginning on heating. When the heating rate is rather high (10°C/s and 1°C/s), the NTD is observed until 350°C or 400°C . For heating at 10°C/s and when increasing the temperature, the resistivity decreases more slowly; no clear increase in the resistivity is measured until 500°C . Heating at a rate of 1°C/s , leads to a small bump at temperatures near 400°C and a NTD between 450°C and 500°C .

For 0.1°C/s the variations of resistivity with temperature are rather complex. Four

stages can be outlined: stage I corresponds to the monotonic NTD observed until 180-200°C, as for the higher heating rates; stage II corresponds to the range of temperature 300°C - 360°C, with a positive temperature dependence; in Stage III, with further temperature increase, a NTD is again measured until 440°C; after 440°C, the resistivity begins to increase gradually with the temperature increase corresponding to Stage IV. To understand the variations of resistivity with temperature for this latter heating rate, samples were heated at the rate of 0.1°C/s, and quenched at different temperatures during the heating stage, i.e. at 350° and 450° and 500° . The specimens were further analyzed by high energy XRD and by TEM.

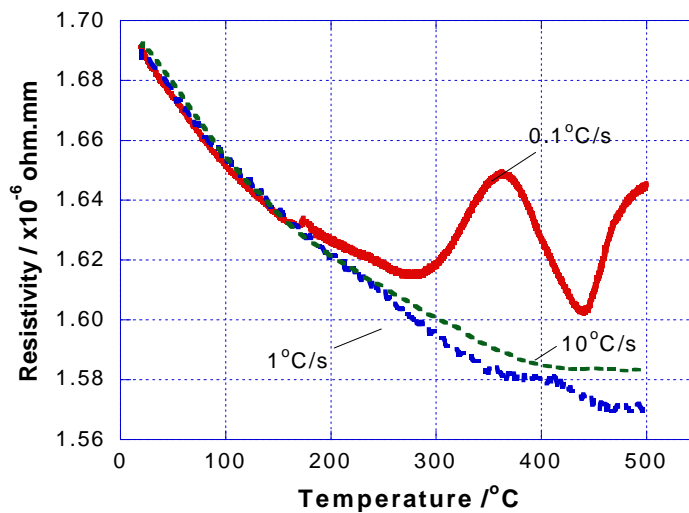


Figure 4-4 Variations of resistivity versus temperature for different heating rates.

IV.1.2. Variation of structure and microstructure during the heating for a heating rate of 0.1°C/s.

The X-ray diffraction patterns obtained at room temperature after quenching from 350°C and 450°C are shown in Figure 4-5. For 350°C, the characterization of the peaks reveals the presence of β and ω phases. The amount of ω has been quantified and estimated equal to 11vol%. For specimen quenched at 450°C, three different

structures are evidenced: β , ω and α'' . The volume ratio of ω is lower (about 2vol%) and meanwhile, the amount of α'' phase is around 10vol.%.

Finally, for the specimen quenched at 500°C (Fig. 4-6), the XRD pattern reveals an increase of the phase precipitated. Several diffraction peaks are observed.

Using Fullprof software, we cannot evidence anymore the ω phase. The different phases that can be identified are the β phase, the α'' phase with an orthorhombic structure, and the α HCP phase. The amount of α is estimated equal to 15.8vol% with cell parameters of $a = b = 2.948 \text{ \AA}$, $c = 4.687 \text{ \AA}$; α'' phase content is 26.7% with crystal parameters of $a = 3.045 \text{ \AA}$, $b = 5.038 \text{ \AA}$ and $c = 4.626 \text{ \AA}$.

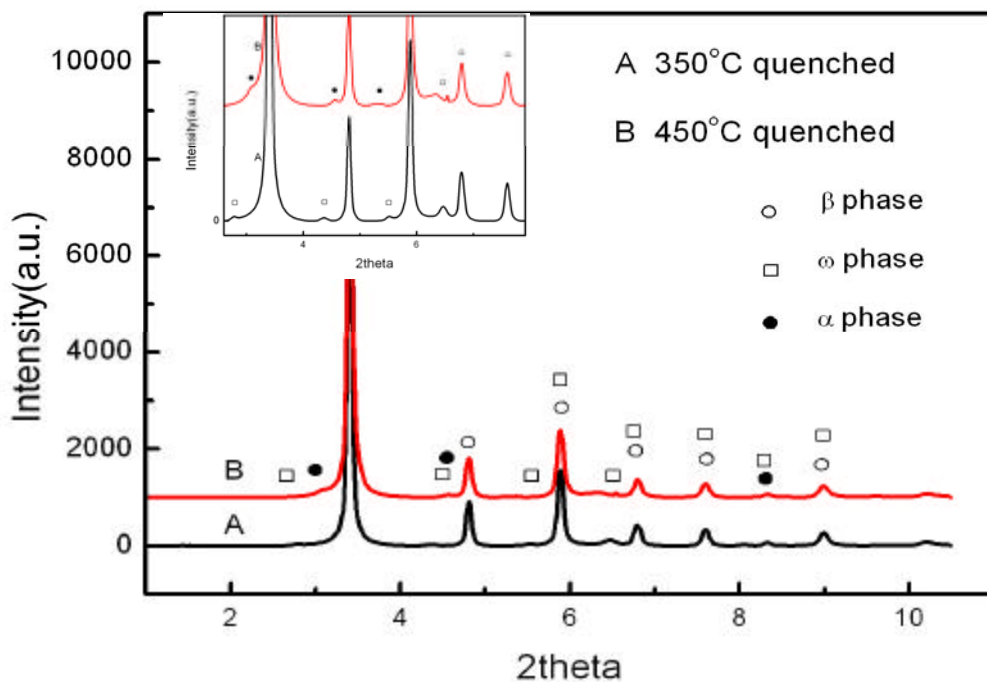


Figure 4-5 XRD patterns for specimens quenched at 350°C and 450°C (heating at 0.1°C/s).

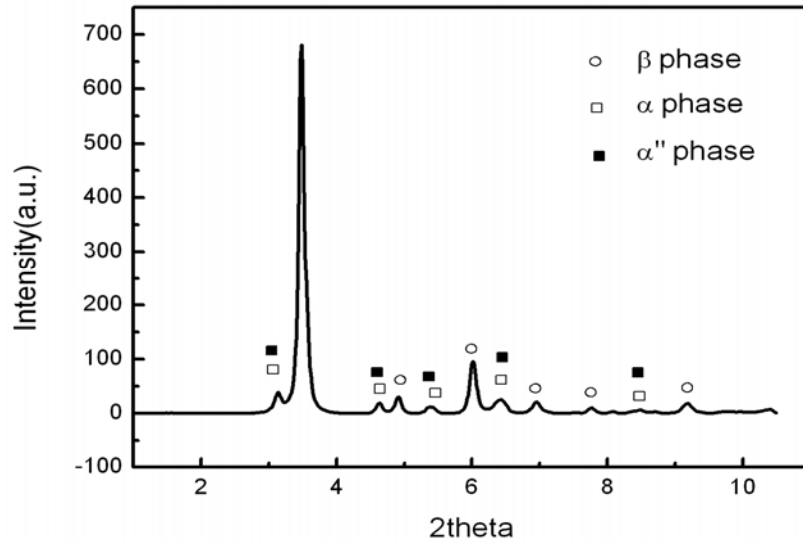


Figure 4-6 XRD pattern for specimen quenched at 500°C (heating at 0.1°C/s).

In addition to these characterizations, TEM observations were performed. Figure 4-7 shows TEM dark field image and its diffraction pattern for specimen quenched from 350°C (heating rate of 0.1°C/s). The diffraction pattern reveals the presence of the hexagonal ω structure. A large density of precipitates is observed, uniformly distributed, which size is a few nanometers. After scaling for the electronic diffraction patterns, the crystal parameters of the formed ω phase are $a = b = 4.692 \text{ \AA}$ and $c = 2.873 \text{ \AA}$. The orientation relationships between β and ω are the following: $[110]_b // [2\bar{1}10]_w$, $(110)_b // (0\bar{1}11)_w$; $[131]_b // [\bar{1}2\bar{1}3]_w$, $(\bar{1}01)_b // (0\bar{1}11)_w$.

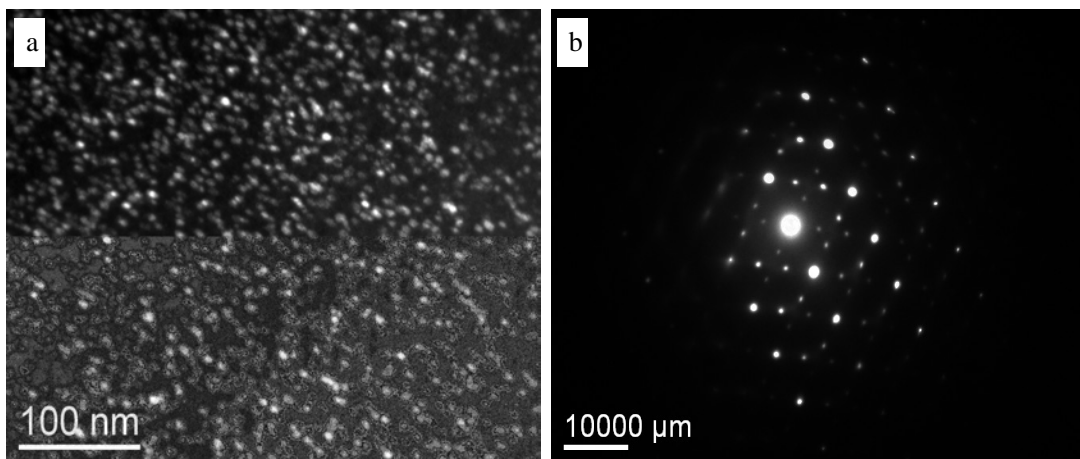


Figure 4-7 TEM dark field image (a) and diffraction pattern (b) for specimen quenched at 350°C (heating of 0.1°C/s).

When the temperature is increased to 450°C changes in the microstructure are also evidenced by TEM. Dark field images and electronic diffraction patterns of the quenched microstructure are shown in Figure 4-8. Dark field images highlight precipitates with two different morphologies. One is acicular (Figure 4-8a), with two main orientations (two possible variants). They are mainly formed with an angle of 60°, and have a length of about 50 nm; the other morphology is particle shape (Figure 4-8b) and has a rather scattered distribution; the size of precipitates is of several nanometers.

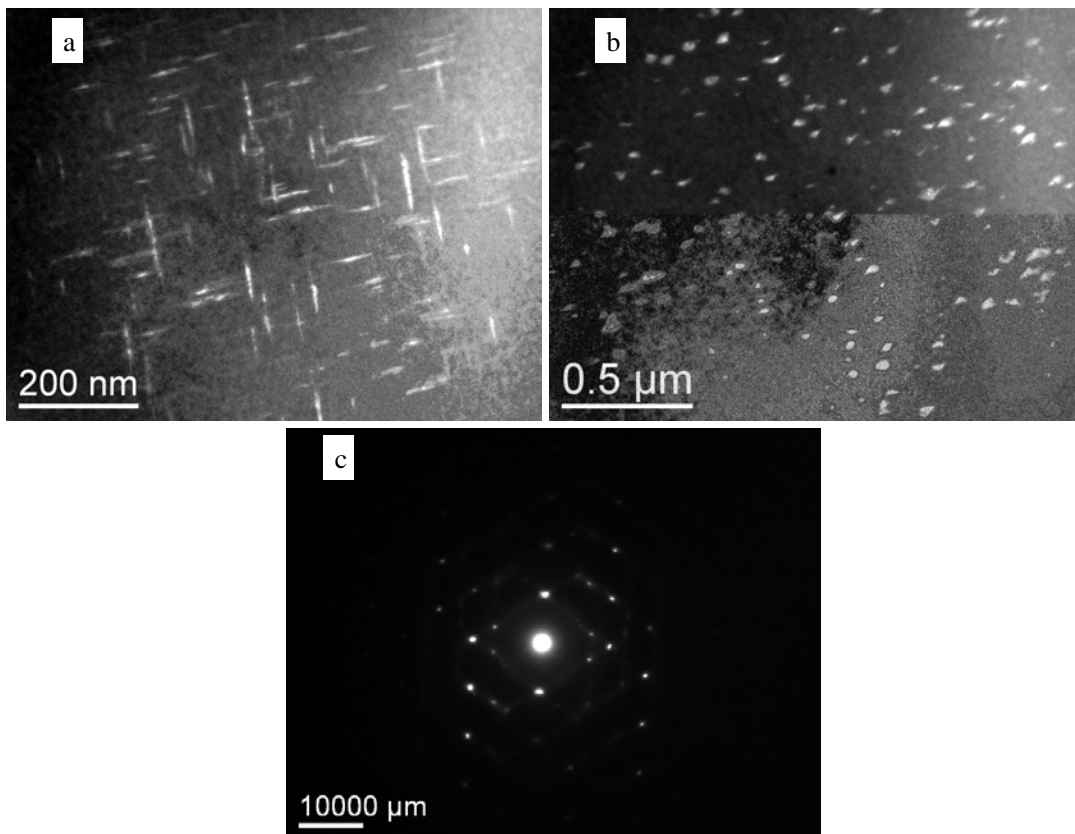


Figure 4-8 TEM dark field images (a, b) and diffraction pattern (c) of specimen quenched at 450°C
(heating at 0.1°C/s)

The acicular precipitates correspond to $(\bar{1}11)$ diffraction spots and can be considered as the orthorhombic α'' structure. Meanwhile, XRD reveals that a small volume of ω

phase still exists; compared with ω phase amount after 350°C, the quantity of ω phase at 450°C is considerably reduced from 11% to about 2%. The presence of ω phase is more difficult to reveal by TEM.

Figure 4-9 shows dark field images and electronic diffraction patterns for the specimen quenched from 500°C after heating at 0.1°C/s. The amount of acicular phase increases and some fuzzy morphology can be observed (Fig. 4-9c).

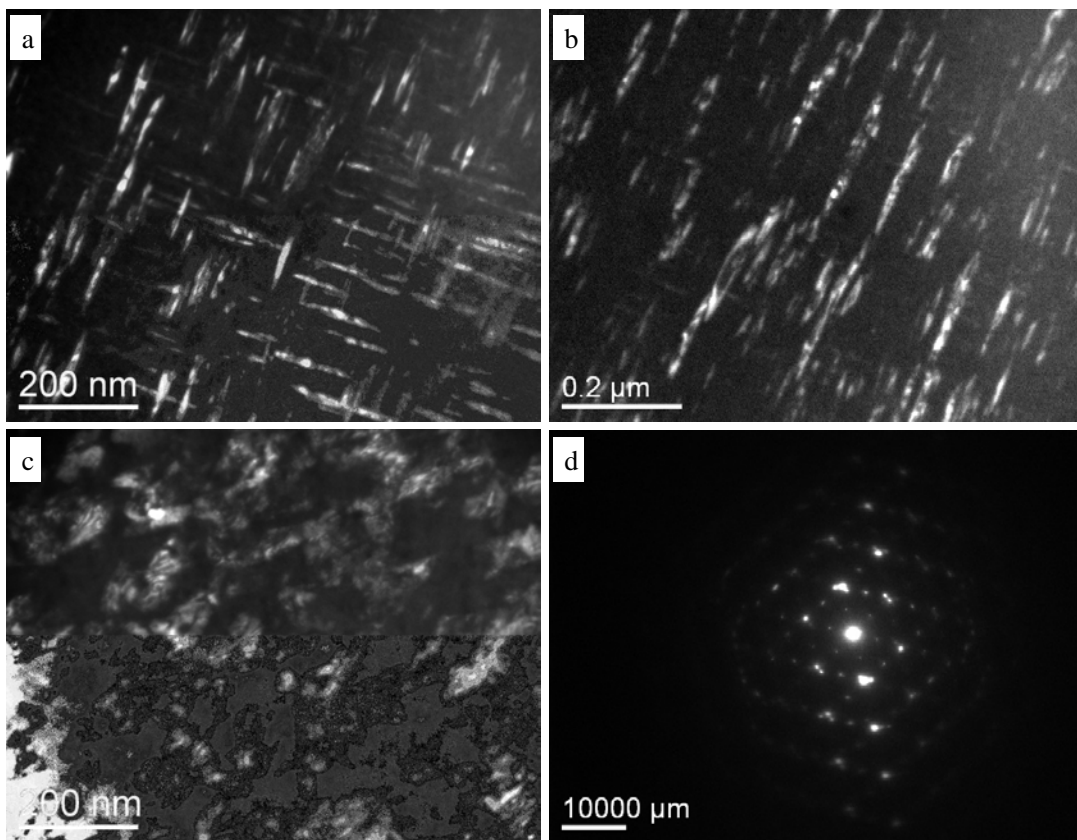


Figure 4-9 TEM dark field images (a-c) and diffraction pattern (d) of Ti-B19 alloy quenched at 500°C (heating at 0.1°C/s).

The additional results obtained by XRD and TEM suggest that the increase of the resistivity in Stage II is associated with the formation of ω phase; The gradual decrease of the resistivity in Stage III, with temperature increase is probably related to a slow transformation process of ω phase into α'' phase; after 440°C, that is Stage IV, the increase of the resistivity with temperature increase is related closely to the

increase in α or α'' phase amount. When the temperature reaches 500°C, the amount of the remaining β is 57.5 vol%. A large part of the transformation took place during the heating step as suggested by resistivity variations. For the higher heating rates investigated, the resistivity of Ti-B19 alloy appears in monotonic lowering process with temperature increase, which represents that no relevant phase transformation process happens in this step.

IV.2. Evolutions during the holding step.

IV.2.1. Evolutions of electrical resistivity variations.

We have previously shown that phase transformation might happen during the heating process of Ti-B19 alloy to the isothermal temperature namely for heating at 0.1°C/s. For the two more rapid heating rates, transformation occurs mainly during the holding step. Figure 4-10 shows the normalized resistivity variations for 10°C/s, and 1°C/s. The transformation kinetics is quite similar.

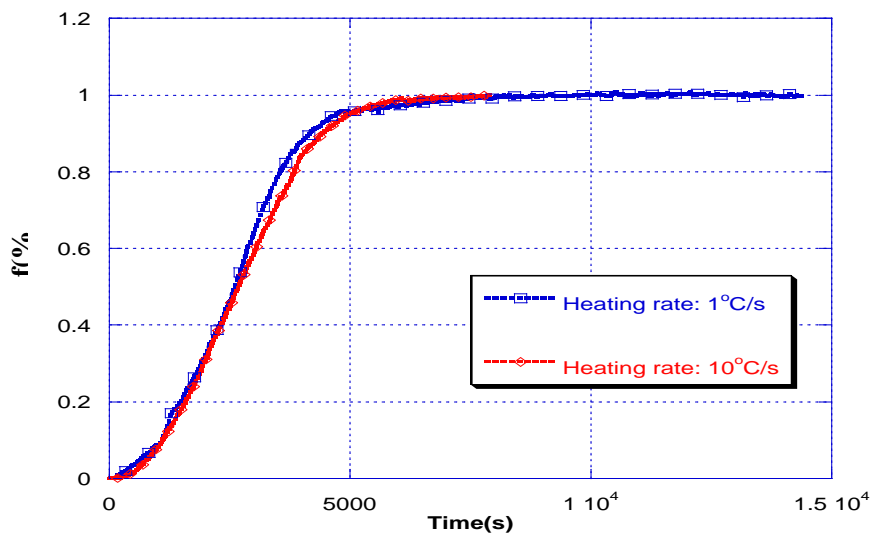


Figure 4-10 Influence of heating rate on isothermal phase transformation kinetics at 500°C after heating at 10°C/s and 1°C/s.

Both curves present a sigmoid shape. No incubation time is clearly evidenced. However, Figure 4-1 suggests an incubation time of about 1300s for the heating rate of 10°C/s and about 200s for 1°C/s. For the slowest heating rate, transformation occurs once 500°C is reached (Fig. 4-1) and is slightly more rapid than for the heating at 10°C/s.

Figure 4-11 shows the logarithm relationship diagram of the phase transformation progress versus time for the two different heating rates. A linear evolution is obtained. For the two different heating rates, the kinetics is the same. The straight line slope which is also the Avrami index of the JMAK function, is $n = 2.17$.

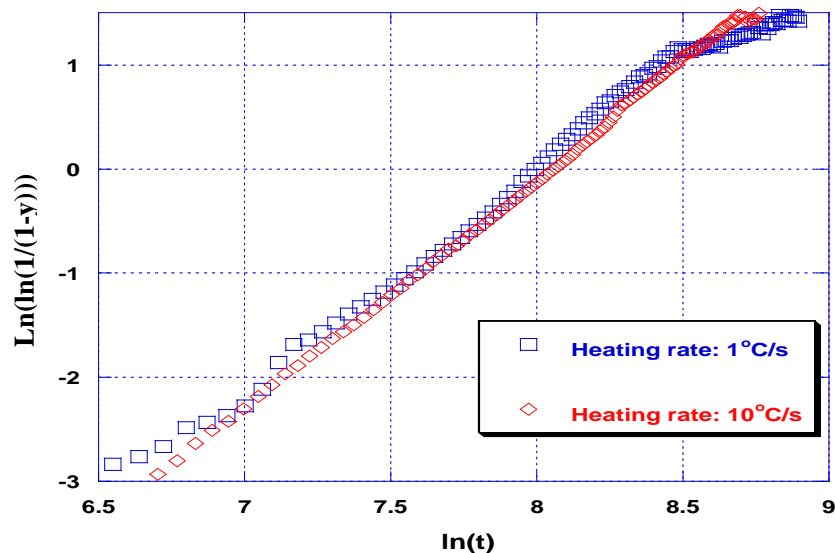


Figure 4-11 Plots of $\ln(\ln(1/(1-f))) - \ln(t)$ of Ti-B19 alloy during the isothermal ageing at 500°C for 10°C/s and 1°C/s heating rate.

IV.2.2. Microstructures and structure obtained after isothermal holding.

We already mentioned that the two rapid heating rates led to a similar microstructure presenting acicular α phase (Figures 4-2 to 4-3). The XRD pattern (Fig.3-21) of the specimen heated at 10°C/s revealed a mixture of two phases (α and β) with a volume fraction of 57.7% α phase.

For the specimen heated at $0.1^{\circ}\text{C}/\text{s}$ and aged 4h at 500°C , TEM observations were performed. Figure 4-12 shows TEM dark field images of the sample heated to 500°C at $0.1^{\circ}\text{C}/\text{s}$, and aged for 4 hours. Figure 4-13 provides the XRD pattern. After aging at 500°C for 4h, only α and β phases are present.

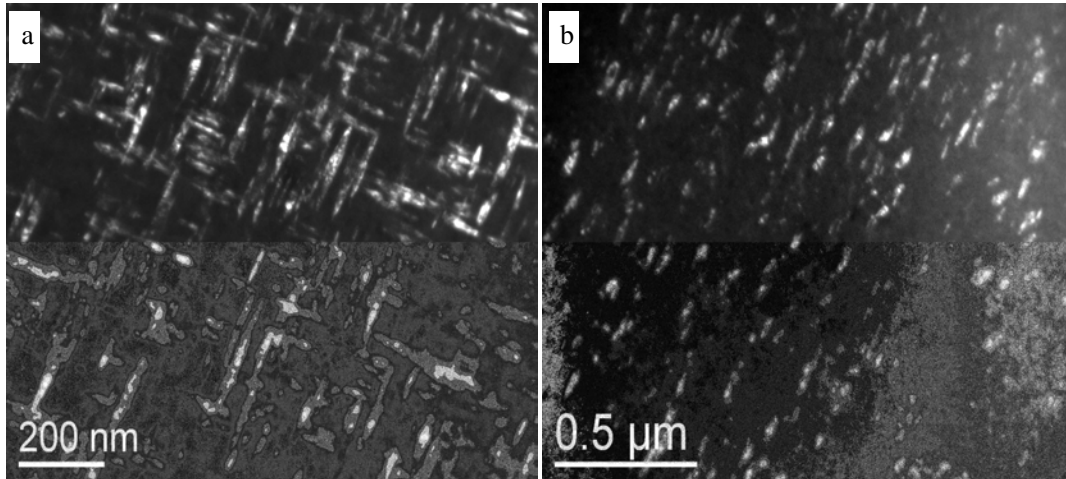


Figure 4-12 TEM images of Ti-B19 alloy after $500^{\circ}\text{C}/4\text{h}$ aging treated with heating rate of $0.1^{\circ}\text{C}/\text{s}$

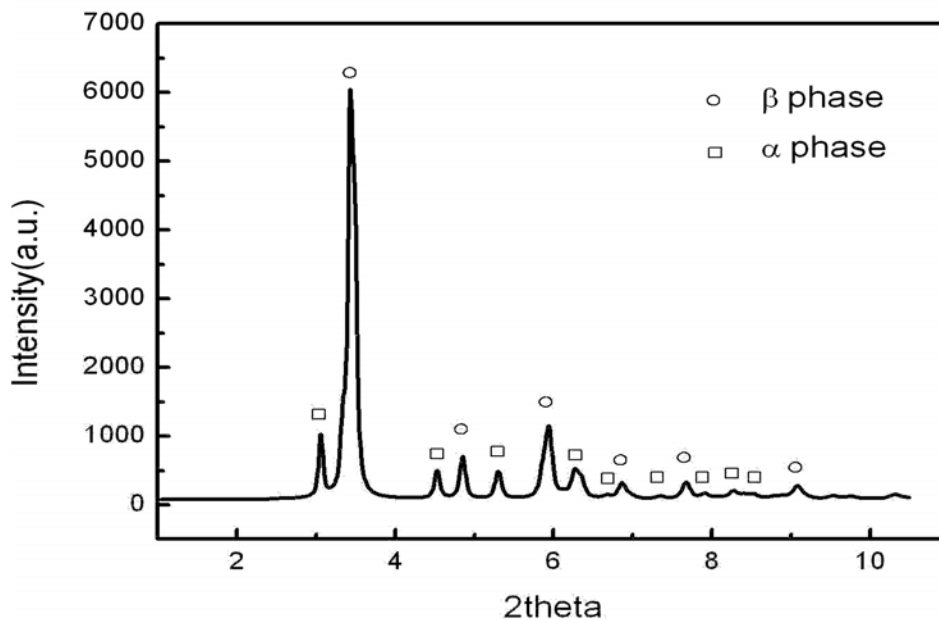


Figure 4-13 XRD pattern after $500^{\circ}\text{C}/4\text{h}$ ageing (heating at $0.1^{\circ}\text{C}/\text{s}$).

Two morphologies of α precipitates are observed, similar to those observed after quenching at 450°C (Figure 4-8). The acicular morphology is still observed, but the

length of the α phase precipitated is a little bit longer than that of specimen quenched from 450°C. Again different precipitates appear with an angle of 60° or in parallel arrangement (Figure 4-12a). The other one is of particle shape and has a diameter of about several nanometers to 10nm in uniform scattered distribution (Figure 4-12b).

IV.3. Brief summary and discussion

- 1) The decomposition of beta metastable structure of Ti-B19 alloy during heating and isothermal aging is dependent on the heating rate. For high heating rates (1°C/s and 10°C/s), the electrical resistivity variations decrease monotonically with temperature increase. The decomposition of the beta metastable phase occurs mainly at the aging temperature. When the heating rate is rather low (0.1°C/s), the resistivity variations with temperature present four domains. ω_{iso} phase is formed in the alloy at 300~360°C; as temperature increases, formation of α'' is observed at the detriment of ω_{iso} . The amount of α'' strongly increases after 440°C. At 500°C, α'' evolves toward the HCP α structure.
- 2) The heating rate has no considerable influence on the final amount of alpha phase in Ti-B19 alloy after 4h aging at 500°C. It affects the kinetics of the phase transformation, and meanwhile, the phase transformation sequences are different. It can be observed that for the isothermal $(\ln(\ln(1/(1-f))))-\ln(t)$ diagrams, at the heating rates of 10°C/s and 1°C/s, Avrami index value of JMA functions is $n=2.17$. The plot of $(\ln(\ln(1/(1-f))))-\ln(t)$ diagram for isothermal resistivity variations at 500°C after heating at 0.1°C/s leads to a $n = 0.67$. This lower n value corresponds to the final step on the transformation (i.e. mainly growth and probably chemical evolutions of the present phases).

- 3) For the lower heating rate (0.1°C/s), a complex transformation sequence is observed with at first, formation of ω phase. ω nuclei are uniformly distributed. These ω precipitates are metastable and act as favorable nucleation sites for the formation of fine acicular precipitates. They gradually disappear with the formation and growth of the acicular phase.

Rather extensive studies have been carried out in order to analyze the role of ω on further precipitation. Most studies on aging of beta metastable phase were done by TEM. In these studies the omega phase is considered as forming α phase^[43,46], the first view is that the α phase nucleus is formed at a certain distance from the ω/β phase interface, due to Al element enrichment, so as to provide perfect conditions for α phase nucleus formation. The second view is that the formation of α nucleus occurs at ω/β phase interface^[45], and it grows consuming β phase and ω phase. Meanwhile, the following orientation relationships are maintained between the three phases, which refer to $(\bar{1}100)_{\omega} // (10\bar{1}0)_{\alpha} // (211)_{\beta}$, $(\bar{1}\bar{1}20)_{\omega} // (0001)_{\alpha} // (0\bar{1}1)_{\beta}$ and $(0001)_{\omega} // (\bar{1}\bar{2}\bar{1}0)_{\alpha} // (\bar{1}11)_{\beta}$. The third view is that α phase nucleus formation is directly formed inside ω phase, and meanwhile, consuming ω phase to grow^[49]. Then, the orientation relationships between α phase and ω phase are as follows: $(2\bar{1}0)_{\omega} // (002)_{\alpha}$, $[001]_{\omega} // [110]_{\alpha}$. From our results, we consider that transformation occurs mainly according to second or third view.

- 4) The analysis performed by high energy XRD evidences the formation of α'' rather than α . α'' is considered as a martensitic transformation product in Ti alloy. Most of α'' appear acicular and possibly contains twin-crystal structure; the phase often appears in metastable β -Ti alloy with many β stable elements, and most of them are formed in high-temperature quenching or isothermal process of Ti alloy^[30,88]. J.I. Qazi et al^[37] have shown for the Ti-35Nb-7Zr-5Ta

that α'' formation relates closely to alloy compositions and the quenching rate; in water quenching conditions, α'' phase can be formed; however, it cannot be formed in the air-cooling condition. Meanwhile, α'' phase quantity is decreased with increase of content of Nb+Ta; they have shown that it is possible to completely suppressed α'' phase formation with an addition of 4.1~4.6% Zr. Meanwhile, increase of interstitial element content can counteract the effect of addition of Zr. Recent in situ XRD studied have clearly evidenced the formation of α'' in Ti 17 alloy during isothermal transformation at 420°C after solution treatment in the high temperature beta range [102]. The formation of α'' phase during the heating process is rarely mentioned. However, some authors report the formation of α'' . O.M. Ivasishin found the existence of orthorhombic α'' structure when studying the ageing process in TIMETAL-LCB alloy and Ti-15-3 alloy [76], and the formation is at the early period of the heating process. Bruneseaux et al [102] have also evidenced the formation of complex transformation sequences depending on the heating rate, with formation of ω prior to α'' and later alpha for low heating rates and formation of α'' for higher heating rates. α'' phase is also a metastable phase, so that following the continuous heating or isothermal process, it will decompose to a stable α phase. That is to say, in general condition, metastable β phase decomposition will first form α'' . For the low heating rate, we have first formation of omega, followed by the formation of α'' at the detriment of omega. Finally α'' transforms into alpha.

- 5) The results obtained show that for the higher heating rates (1°C/s and 10°C/s) the transformation occurs mainly during the holding stage at 500°C and the kinetics correspond to that of α formation. α morphology is acicular, and precipitates have a length of about 10 μm . For a heating rate of 0.1°C/s, a complex transformation sequence occurs during heating with successive

formation of ω , α'' and α . After 4 hours aging, α precipitates have a much lower size. Their length is about 0.1 μm , 100 times lower than for the highest heating rates. This difference is attributed to the higher nucleation sites for α'' and α gained through the precipitation of ω .

V. EFFECT OF PLASTIC DEFORMATION ON PHASE TRANSFORMATION OF TI-B19 ALLOY DURING AGING

Plastic deformation has important influences on isothermal phase transformation kinetics of titanium alloy. Indeed, during the aging process, plastic deformation changes the phase transformation kinetics in a similar way as the isothermal temperature, aging time and heating rate. To study the influence of plastic deformation on the microstructure formation, specimens were plastically deformed (42% and 53%) at room temperature in the beta metastable state (i.e. after solid solution treatment at 900°C/10min followed by quenching at 20°C/s). Then, the specimens were heated to 500°C at the three different rates of 10°C/s, 1°C/s and 0.1°C/s and were hold at that temperature for 4h.

V.1. Resistivity variation during heating and aging processes

V.1.1. Resistivity variation in the heating range

Figure 5-1 shows the resistivity variations versus temperature (time) for specimen with 42% prior deformation and for different heating rates. As for the un-deformed specimens, there are several differences in the resistivity variations with temperature when the heating rates differ. When the heating rate is 10°C/s, the resistivity appears in a monotone decreasing trend while the temperature increases; when the heating rate is 1°C/s and 0.1°C/s, the resistivity variations are more complex: two stages are observed. In the first stage, between 20 and 320°C, the resistivity decreases

monotonically with the temperature increase. It can be emphasized that the slope between 100°C and 250°C differs for the undeformed specimen and the deformed ones. When the temperature approaches 320°C, the rate at which resistivity decreases becomes lower; when the temperature exceeds 320°C, the resistivity starts to increase with temperature (Stage II). For the heating rate of 0.1°C/s, the increase of resistivity with temperature is obviously higher than for 1°C/s.

The comparison of the above variations to the one obtained for un-deformed specimen suggests that there are considerable differences between the resistivity variations. In the un-deformed condition, the resistivity variations with temperature when being heated at 0.1°C/s include four stages, and for 1°C/s, the resistivity shows a monotone decrease with the temperature increase. For specimens 42% deformed and heated at 0.1°C/s and 1°C/s, the resistivity variations with temperature include only two stages.

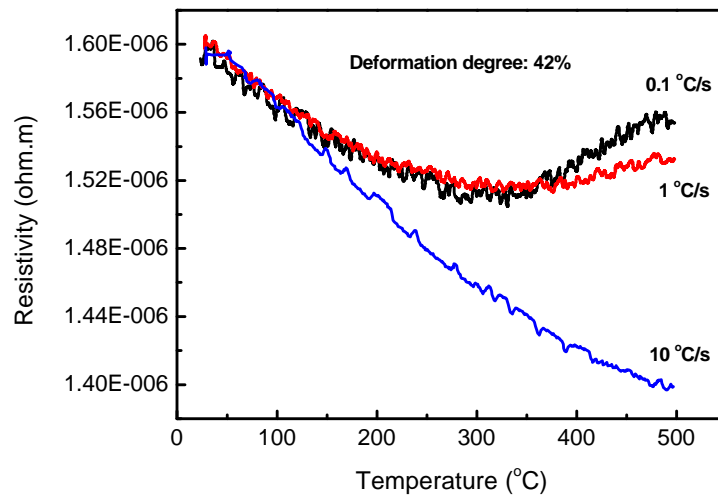


Figure 5-1 Resistivity variations with temperature during heating to 500°C at different heating rates for 42% prior deformation.

Figure 5-2 shows the resistivity variations during heating for 53% deformation¹. The

¹ The resistivity values have been shifted in order to have the same initial value at room temperature.

resistivity variations with temperature are basically the same as for 42% deformation. When heated at 1°C/s and 0.1°C/s , the resistivity variations still include two stages with the temperature increase except that the temperature for which resistivity increases is slightly increased: if heated at 1°C/s , the inflexion temperature is 380°C ; if heated at 0.1°C/s , the inflexion temperature is 330°C . A change in the slope of resistivity variations with temperature is also observed near $100\text{-}150^{\circ}\text{C}$ for 1 and 0.1°C/s .

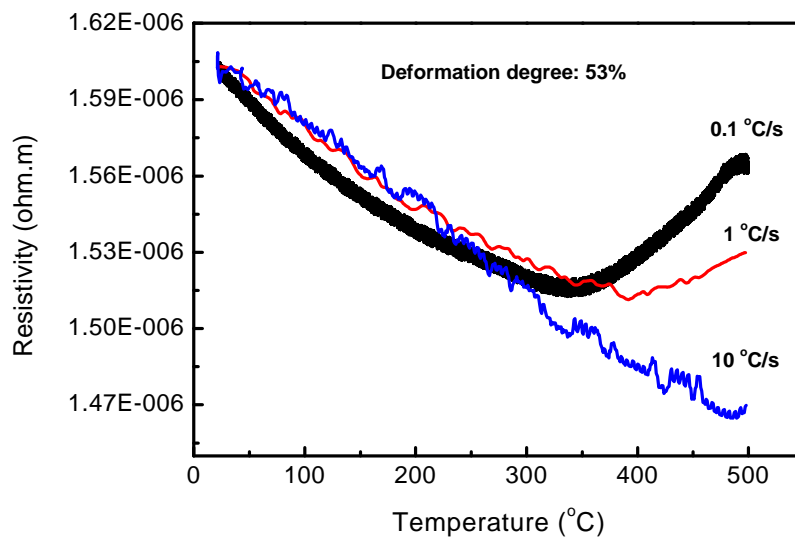


Figure 5-2 Resistivity variations with temperature during heating to 500°C at different heating rates for 53% prior deformation.

To evidence the effect of deformation on the resistivity variations we have compared the resistivity variations with temperature for the un-deformed specimen and the specimens with 42% deformation and 53% deformation for each heating rate of 10°C/s , 1°C/s and 0.1°C/s . Results are shown in Figures 5-3, 5-4 and 5-5 respectively.

When heated at 10°C/s (Figure 5-3), the resistivity shows a monotone decrease with temperature increase; the slopes are slightly different, but the overall trend is not changed. Therefore, it can be considered that almost no phase transformation

happens in the heating stage during rapid heating in all three conditions: undeformed, 42% deformation degree and 53% deformation degree.

When heated at 1°C/s , (Figure 5-4), the pre deformation leads to rather high changes in the variations of resistivity during the heating stage. For the un-deformed specimen, the resistivity shows a constant decrease with temperature increase with almost no phase transformation; a slight change in slope is observed when reaching 500°C . For specimen with 42% deformation, the resistivity variations curve has two parts; The first part which is similar to the un-deformed specimen, and a second one for which the slope is 0 or positive for temperatures above 320°C suggesting that phase transformation happens; for 53% deformation, the resistivity variations curve is also composed of two parts and the zero or positive slope is observed above 380°C . From these results we can first conclude that room temperature deformation favors the phase transformation during heating. Transformation begins at 320°C and 380°C for the two deformation conditions.

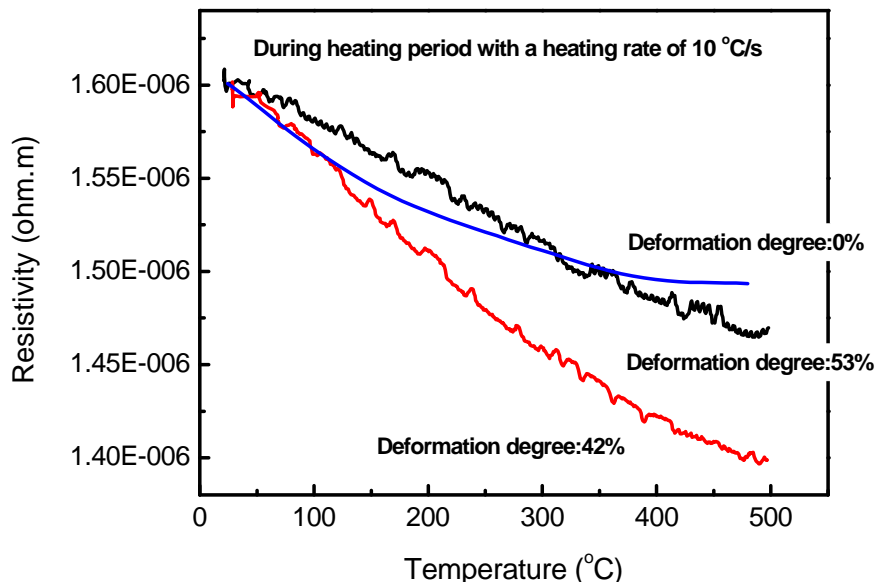


Figure 5-3 Resistivity variations versus temperature for the heating rate of 10°C/s and different initial states (undeformed, prior deformation degree of 42 and 53%)

When heated at 0.1°C/s (Figure 5-5), the differences are even higher. In the

temperature range 20°C - 250°C the resistivity variations with temperature are quite similar for un-deformed and deformed specimens. However, above 250°C, the behavior is modified. For the un-deformed specimen, the resistivity variations curve with temperature includes four stages, while for the deformed specimens only two stages are obtained. For the un-deformed specimen the resistivity increases at temperatures above 300°C. This first increase has been associated with the precipitation of ω phase. During further heating a decrease in the resistivity was obtained followed by a further increase associated with the formation of α'' or α phase. For the deformed specimen, the increase of resistivity is observed at temperatures higher than for the un-deformed one (about 350°C). The complex behavior observed for the un-deformed specimen is not observed.

Further results (in Section 5.3) obtained by X-ray and TEM suggest that $b \rightarrow a + w$ transformation happens in the second stage of the resistivity variations with temperature for pre-deformed specimens heated at of 1°C/s and 0.1°C/s.

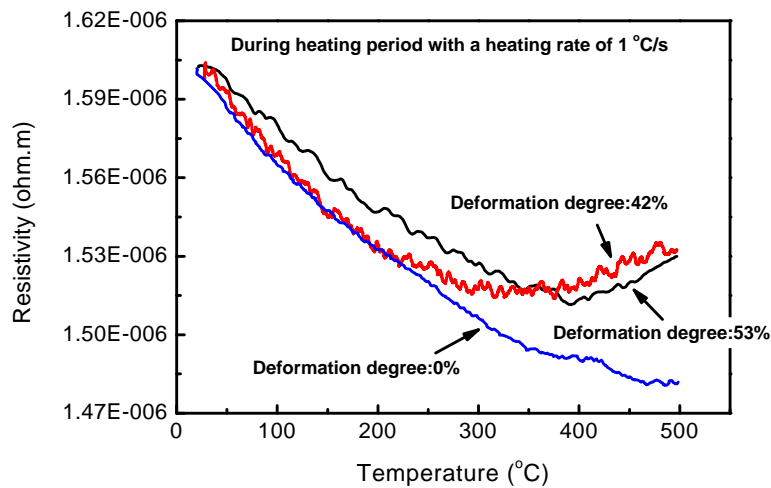


Figure 5-4 Resistivity variations with temperature for the heating rate of 1°C/s and different initial states (un-deformed, prior deformation of 42 and 53%).

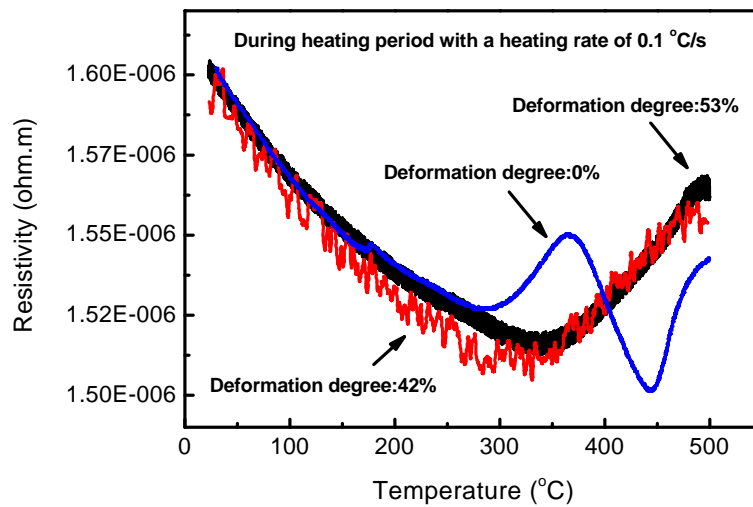


Figure 5-5 Resistivity variations with temperature for the heating rate of 0.1°C/s and different initial states (un-deformed, prior deformation of 42 and 53%).

V.1.2. Resistivity variations during holding at 500°C.

Figure 5-6 shows the isothermal resistivity variations versus time during aging at 500°C for specimen with 42% deformation, and for the three heating rates of 10°C/s, 1°C/s and 0.1°C/s. To compare the changes in resistivity variations, a same value has been assigned at the beginning of holding at 500°C. The higher amplitude of resistivity variations during holding is observed for the higher heating rate.

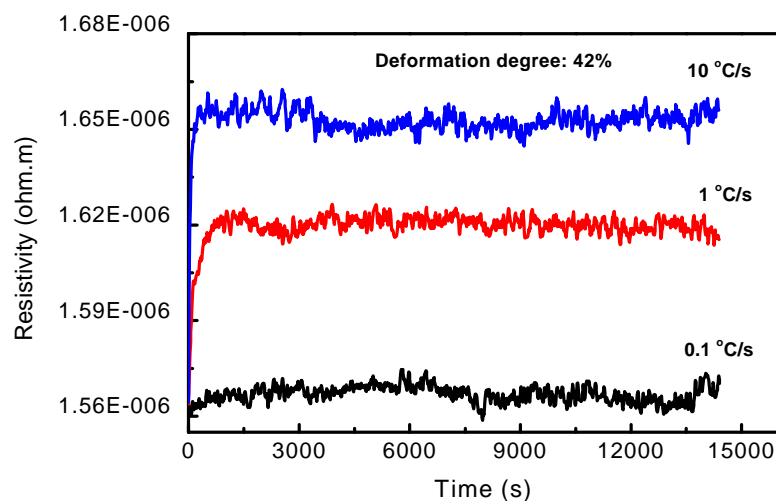


Figure 5-6 Resistivity variations with holding time at 500°C for different heating rates (10°C/s, 1°C/s and 0.1°C/s). Prior deformation degree is of 42%.

Indeed when heated at 10°C/s , almost no β nor α'' or α phase transformation happens in the heating stage; however, if heated at 1°C/s and 0.1°C/s , phase transformation takes place in the heating stage and the amplitude of the resistivity increase during holding is lower. Therefore, phase transformation kinetics for the three deformation conditions are slightly different during the isothermal holding at 500°C .

Figure 5-7 shows resistivity variations versus after 53% deformation for the three different rates of 10°C/s , 1°C/s and 0.1°C/s . The amplitude of resistivity variations after heating at 10°C/s is again far higher than those at 1°C/s and 0.1°C/s ; meanwhile, when heated at rates of 1°C/s and 0.1°C/s the changes during the isothermal range are much lower, and a decrease in electrical resistivity is even measured.

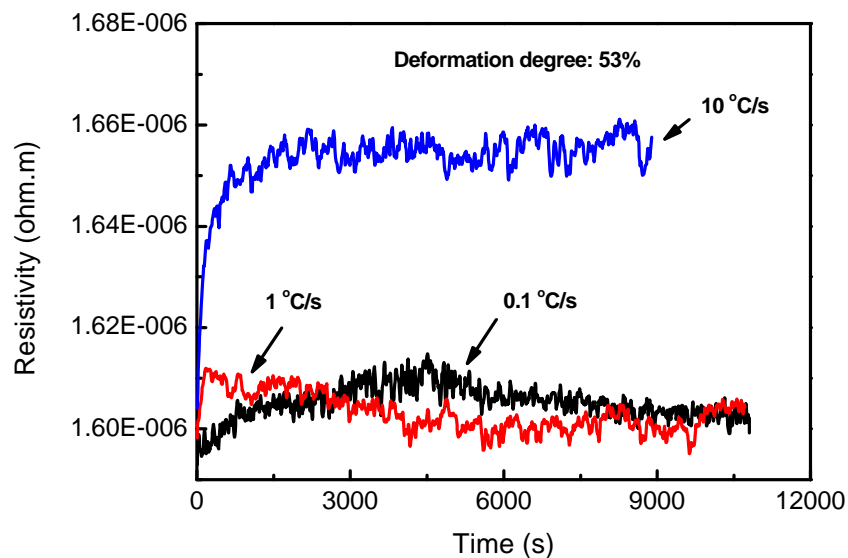


Figure 5-7 Resistivity variations versus holding time at 500°C for different heating rates (10°C/s , 1°C/s and 0.1°C/s). Prior deformation degree is of 53%.

To further analyze the influence of deformation and heating rate on the resistivity variations, the isothermal evolutions at 500°C for the un-deformed specimen and those for specimens with 42% deformation and 53% deformation are compared for the three heating rates of 10°C/s , 1°C/s and 0.1°C/s (Figures 5-8, 5-9 and 5-10

respectively).

When heated at 10°C/s , almost no phase transformation happens in the heating range. Phase transformation mainly takes place during the isothermal holding. Figure 5-8 shows that for the deformed specimens the resistivity reaches the maximum value at a lower time. The precipitation kinetics is strongly increased. The end of the transformation is reduced from 6000s to 300s (for 42% deformation). Moreover, the sigmoid shape of the resistivity variations obtained for the un-deformed specimen is no more observed; the incubation period is clearly suppressed. Considering the amplitude of resistivity variations, the highest increase of resistivity is observed for the un-deformed specimen. For deformed specimens the amplitude is lower. The lowest value is obtained for the specimen with 42% pre-deformation.

When heated at 1°C/s (Figure 5-9), the resistivity variations for the un-deformed specimen is basically the same as for heating at 10°C/s ; almost no phase transformation happens in the heating stage, and phase transformation mainly takes place in the isothermal stage. After room temperature deformation, the time that the resistivity reaches the peak value is considerably shortened. Again the transformation kinetics is strongly accelerated. Comparing the two deformation levels, the higher the deformation amount, the lower the resistivity peak value will be.

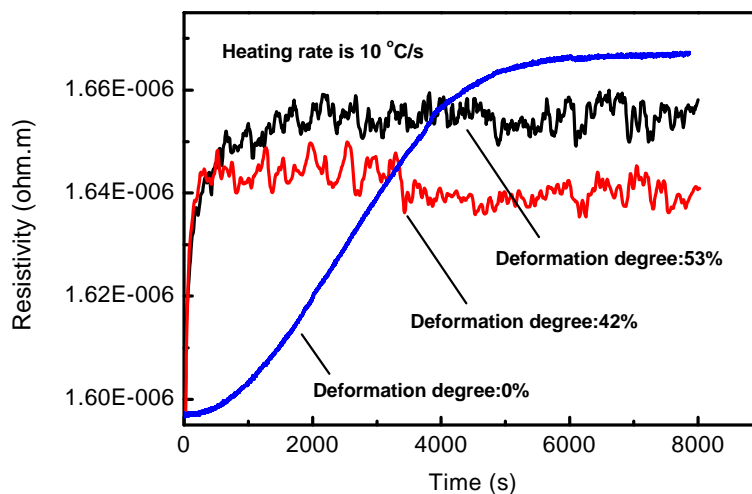


Figure 5-8 Resistivity variations versus holding time at 500°C for three different initial conditions and the heating rate of 10°C/s .

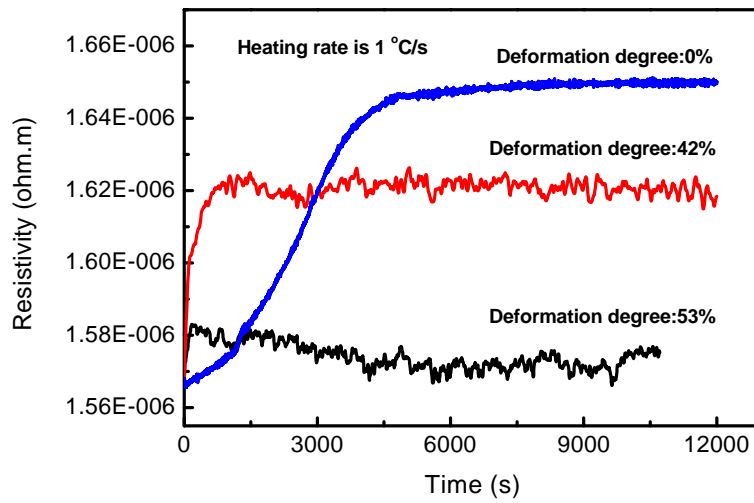


Figure 5-9 Resistivity variations versus holding time at 500°C for three different initial conditions and the heating rate of 1°C/s.

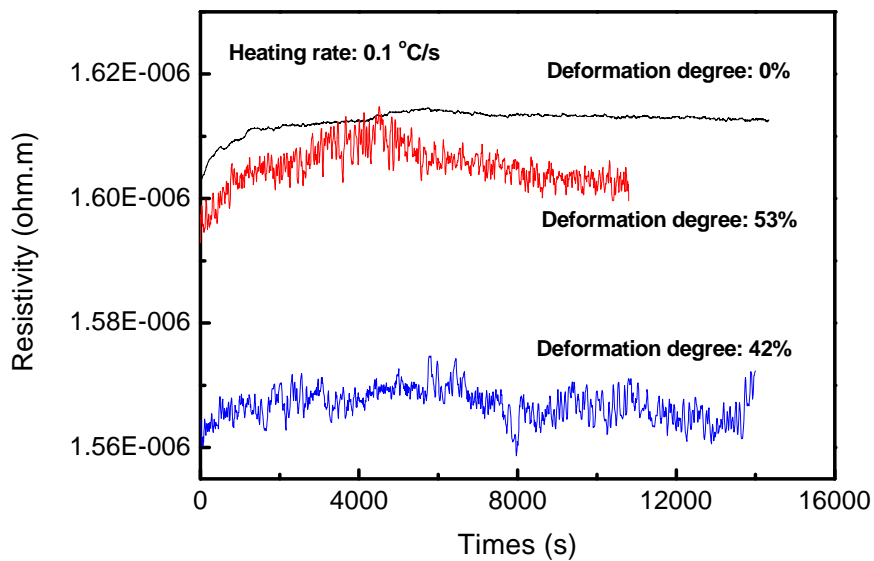


Figure 5-10 Resistivity variations versus holding time at 500°C for three different initial conditions and the heating rate of 0.1°C/s.

For 0.1°C/s (Figure 5-10), the main difference between the un-deformed specimen, and the specimens with 42% deformation and 53% deformation lies in the resistivity peak value. The resistivity peak value after 53% deformation is higher than that after 42% deformation.

V.2. Isothermal phase transformation kinetics

Assuming that the increase of resistivity is associated with the phase transformation amount, Figures 5-9 and 5-10 suggest that, room temperature deformation strongly affects the transformation kinetics during the heating stage and during the holding at the aging temperature. For the lower heating rates (1°C/s and 0.1°C/s) precipitation begins during the heating. Thus during the holding stage, the transformation will progress. The kinetics will thus not correspond to the complete isothermal transformation from 100% beta metastable to $\alpha+\beta$. For 42% deformation, and when the heating rate is 1°C/s , the phase transformation kinetics has a parabolic shape; the overall transformation process needs about 800s. For 0.1°C/s , the variations during holding are noisy, small and cannot considerably represent the phase transformation process.

Compared with phase transformation kinetics process in un-deformed specimen, room temperature deformation has rather high influences on the isothermal behavior. The kinetics of the isothermal a phase transformation is strongly increased; the time for which the transformation is completed is shortened by more than 90%. However the amplitude of resistivity changes is reduced.

For specimens with a prior deformation of 53%, the transformation kinetics for heating conditions of 10°C/s reveals again a parabolic shape, and the overall process needs only about 300s before transformation is finished. For 1 and 0.1°C/s , the amplitude of resistivity variations is low and noisy. Moreover a decrease in the resistivity is observed. We cannot express any transformation kinetics for these conditions.

In a general approach, we can attribute the acceleration of transformation kinetics to the increasing amounts of defects resulted from the deformation of the β grains. The

increase in the density of nucleation sites favors the nucleation of ω , α'' or α on the intra granular defects as well as the increased amount of boundaries.

V.3. Influence of deformation on microstructure evolutions.

Figure 5-11 shows the initial microstructure, before aging, i.e. the microstructure of the alloy after solution treatment in the beta range and plastic deformation at room temperature. Compared with the un-deformed state (Figure 3-7), the plastic deformation leads to defects in the grains and at grain boundaries, dislocation lines are clearly evidenced. For 42% deformation the average β grains size (about 100 μm) does not vary too much; for 53% deformation, defects are further increased. Moreover, fragmentation happens in some β grains.

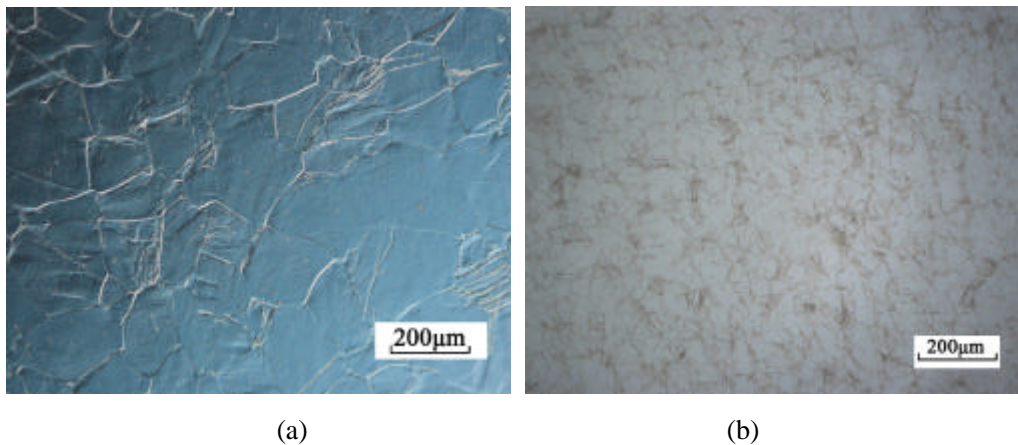


Figure 5-11 Microstructures of Ti-B19 alloy after beta solid solution treatment and followed by (a) 42% deformation; (b) 53% deformation

Figure 5-12a and 5-12b show the final microstructure of specimens aged 4h at 500°C (heating rate of 10°C/s) and with a prior deformation of 42 and 53% respectively; Figure 5-13 shows the XRD patterns (conventional laboratory characterization). The structure after aging at 500°C is a mixture of acicular α phase and β phase. The quantitative analysis of the X-ray diffraction results leads to an α amount of 41vol.% for specimen with 42% deformation and of 32vol.% for specimen with 53%

deformation (Table 5-1). The α volume fraction for the un-deformed specimen is 58%. The pre-deformation restrains the amount of α formed; the bigger the pre-deformation, the smaller the α phase amount.

Table 5-1 α phase amounts after 4h aging at 500°C for different heating rates and pre-deformation.

Heating rate	Volume fraction of α phase (vol.%)		
	Un-deformed	42% deformed	53% deformed
10°C/s	58	41	32
0.1°C/s	53	33	30

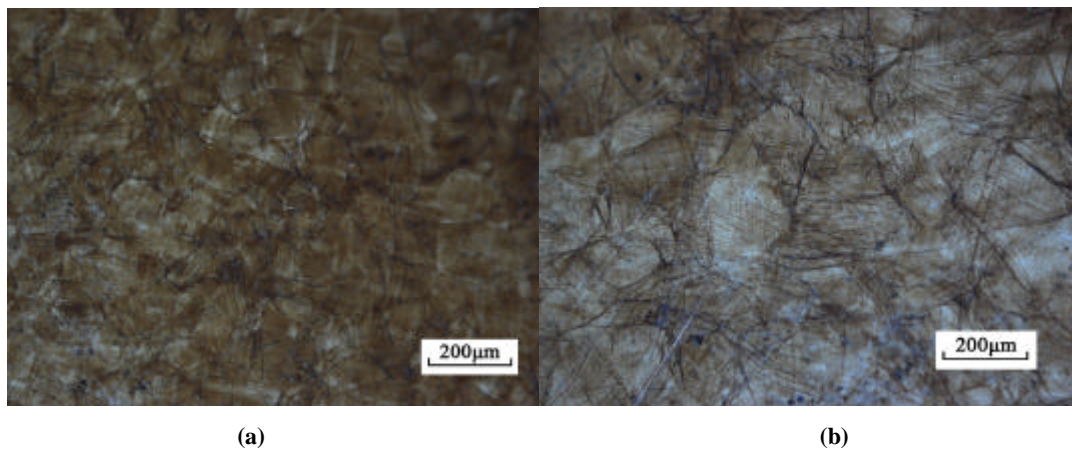


Figure 5-12 Microstructures after 4h aging at 500°C(rate of 10°C/s). (a) 42% deformation; (b) 53% deformation

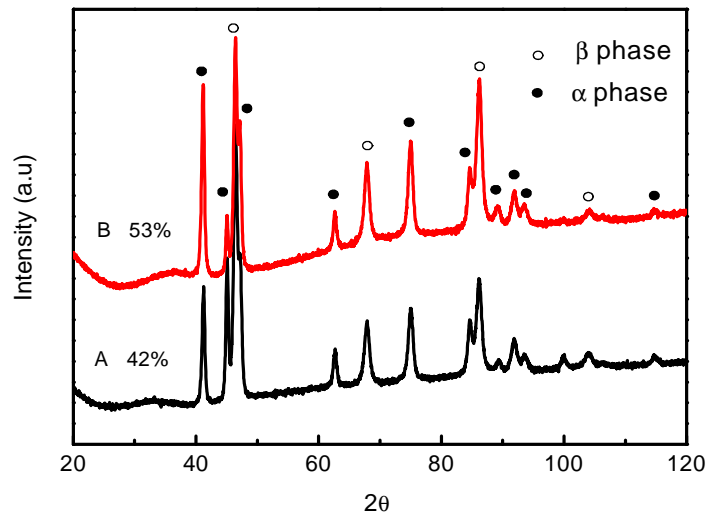


Figure 5-13 X-ray diffraction patterns after 4h aging at 500°C (rate of 10°C/s).

For the lower heating rates (1°C/s and 0.1°C/s), the analysis in 5.1.1 suggests that, pre-deformation has considerable influence on the phase transformation during heating (the resistivity curves present two stages, with a “V” shape) and the deformation amount influences mainly the temperature at the “V” shaped inflection point (Figure 5-4 and 5-5).

We thus can consider that, when heated at 1°C/s, the phase transformation sequence for 42% pre-deformation and 53% pre-deformation should be basically the same, and meanwhile, the microstructures should also substantially be the same. To further study the influence of room temperature deformation on the phase transformations during heating at 1°C/s, a specimen with 42% pre-deformation was heated at 1°C/s up to 500°C and quenched, and specimens with 53% pre-deformation were also heated at 1°C/s to 380°C and 500°C and quenched at those temperatures. Optical micrographs for the two deformed specimens (42 and 53%) heated at 1°C/s and quenched when reaching 500°C are shown in Figure 5-14. They reveal that acicular α phases exist at grain boundaries and on intra granular defects.

XRD pattern and TEM results are respectively shown in Figures 5-15a and 5-16a and b for specimen with 42% pre-deformation, quenched at 500°C. Those for

specimen with 53% pre-deformation and quenched at 380°C, are respectively given in Figures 5-15b and 5-16c and d.

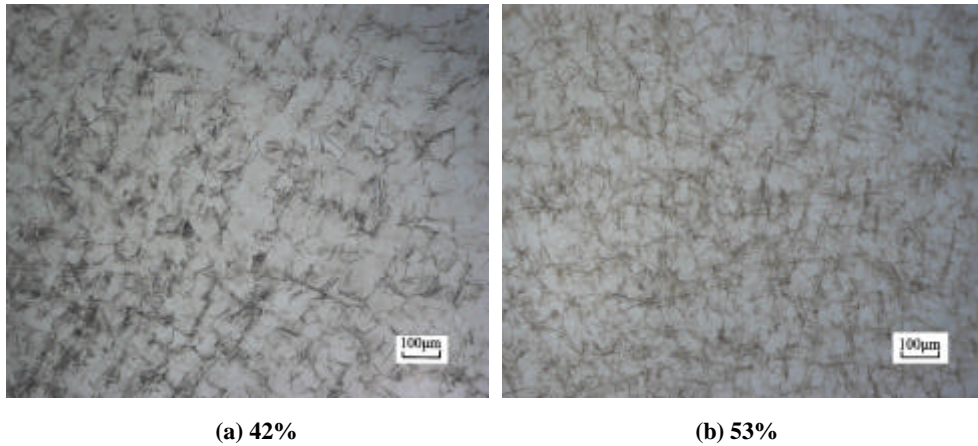
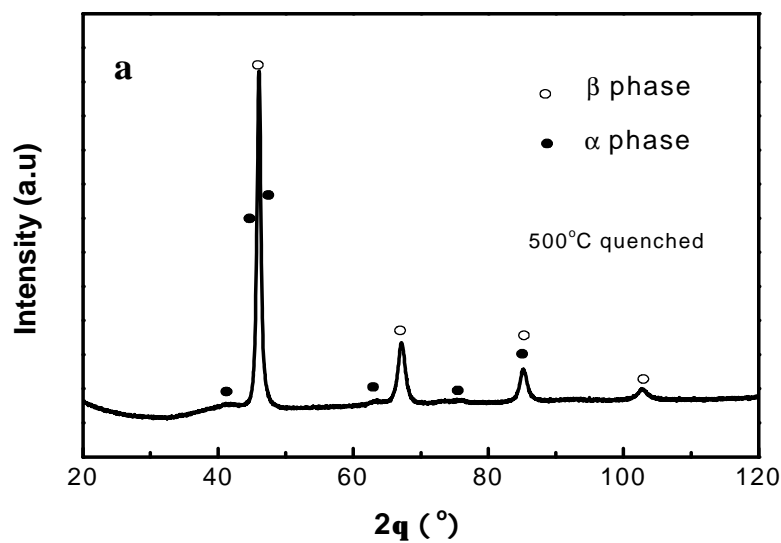


Figure 5-14 Microstructures after quenching at 500°C with a heating rate of 1°C/s (OM)

The TEM results suggest that $b \rightarrow w + a$ transformation happens to the deformed specimens during heated from room temperature to 500°C at the rate of 1°C/s. w is finely dispersed in the β grains (Figure 5-16a and c). One can mention that there is no evidence of the existence of w phase on the X-ray diffraction patterns due to the little amount of w phase. Moreover these patterns were obtained by a conventional X-ray source, with less sensitivity that the synchrotron source.



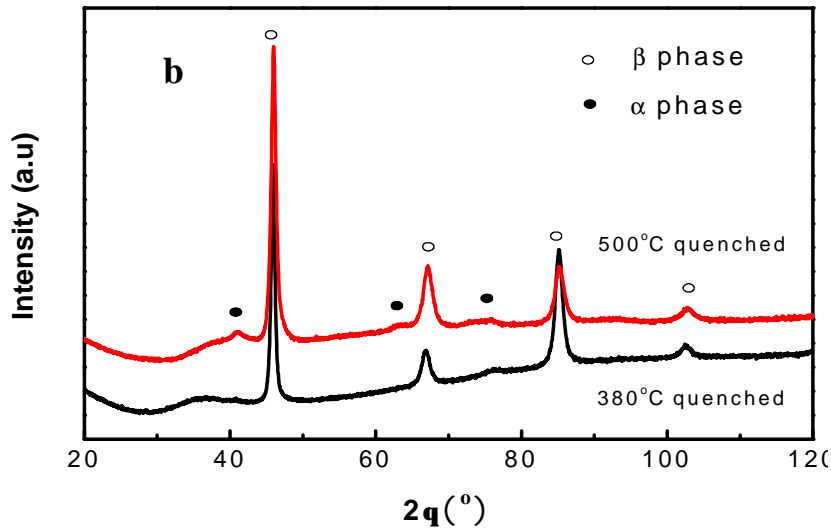


Figure 5-15 X-ray diffraction pattern for specimens heated at 1°C/s.
 (a) 42% deformation, 500°C quenched; (b) 53% deformation, 380°C and 500°C quenched.

The amount of α phase was determined from X ray data. For specimen with 42% pre-deformation and heated to 500°C, the α phase amount is 11 vol.%; the amount of ω is more difficult to estimate, since ω particles are small (diameter of 8nm) and the diffraction peaks are close to those of the β phase. For specimen with 53% pre-deformation, and heated to 500°C, the α phase amount is 6vol.%; equally, ω phase cannot be distinguished on X-ray diffraction pattern.

The present results allow confirming the precipitation during heating at 1°C/s, as suggested by the resistivity variations. Such precipitation did not occur for the undeformed specimen. The precipitation during heating is thus favored by the deformation at room temperature.

However, the lower amount of α phase when deformation amount increases suggests that pre deformation has restraining effects on the α phase amounts; the higher the pre-deformation is, the smaller amount of α phase transformation will be. This effect can be associated with the presence of internal stresses or the increase of strain energy associated with the transformation. Indeed, on one hand internal stresses are generated due to the strain incompatibilities between grains. Those stresses may be

unfavorable for further transformations. On another hand, the strain energy associated with the misfit stresses may be enhanced for the deformed specimens^[103].

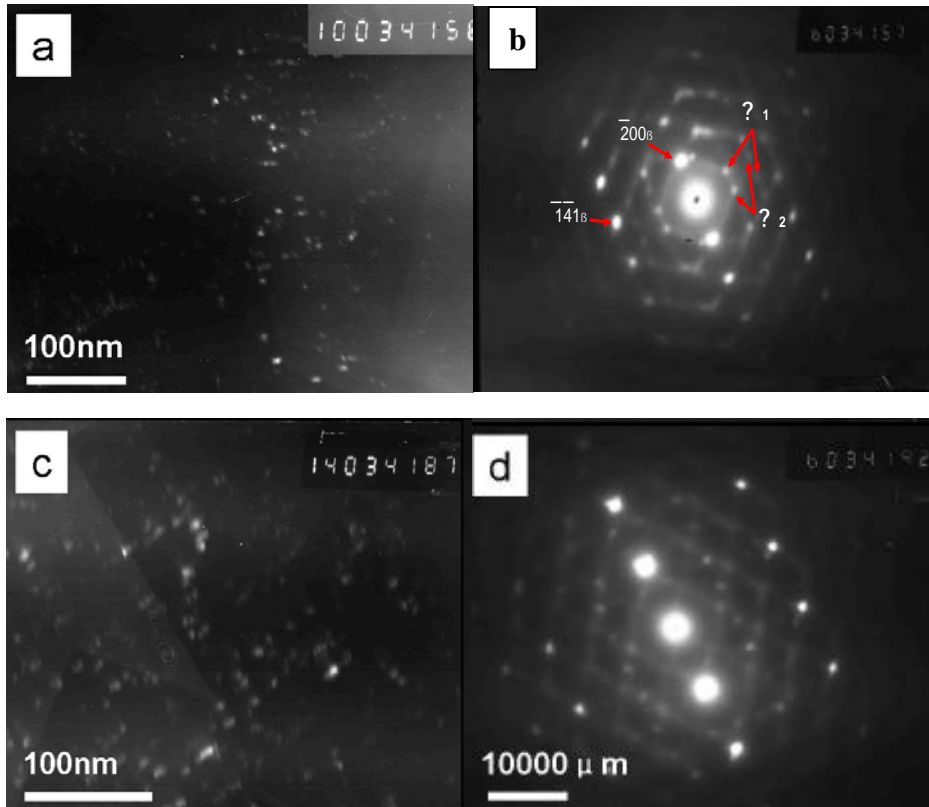


Figure 5-16 TEM dark field image (a) and diffraction pattern (b) of specimen with 42% deformation degree heated to 500°C at 1°C/s; TEM dark field image (c) and diffraction pattern (d) of specimen with 53% deformation and heated to 380°C at 1°C/s.

When heated at 0.1°C/s, the variations of resistivity with temperature appear for both deformation conditions in “V” shape (Figure 5-5) suggesting that the phase transformation sequence for specimen with 42% deformation degree and 53% deformation degree is basically the same. The resistivity variations were different for the undeformed specimen.

TEM observations were realized on specimen quenched during heating. Figure 5-17a (42% deformed quenched at 350°C) shows the dark field image with a selected diffraction spot of (014) and indicates the dispersed precipitates distribution in the parent phase in deformed specimens heated at 0.1°C/s. Figure 5-17b show the

electron diffraction pattern allowing identifying the precipitates as ? phase.

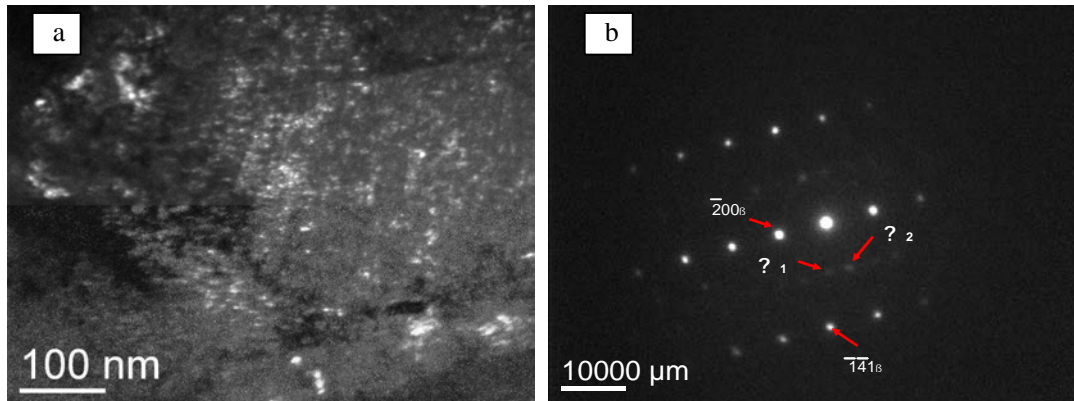


Figure 5-17: TEM dark field image (a) and diffraction pattern (b) of Ti-B19 alloy with 42% deformation degree when heated to 350°C at 0.1°C/s.

The precipitate size is around 5nm; since ? phase particles are rather fine and the quantity is limited, it is very difficult to observe their diffraction peaks on XRD (Figure 5-19a); only parent phase peaks observed.

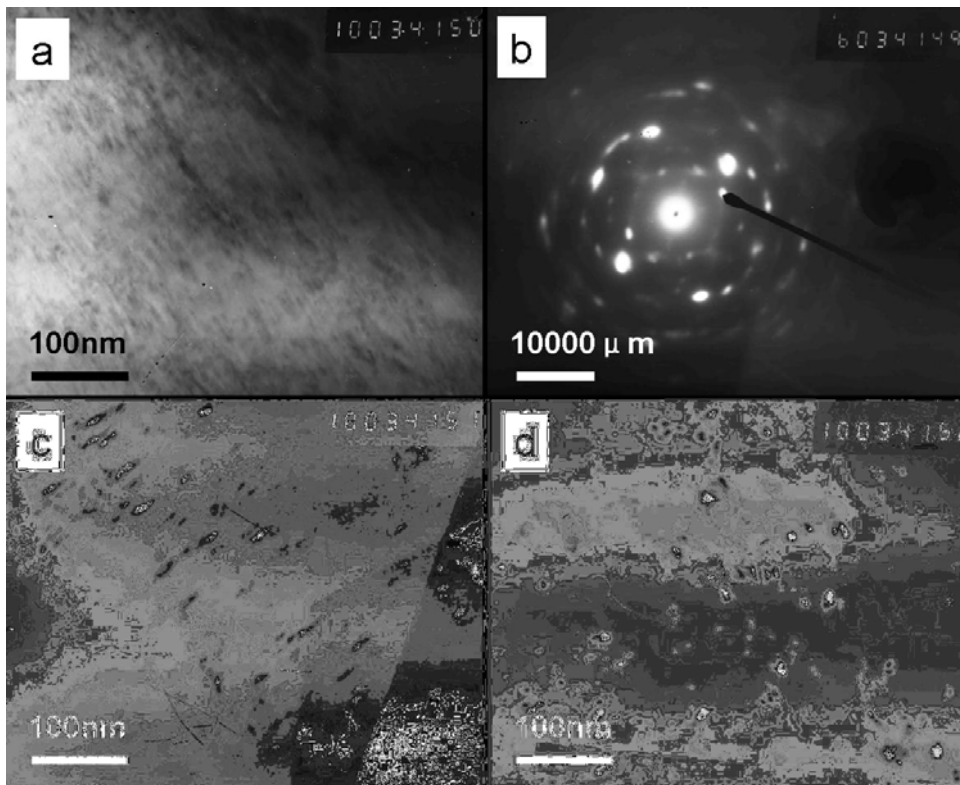


Figure 5-18: TEM bright field image (a), diffraction pattern (b) and dark field image (c, d) of Ti-B19 alloy with 53% deformation degree when heated to 500°C at 0.1°C/s.

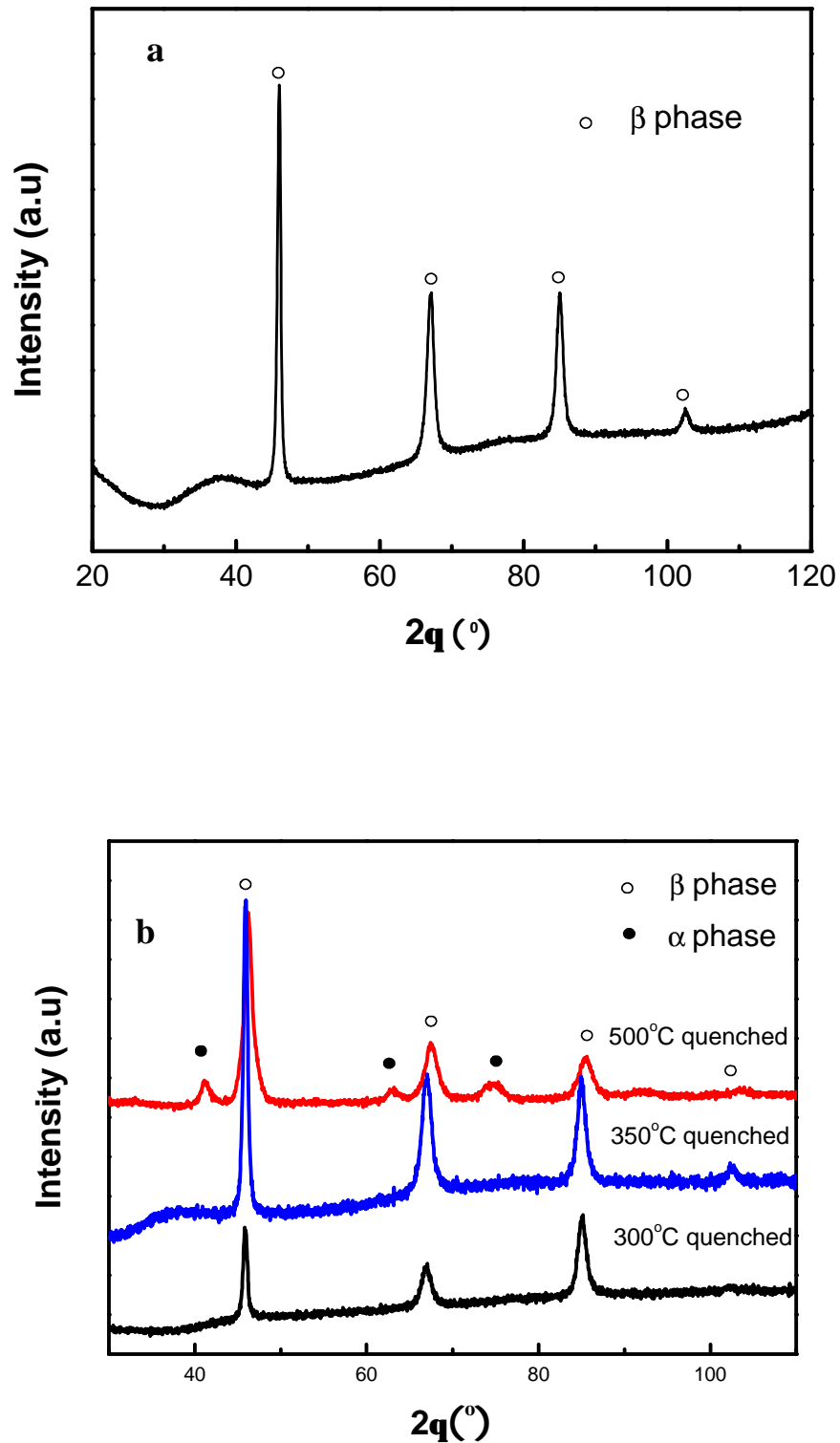


Figure 5-19 X-ray analysis results of quenched specimen during heating to 500°C at a rate of 0.1°C/s: (a) quenching at 350°C with 42% deformation degree; (b) quenching at 300°C, 350°C and 500°C with 53% deformation degree.

For specimens with 53% pre-deformation, XRD patterns obtained for specimens

quenched at 300°C, 350°C and 500°C are shown in Figure 5-19b. Diffraction peaks of the α phase are clearly observed for specimen quenched at 500°C, but for specimens quenched at 300°C, 350°C, the α phase peaks are absent.

The quantitative analysis leads to an α phase amount of 17 vol.% in the specimen quenched at 500°C. TEM micrograph (Figure 5-18c) suggests that the α phase morphology is acicular with a length of about 30nm and a width of about 4nm. Precipitates are parallel distributed, with a single orientation.

For the heating rate of 0.1°C/s, one could consider from the electrical resistivity curves that transformation is almost completed during the heating stage (increase of resistivity of about $6 \cdot 10^{-9}$ ohm.m on heating, while the increase is less than $2 \cdot 10^{-9}$ ohm.m during the isothermal stage). However, the amount of α phase determined for specimen (53% deformed) quenched at 500°C does not confirm this result. Indeed, only 50% of the total amount of α is formed during the heating stage until 500°C (considering that all results can be reproduced). The resistivity variations have thus to be considered carefully. Indeed, this property is sensitive to the transformation amount as well as to the defects amounts. Any changes in the defects structure could lead to a change in the resistivity value. Thus if recovery takes place during slow heating conditions as well as during aging, the resistivity variations will result from a combination of recovery and phase transformation. Further in situ characterizations should be conducted to analyze these results.

Table 5-2 α phase amount after aged at 500°C for time, heating rates and predeformation degree.

Heating and Aging condition		Volume fraction of α phase (Vol.%)		
		Un-deformed	42% deformed	53% deformed
0.1°C/s	500°C, 0min.	43	/	17
	500°C, 4h	58	41	32
1°C/s	500°C, 0min.	16	11	6

The amounts of α phase obtained for different deformation conditions are reported in

Table 5-2. These results confirm the restraining effect of the deformation on the amount of α phase formed. It would be interesting to further study the effect of the deformation, with additional experiments and a deep characterization by TEM of the phase morphologies in order to precise the role of the deformation.

V.4. Brief Summary

The results obtained show that pre-deformation of the beta metastable phase leads to rather high differences on the precipitation during aging.

1. During the heating stage, the resistivity variations with temperature are modified, namely for the heating rates of 1 and 0.1°C/s. For 10°C/s, the resistivity during heating presents a monotone decrease with the temperature increase; for 1°C/s and 0.1°C/s, the resistivity variations with temperature include two parts and appear in “V” shape. This is associated with the $\mathbf{b} \rightarrow \mathbf{a} + \mathbf{w}$ transformation. Meanwhile, deformation amount modifies the “V” shape inflection point temperature.
 2. The amplitudes of the resistivity variations during holding at 500°C are tightly related to the heating rate. For a pre-deformation of 42%, the higher the heating rate is, the higher the resistivity peak value will be; for 53% deformation, the resistivity peak value reaches the maximum value for specimen heated at 10°C/s; for heating at 1°C/s and 0.1°C/s, the resistivity variations with time are rather complex, but the curves are basically close to each other.
 3. Deformation has rather high influence on the kinetics of the isothermal evolutions. a phase transformation kinetics are considerably increased: no incubation period is observed, and the transformation time is shortened by over
-

90%. Microstructure observations have confirmed that pre-deformation results in distortion of metastable β grains. Defects in the grain and at grain boundaries are increased, and even cause some grain fragmentation. More favorable nucleation sites for precipitation of γ phase or α phase are provided and in consequence the precipitation kinetics is accelerated; when heated at rates of 1°C/s and 0.1°C/s , $\beta \rightarrow \alpha + \omega$ transformation happens in the heating stage; γ phase appears in particle shape, and α phase has a fine acicular morphology. Both phases are uniformly distributed in the parent grain.

4. Meanwhile, the pre-deformation restrains the α phase transformation, i.e. after 4h aging, the α phase amount is lower as the deformation amount increases. Similarly, during heating and for a same heating rate, the amount of precipitated alpha phase is lower for the higher pre-deformation amount. This decrease in transformation amount is related to the existence of internal stress caused by room temperature deformation and/or to an increase in the deformation energy associated with the transformation.

VI. PHASE TRANSFORMATION OF TI-B19 ALLOY DURING CONTINUOUS COOLING

The study of isothermal transformation (Chapter 3) provides reliable results for the effect of temperature, heating rate on the isothermal phase transformation kinetics, the microstructure evolutions of Ti-B19 alloy. However in fact, heat treatment processes of metal and alloys also include continuous temperature variations that influence the microstructure formation and in consequence the application properties of the alloys^[88,107]. During continuous cooling, the driving force of the phase transformation varies with time due, on one hand to the change in temperature (the driving forces increases as temperature decreases), and on another hand to the progress of the transformation (the driving force decreases as transformation progresses). The nature of the transformation and the transformation kinetics are thus dependent on the continuous cooling rate^[45]. Previous studies have shown that depending on the cooling rate, metastable β phase in Ti alloy can be transformed into stable α phase, or metastable phases as martensite α' (or α'') phase, β' phase or over-cooled (metastable) β ^[70,108,109]. In this chapter, we analyze the kinetics of phase transformation for different cooling rates (0.03~1°C/s) for the Ti-B19 alloy after solution treatment in the beta temperature range at 900°C for 10min. Kinetics evolutions are characterized by in situ electrical resistivity. Resulting microstructure are observed in order to establish the CCT curve for the continuous cooling process for the alloy.

VI.1. Influence of the cooling rate on the microstructure evolution in Ti-B19 alloy.

It has been mentioned that Ti-B19 alloy is a typical metastable β Ti alloy with rather good quenching penetrability, so that high-temperature metastable β phase can be maintained to room temperature even quenched with a cooling rate of 1°C/s . We have previously shown (Figure 3-7) that the microstructure observed for a cooling rate of 20°C/s is that of a completely β metastable phase without stable α phase. The microstructures obtained for lower cooling rates in the range 1°C/s to 0.03°C/s are shown as Figures 6-1a to 6-1e. For a cooling rate of 1°C/s no α precipitation is observed (Figure 6-1a). When cooling rate decreases, the amount of α phase increases. Cooling rates of 0.2°C/s and 0.1°C/s , lead mainly to the formation of α on the most favorable nucleation i.e. at the beta/beta grain boundaries. α grows and lamellar α Widmanstätten colonies are formed, parallel and with a same orientation. Such morphologies are also observed for 0.06°C/s . When decreasing the cooling rate, ((Fig.6-1d and 6-1e)) the growth of Widmanstätten colonies is favored and additional intragranular precipitation occurs. We can notice that even for a cooling rate of 0.03°C/s , the transformation is not completed. Indeed, some un-transformed matrix is still observable.

Different authors have studied the transformation behavior during continuous cooling process. They analyzed the resulting α phase morphologies in Ti alloys [95,101~103,108]. It was shown that the amount of Widmanstätten colonies as well as the amount of intragranular α phase is dependent on the cooling rates. For a constant total amount of α phase, the relative amount of intragranular α phase will be increased with the increase of the cooling rate, but on the contrary, the amount of Widmanstätten colonies will be decreased. In the present case, the amount of α

phase is not constant for the increasing cooling rates. It decreases as cooling rate increases.

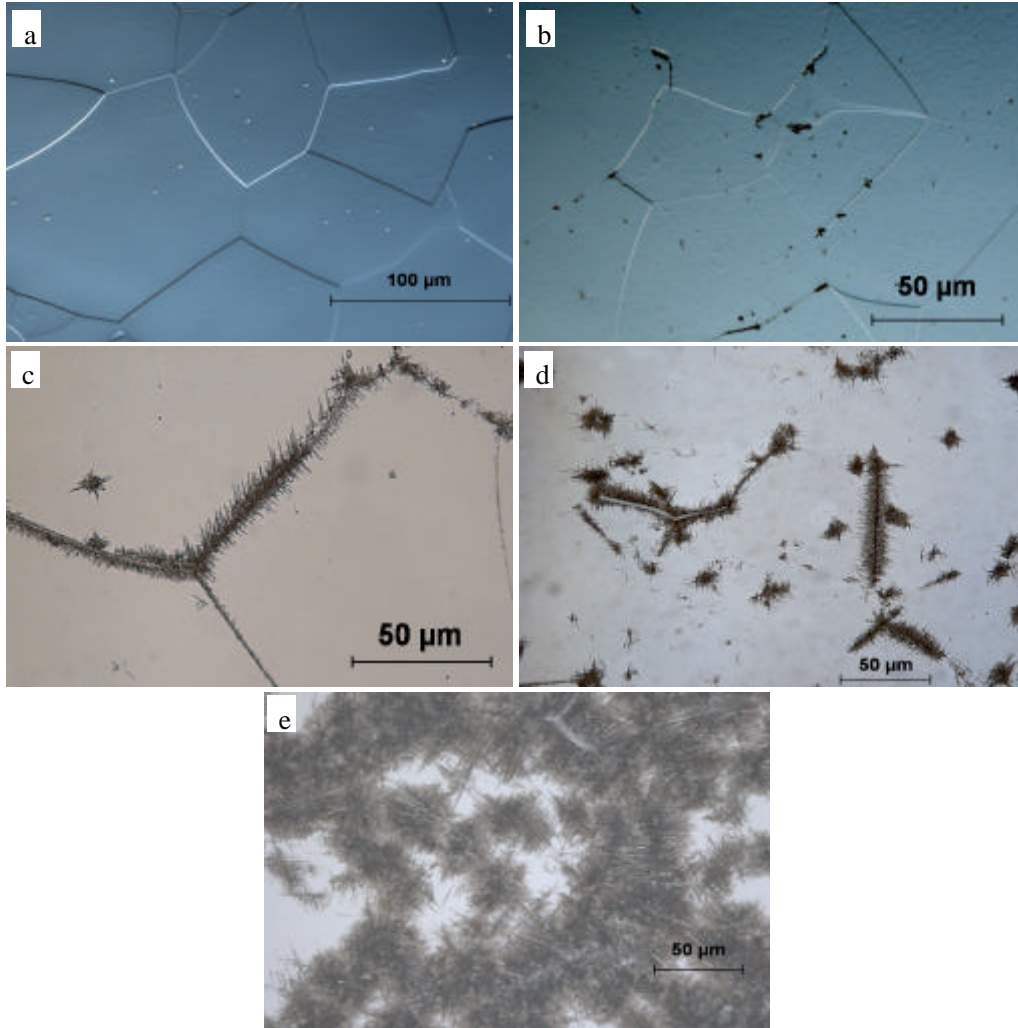


Figure 6-1 Microstructures (OM) of Ti-B19 alloy obtained after continuous cooling of 1? /s(a), 0.2? /s(b), 0.1? /s(c), 0.06? /s(d), 0.03? /s(e).

VI.2. Resistivity variations during continuous cooling.

In order to compare the behaviour during cooling, we have plotted Figure 6-2, the resistivity variations versus temperature for 5 different cooling rates. Two groups can be defined according to the cooling rate. For the lowest cooling rate (0.03°C/s), the

resistivity variations can be separated into three stages, while for the other cooling rates mainly two stages are evidenced. In the initial cooling stage (Stage I), the resistivity decreases while temperature decreases. This decrease is associated with the decrease of resistivity with temperature.

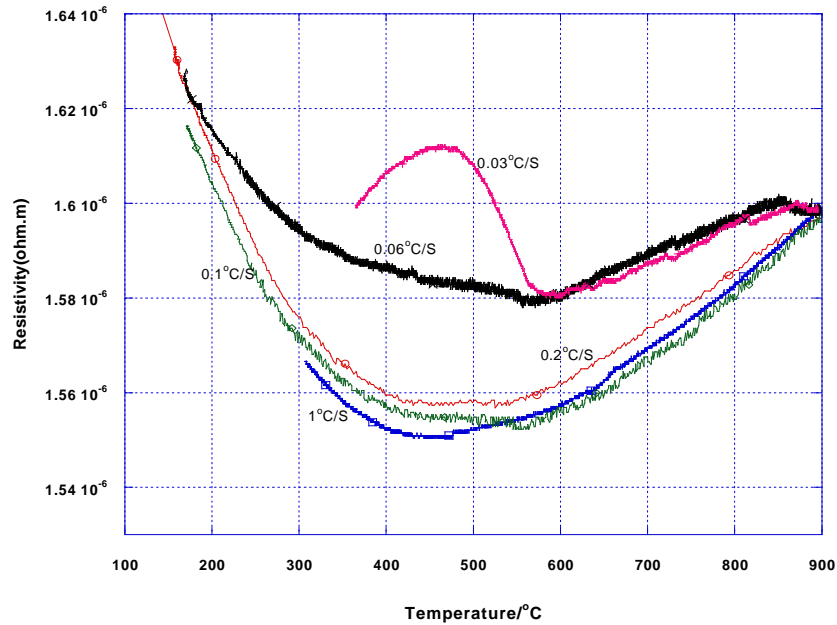


Figure 6-2 Resistivity variations of Ti-B19 alloy during continuous cooling for different cooling rates varying from 0.03 to 1? /s.

When thermodynamic and kinetics conditions allow phase transformation to occur, nucleation and growth of α starts; the increasing amount of α phase amount causes an increase in resistivity; the general expression is that the alloy resistivity during cooling rises quickly with temperature decrease; this stage is Stage II of the resistivity variations with temperature shown in Figure 6-2 for the cooling rate of 0.03°C/s and defined in Figure 6-3; when $b \rightarrow a + b$ phase transformation is almost finished, the alloy resistivity decreases again with the temperature; this is Stage III of the resistivity variations with temperature. Thus, for the cooling rate of 0.03°C/s, the beginning of the transformation occurs at 600°C, and the

transformation stops near 450°C.

For the higher cooling rates the behavior is different. Optical microscopy revealed that cooling at 1 and 0.2°C/s led to almost no transformation. Thus the resistivity variations for the metastable β without α formation results in a decrease of the resistivity as temperature decreases (stage I) followed by some increase in the resistivity at temperature lower than 450°C (as mentioned in chapter 3). For 0.06°C/s, a clear change in the slope (from negative to positive) is observed at 550°C. This change is associated with α formation in small amounts as shown in Figure 6-1d by OM. The small increase of resistivity can be associated with the amount of α precipitated. Comparing the two cooling rates (0.03°C/s and 0.06°C/s) shows that the beginning temperature is decreased, as cooling rate is increased, and the amount of α formed is decreased. For the higher cooling rates, the transformation may occur between 570°C and 430°C for 0.1°C/s and near 540°C-430°C for 0.2°C/s. The associated resistivity “increase” is extremely low.

Moreover, for the two lower cooling rates, the slopes of resistivity variations with temperature in stage I is lower than those for the higher cooling rates. These may be associated with some oxygen diffusion during the experiment that cannot be avoided and that leads to some change in the slope.

Resistivity variations and microstructure observations show that cooling rate influences the $b \rightarrow a + b$ phase transformation kinetics.

In order to further analyze the transformation kinetics, the evolutions obtained for 0.03°C/s are considered. The resistivity variations with time are shown Figure 6-3. The three stages previously defined are illustrated. The transformation range, that is Stage II where $b \rightarrow a + b$, occurs between points A and B. The variations of resistivity look rather similar to the resistivity variations with time in the isothermal

aging process.

In Figure 6-3, we consider that the curves in Stages I, II and III are respectively $R_1(t)$, $R(t)$ and $R_2(t)$. Similarly to the isothermal transformation, the resistivity variations are analyzed with the method used in Figure 3-4; that is to say, focused on Stage II of $b \rightarrow a + b$ phase transformation, the relative resistivity is $\Delta R(t)/R_1(t)$ and $\Delta R(t) = R(t) - R_1(t)$; $R_2(t)$ can be considered as the resistivity variations with time at the end of the transformation (when the transformation amount does not progress anymore). $\Delta R_{\max}(t)$ is the maximal resistivity change associated with the transformation. It is given by $\Delta R_{\max}(t) = R_2(t) - R_1(t)$.

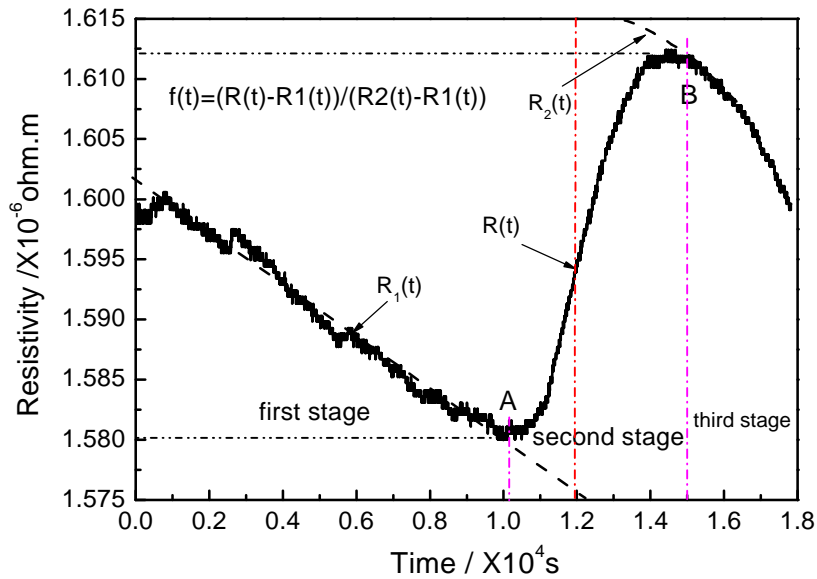


Figure 6-3 Resistivity variations with time during continuous cooling at 0.03? /s

As the cooling rate is constant, a linear relation exists between time t and the temperature T . The $b \rightarrow a + b$ phase transformation extent can thus be expressed as follows:

$$f(T) = \frac{R(T) - R_1(T)}{R_2(T) - R_1(T)} \quad (6-1)$$

For this relation, we can gain the transformation kinetics knowing $\Delta R_{\max}(t) = R_2(t) - R_1(t)$, and the relationship between ΔR_{\max} and the amount of phase formed. If for ΔR_{\max} the amount of α formed is the equilibrium one, the transformation progress is 1. We thus obtain the relationship between phase transformation degree and time during continuous cooling. We have used this method in order to get the kinetics of the transformation versus time for the cooling rate of 0.03°C/s . The result is shown in Figure 6-4. It can be observed that the phase transformation progresses with a similar regularity as for the isothermal phase transformation.

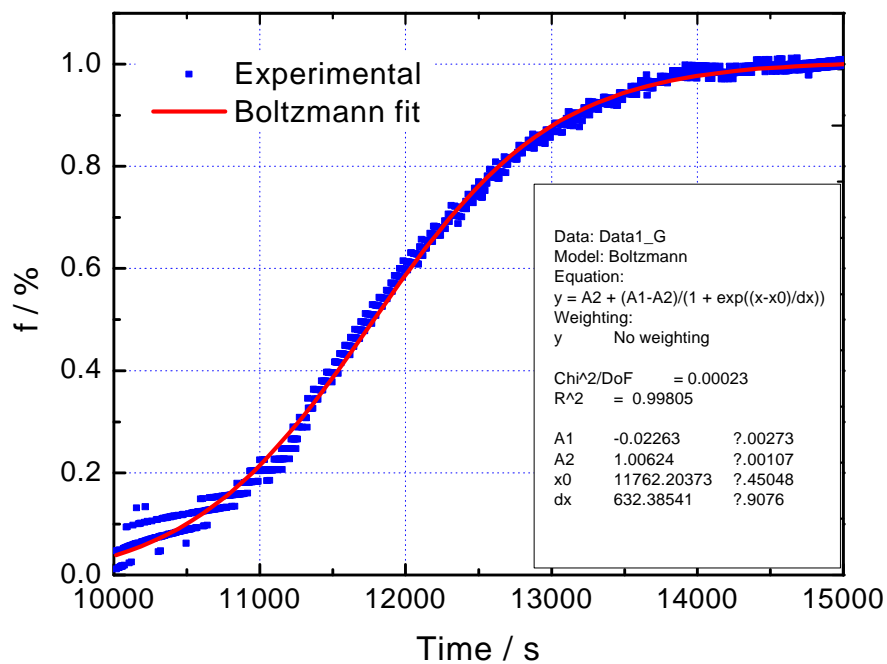


Figure 6-4 Phase transformation kinetics during continuous cooling from 900°C at 0.03°C/s .

VI.3. Establishment of phase transformation kinetics functions

During isothermal transformation and continuous cooling transformation, the kinetics of the transformation is a function of the nucleation rate and the growth rate, which depend both on temperature and transformation mechanisms. This leads to difficulties in description of the kinetics during continuous cooling. Figure 6-3 shows the regularity of the resistivity variations with time during continuous cooling; it suggests that, for the selected cooling rate, the continuous cooling process for Ti-B19 alloy can be understood as a superposition of several instantaneous isothermal phase transformation processes. Considering a simplified approach, each instantaneous isothermal process complies with the JMAK relationship, for which it is possible to analyze phase transformation kinetics with the integral method.

Based on this idea, Scheil's additivity principle^[107] is used for analyzing the phase transformation kinetics during continuous cooling; that is to say, additivity is considered for the incubation period ratio and for the phase transformation progress. This principle can be considered as follows: supposed that $t_a(T)$ is the duration for which the isothermal phase transformation progress reaches f_a at temperature T, t is the duration for which the phase transformation progress during continuous cooling reaches f_a , then, the additivity condition can be expressed as follows:

$$\int_0^t \frac{dt}{t_a(T)} = 1 \quad (6-2)$$

However, in the continuous cooling process of Ti-B19 alloy, $\mathbf{b} \rightarrow \mathbf{a} + \mathbf{b}$ phase transformation rate can be expressed as follows:

$$df / dt = h(T) / g(f) \quad (6-3)$$

$h(T)$ and $g(f)$ are respectively functions versus temperature and the new phase transformation extent; for any phase transformation pathway

$$\int_0^t h(T) dt = \int_0^t g(f_a) df = G(f_a) \quad (6-4)$$

As for the transformation progress f_a at a temperature T_a :

$$h(T) = G(f_a) / t_a(T) \quad (6-5)$$

If substituted it into Formula (6-4), the following function can be gained:

$$t_a(T)(df / dt) = G(f_a) / g(f) \quad (6-6)$$

Therefore:
$$g(f) / (t_a(T)(df / dT)) = G(f_a) \quad (6-7)$$

Put Formula (6-7) into Formula (6-2), and the following function can be gained:

$$\int_0^t \frac{dt}{t_a(T)} = \int_0^f \frac{df}{t_a(T)(df / dt)} = \int \frac{g(f)df}{G(f_a)} = \frac{G(f)}{G(f_a)} \quad (6-8)$$

Therefore, Formula (6-8) is a general formula based on the additivity principle, which leads to a general regularity between the phase transformation extent and the temperature changes.

When $\mathbf{b} \rightarrow \mathbf{a} + \mathbf{b}$ phase transformation happens during continuous cooling, α phase nucleates at different nucleation sites and the growth rate is dependent on the morphology of the precipitates ^[81,101]. For grain boundary nucleation, it can happen

at the β grain boundary or on spatial angle nucleus or on grain edges. The integral Formula (6-2) is dependent on the grain dimensions and the nucleation sites and growth conditions. According to the phase transformation theory with nucleation on different sites^[107], several expression of $G(f)$ were proposed:

$$\begin{aligned}
 &\text{For grain boundary nucleus formation } G(f) = -\ln(1-f)/2 \frac{A^B}{V} \\
 &\text{For grain edge nucleus formation } G(f) = \left[-\ln(1-f)/\mathbf{p} \frac{L^E}{V} \right]^{\frac{1}{2}} \\
 &\text{For spatial angle nucleus formation } G(f) = \left[-\ln(1-f)/\left(4\mathbf{p} \frac{\dot{N}^C}{V} \right) \right]^{\frac{1}{3}}
 \end{aligned} \quad \left. \vphantom{\begin{aligned} & \\ & \\ & \end{aligned}} \right\} \quad (6-9)$$

Wherein, f means the phase transformation volume ratio; A^B means the total area of grain boundaries at which the transformation occurring with nucleation sites on grain boundaries; V is the volume; L^E/V means the grain boundary edge length per unit volume; \dot{N}^C means the specific spatial angle nucleus formation rate, which is also named as the nucleus formation rate per spatial angle. Merge Formula (6-8) with a general expression of Formula (6-9), and the $\ln(1-f)$ expression of $\mathbf{b} \rightarrow \mathbf{a} + \mathbf{b}$ phase transformation progress for Ti alloy in the continuous cooling condition is as follows:

$$\ln(1-f) = \ln(1-f_a) \left\{ \int_0^t \left[\frac{dt}{t_a(T)} \right] \right\}^m \quad (6-10)$$

Wherein, m is related to the growth process and the geometry of the precipitates.

In these conditions, the kinetics of the phase transformation during continuous cooling can be expressed as follows:^[107]

$$f_a = 1 - \exp\{-K(T)t_a^m\} \quad (6-11)$$

Wherein, m is Avrami index (as the n in isothermal transformation); the phase transformation rate constant $K(T)$ depends on the temperature and is as follows:

$$K(T) = K_0 \exp\left(-\frac{E}{RT}\right) \quad (6-12)$$

Put Formula (6-11) into Formula (6-10), the following function can be gained:

$$\ln(1-f) = \left[-K(T)t_a^m \left[\int_0^t \frac{dt}{t_a(T)}\right]^m\right] \quad (6-13)$$

That is to say,
$$\ln(1-f) = \left[-K(T)\left[\int_0^t dt\right]^m\right] \quad (6-14)$$

Therefore, the $\mathbf{b} \rightarrow \mathbf{a} + \mathbf{b}$ phase transformation progress during continuous cooling can be expressed as follows:

$$f = 1 - \exp\left\{-\left[K_0 \exp\left(-\frac{E}{RT}\right)\right]\left[\int_0^t dt\right]^m\right\} \quad (6-15)$$

From results in Chapter 3, we can estimate a mean activation energy for the transformation $E= 4.17415 \times 10^5$ J/mol and the phase transformation frequency factor $K_0= 9.5454 \times 10^{17}$. As transformation proceeds only for temperatures lower than T_β we express the temperature variations versus the time variations and taking T_β for Ti-B19 alloy equal to 1033K. Therefore, it is possible to gain the following relationship between the continuous cooling phase transformation progress and the time t (temperature T) as well as the cooling rate with Formula (6-15):

$$f(t) = 1 - \exp \left\{ - K_0 \left(\int_0^t \exp \left(- \frac{E}{mR(1033 + C_v t)} \right) dt \right)^m \right\} \quad (6-16)$$

Wherein, C_v is the cooling rate. This expression does not take into account any change of the equilibrium amount of alpha with temperature. If the maximal amount of α phase is nearly constant in a given temperature range, the approach can be used. Since the experimental data are limited, it is necessary to estimate the magnitude of Avrami index m , in order to further analyze the phase transformation kinetics during continuous cooling. Generally speaking, in a certain temperature range, m value is close to n value obtained for isothermal transformation kinetics. It can be observed in Figure 6-2 that the starting transformation temperature is about 600°C, therefore, the n values of isothermal transformation at 600~700°C are used. We have obtained at 600°C a value equal to $n= 1.3$. Therefore, the Avrami index in the continuous cooling process is $m= 1.3^2$.

Several calculations have been made using relation (6-16) for different cooling rates and different m values. They are developed in appendix 1.

The calculated transformations kinetics for 0.03°C/s and $m=1.3$ is given Figure 6.5 and is compared to the experimental results.

Quite similar evolutions are obtained for the calculated and measured kinetics. The duration of the transformation is nearly the same as well as the progress of transformation versus time.

For the calculated results, transformation begins very early, at the beginning of the cooling under T_β . Such behavior is not observed experimentally. It results from not

² We must emphasize that we take data that were obtained for precipitation during aging. We make thus implicitly the hypothesis that the mechanisms and kinetics of nucleation and growth are similar for continuous cooling and isothermal transformation during aging.

taking into account the incubation period independently. When analyzing these results with corresponding temperature variations, discrepancies are however obtained between experiment and calculation. Indeed, for calculation results, 10% of transformation occurs at 715°C (1500s) and 50% at 685°C. Experimental resistivity variations do lead to noticeable amounts of transformation at these temperatures. Moreover, for the calculated kinetics, the end of transformation is 620°C.

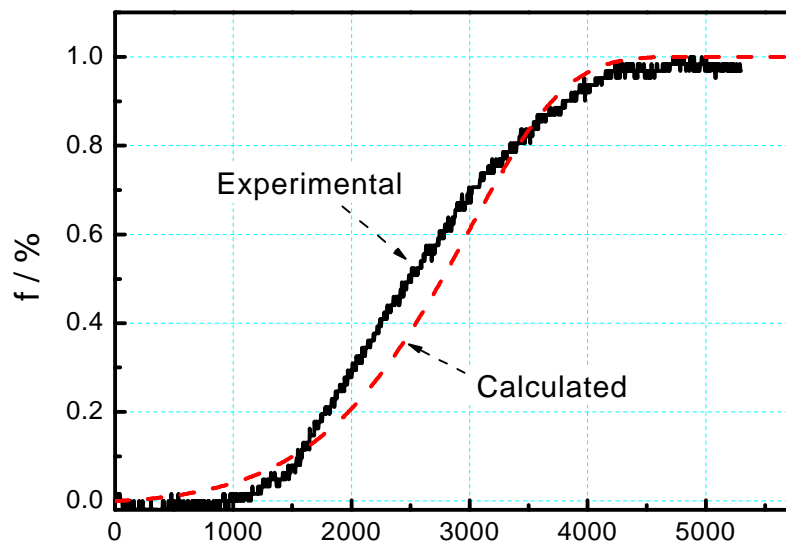


Figure 6-5 Comparison between the calculated and experimental results of phase transformation kinetics for Ti-B19 alloy during continuous cooling from 900°C at 0.03°C/s.

Thus if the transformation progress versus time have nearly the same trends, differences exist in the time/temperature scale. The differences can be attributed on one hand to the fact that the incubation period is not taken into account independently, and also that the data that have been used correspond to transformation on aging. Moreover, the model used is a global model and does not taken into account all the transformation details. Additional studies have to be performed both for experiments and modeling. For experiments, it would be necessary to obtain transformation kinetics at lower cooling rates, as well isothermal

kinetics after direct quenching from the beta temperature range. For modeling, calculations should be realized taking into account incubation time and transformation progress independently, and new developments should allow calculating the volume amount of α phase.

VI.4. Brief summary

- 1) Transformation of Ti-B19 alloy during continuous cooling from the β phase temperature range occurs by nucleation and growth. For the cooling conditions studied, the preferential nucleation sites of α are β grain boundaries. With the decrease of the cooling rate, the growth of the α phase nucleated at grain boundaries is favored; meanwhile, nucleus formation starts on intracrystalline sites, so that the α phase quantity is increased. According to test observations, the critical cooling rate of α phase formation is about 1°C/s . Even, poor transformation amounts are obtained for cooling rates varying from 0.2°C/s to 0.03°C/s .
- 2) Using Scheil superposition principle and JMAK functions, the phase transformation kinetics during continuous cooling has been analyzed for Ti-B19 alloy. The following function has been proposed to describe the phase transformation kinetics:

$$f(t) = 1 - \exp \left\{ - K_0 \left(\int_0^t \exp \left(- \frac{E}{mR (1033 + C_v t)} \right) dt \right)^m \right\}$$

Wherein, when the cooling rate is smaller than 0.08°C/s , $m=1.3$. The equation allows describing good trends for the evolutions of transformation progress with time, but transformation temperature range is too high.

VII. RELATIONSHIPS BETWEEN MICROSTRUCTURE AND MECHANICAL PROPERTIES OF TI-B19 ALLOY

Ti-B19 titanium alloy is a new β metastable alloy that should have both high strength and reasonable plasticity. In order to design the optimal treatment, it is essential to establish the relationships between microstructure and mechanical properties. In quenching and aging processes, the phase transformations sequences of Ti-B19 alloy are rather complicated. In order to gain a comprehensive behavior of the properties, we characterized the mechanical properties for specimens obtained after controlled treatments. In this thesis, main concerns include influences of volume fraction, shape, distribution and particle size of the formed phase against mechanical characteristics. Chapter 3 covers the microstructure developments of Ti-B19 titanium alloy after isothermal aging in the temperature range of 300°C-700°C. The research in this chapter focuses on the relationships between the microstructures formed during aging, and the tensile properties of Ti-B19 alloy determined at room temperature.

VII.1. Mechanical characteristics of Ti-B19 alloy after solution aging

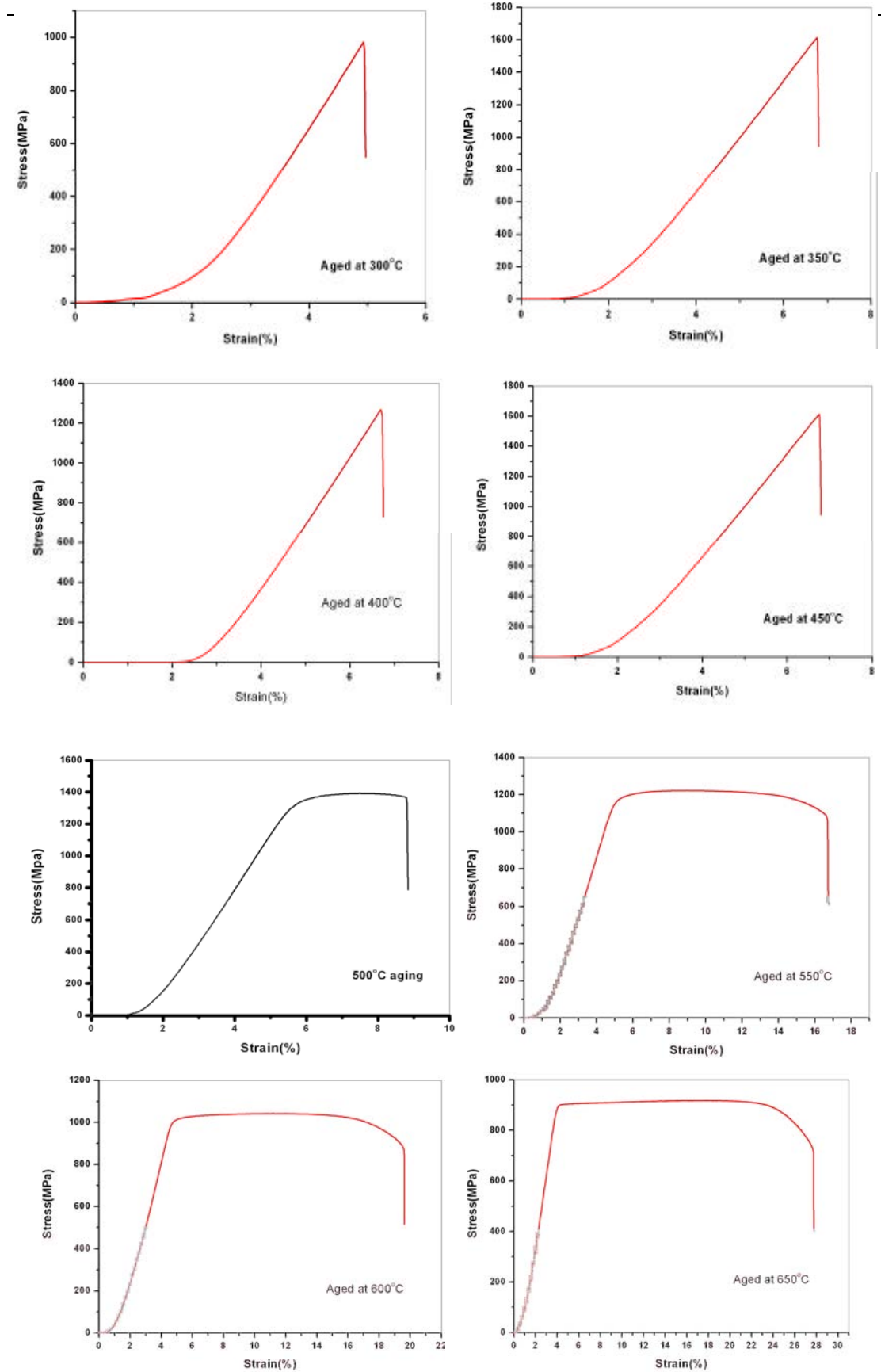
Figures 7-1 show the engineering stress strain curves got from tensile tests of different specimens that were aged at different temperatures after solution treatment at 900°C for 10min and further quenching. Tensile tests were done using the INSTRON 5581 testing machine. The engineering strain is calculated from the relative value, i.e. elongation divided by the length of designed standard working

distance. The elongation is obtained by the measurement of the machine. Nevertheless, the plastic elongation at failure can be determined taking into account the elastic deformation of the specimen and the machine. The testing results lead to the yield and ultimate strength (respectively σ_s and σ_b) as well as to the plastic elongation at failure (δ_s) and the area reduction (Ψ).

The stress-strain curves obtained (Figures 7-1) show that for specimens aged at 300°C, 350°C, 400°C and 450°C failure occurred in the elastic deformation range. For specimens aged at temperatures equal or higher than 500°C, the stress-strain curves present the elastic and plastic ranges. The changes in behavior are dependent on the nature, amount and size of the phases present after aging.

The variations of tensile strengths (yield strength σ_s and ultimate strength σ_b) obtained for specimens aged at different temperatures ranging from 500 to 700°C are given Figure 7-2. The values obtained after aging at temperatures ranging between 300~450°C are not included due to the brittle failures obtained. For aging temperatures higher than 500°C (as shown in Figure 7-2), a constant decreasing in the tensile strength with the aging temperature increasing is obtained. For these aging temperatures, only α and β phases are present. The changes in mechanical properties are thus tightly related to the amount and morphologies of the two present phases. With the increase in aging temperature, the volume fraction of α phase is decreased, and the width of the α precipitates is enlarged; this will result in a decrease in the tensile strength and an increase in the elongation (Figure 7-3, discussed later). The relationship between the tensile strength and the volume fraction of alpha phase will be further discussed in section 7.2.

Phase transformations and microstructure evolutions in metastable beta titanium alloy Ti-B19



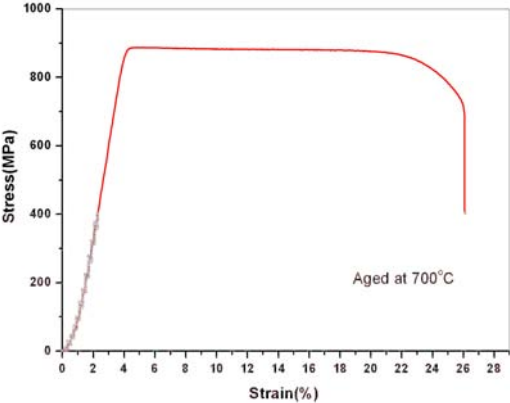


Figure 7-1 Stress-strain curves of Ti-B19 alloy specimens aged at different temperature

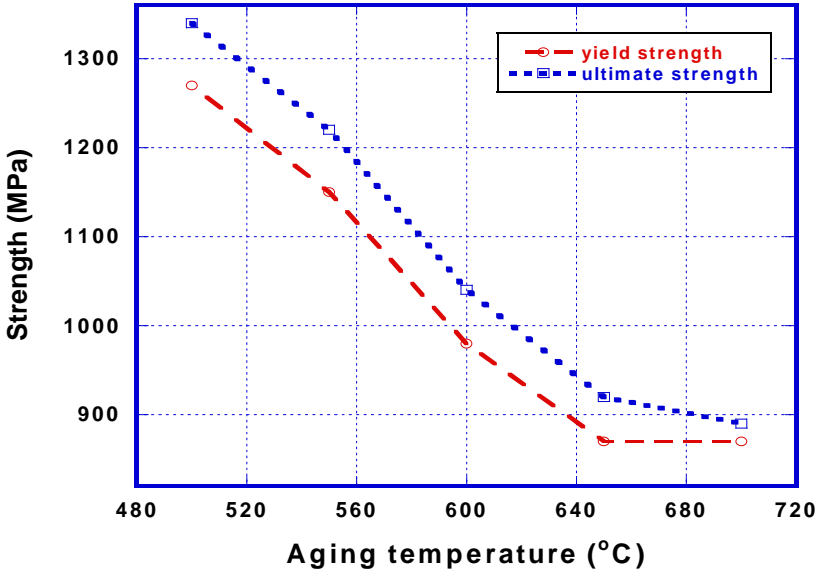


Figure 7-2 Variations of tensile strength with the aging temperature

The variations of the plastic elongation as well as the area reduction of Ti-B19 alloy as a function of the aging temperature (500~700°C) are given in Figure 7-3. It can be seen that when the aging temperature increases, ductility of the alloy is increased obviously as a whole. This is also mainly due to the microstructure evolutions in those temperatures, such as the volume fractions, the size and the morphologies etc. (shown in Chapter 3) as we mentioned above.

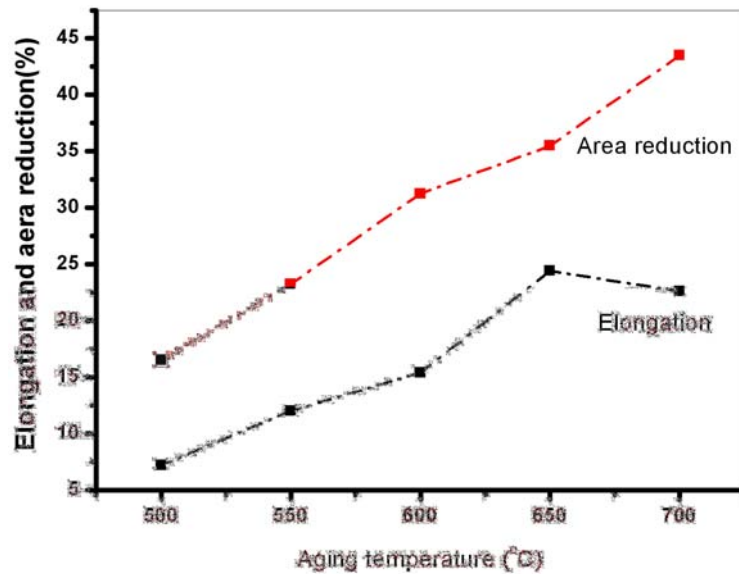


Figure 7-3 Variations of elongation and area reduction as a function of the aging temperature

If we analyze the changes of tensile strength and elongation simultaneously, we can observe that the alloy strength reaches the maximum when the aging temperature is 450°C , while the plasticity is rather poor; when the aging temperature is higher than 500°C , the strength decreases and the plastic elongation increases. When the aging temperature is in the range of $510\text{--}540^{\circ}\text{C}$, a nearly good compromise between ductility and high tensile strength is obtained as shown by the additional experiments for specimens aged between $510\text{--}540^{\circ}\text{C}$. The stress-strain curves are shown in Figure 7-4, and the corresponding relationship among the yield strength, elongation and aging treatment temperature are given in Figure 7-5

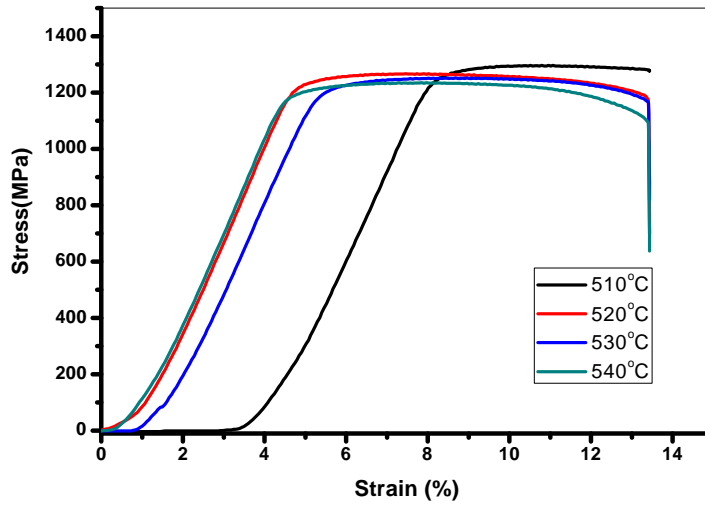


Figure 7-4 Experimental stress-strain curves of Ti-B19 alloy for aging temperatures of 510~540°C

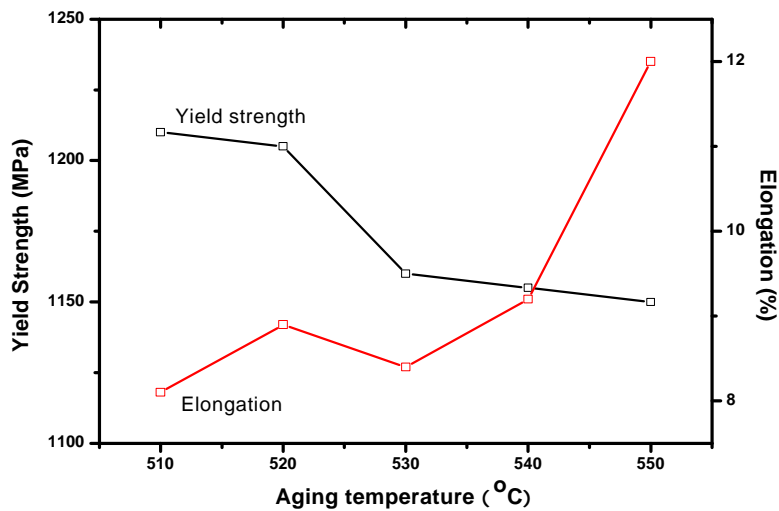


Figure 7-5 Variations of yield strength and elongation with aging temperature (510~550°C) of Ti-B19 alloy

VII.2. Influences of volume fraction of precipitated phases on mechanical characteristics of Ti-B19 alloy.

For aging temperature of 300°C and 350°C, the mechanical properties of poor ductility and higher strength are related to the presence of isothermal ω phase formed during the aging treatment. Figure 7-1 suggests that the alloy strength and

plasticity are rather good after 20h aging at 300°C. The high strength can easily be understood. From Figure 3-10 in Chapter 3, it can be seen that the volume fraction of ω phase is about 27%; wherein, ω phase appears as spherical precipitates with a size of about several nanometers, uniformly dispersed in the matrix. Since the ω particles are fine and dispersed, they will act as obstacles for dislocations motion, thus leading to an increase in the tensile strength. The good ductility is surprising considering the literature results. For specimen aged 20 hours at 350°C, the three following phases are present: ω phase, α phase and β phase; the volume fraction of ω phase is decreased to about 5%, and the volume fraction of α phase is about 13%; wherein, ω phase is distributed uniformly and appears in particle shape; but α phase is mainly distributed within the β grain by dispersed fine acicular shape. For that aging temperature, the failure has a brittle character.

Micrographs of the fractured profiles for the two aging temperatures are given in Figure 7-6. It is generally thought that ω phase might lower toughness and ductility, but can increase the alloy's hardness. The work in this thesis also suggests that the ω phase in dispersed distribution in the matrix can take certain effects in intensifying the tensile strength and plasticity of the alloy; however, when ω phase further grows and starts to transform into α phase, the tensile strength will increase considerably and the ductility will decrease.

When the aging temperature is higher than or equal to 400°C, the microstructure after aging is a mixture of α'' and/or α phases and β phase. For the temperatures of 500°C, the microstructure is a mixture of α and β phases. The mechanical characteristics of the alloy relates to volume fraction, shape, distribution and size of α (possibly α'') phase.

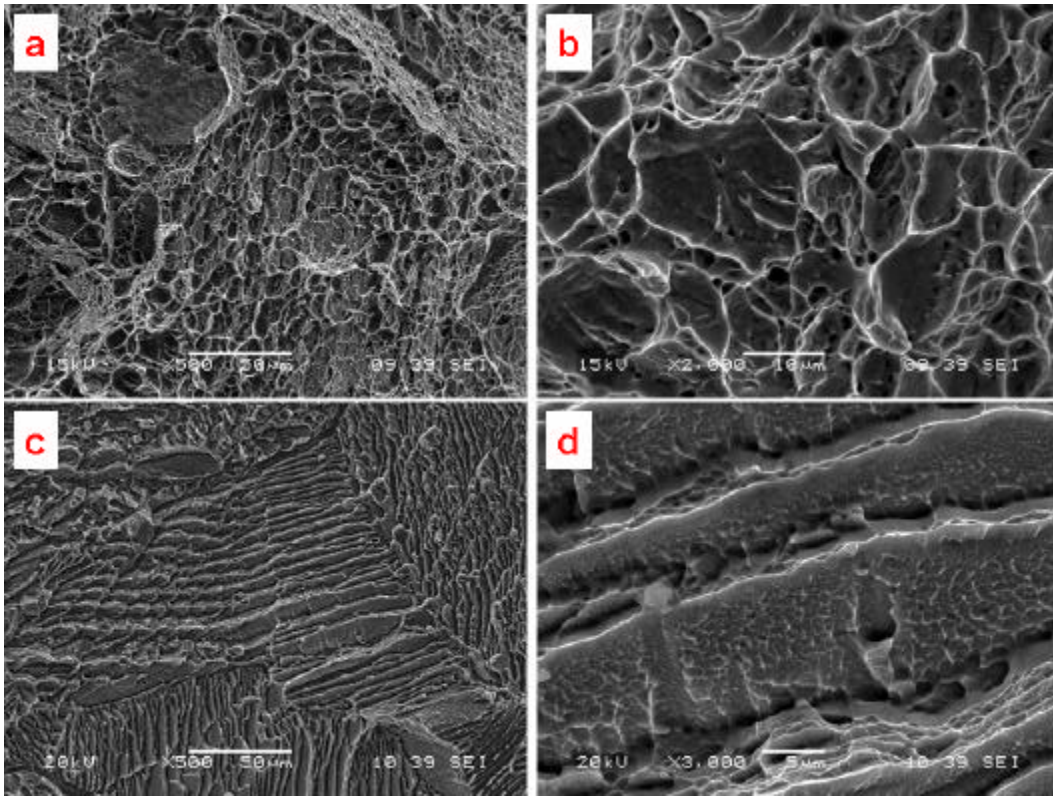


Figure 7-6 Fractured profiles of alloy after 300° and 350° aging
(a) 500° -300° (b) 2000° -300° (c) 500° -350° (d) 3000° -350°

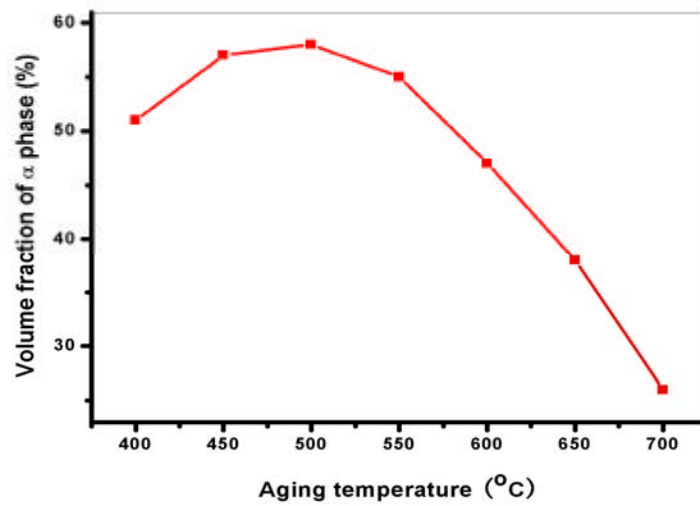


Figure 7-7 change curve of a phase volume fraction with aging temperature

The variations of α phase volume fraction with aging temperature are shown Figure

7-7. The maximal α volume fraction is obtained at 450-500°C. Due to kinetics reasons, when the aging temperature is 400°C, the transformation amount is lower than the maximum amount that can be formed at this temperature. For aging temperatures higher than 500°C, α transformation volume is decreased for thermodynamic reasons.

Figure 7-8 shows the variations of yield strength and elongation as a function of the α (possibly α'') volume fraction obtained after aging at temperatures in the range from 550°C to 700°C. For the same reason mentioned in section 7.1, the other aging temperatures are not included. The yield strength and the elongation at failure have a very tightly relationship with the volume fraction of precipitated α phase. It can be seen that the yield strength of Ti-B19 alloy is increased from 870MPa to 1150MPa with the increase of α volume fraction from 25 to 55%. At the same time the elongation decreased from about 20% to 10%. When α phase volume fraction is between 26 and 38%, the yield strength is nearly constant; but, when α volume fraction is higher than 38%, the strength increases rapidly, and the corresponding elongation also decreased quickly. These changes agree quiet well with the common rules in titanium alloys.

Figure 7-9 shows the micrographs of the fracture surface of the specimen aged at 400°C and 550°C. After 18h aging at 400°C, numerous acicular precipitates are formed, with different arrangements. Some precipitates are aligned in certain directions to form “tire-shaped” patterns, and α fine acicular precipitates are formed with an angle of 60°. These special morphology and arrangement can strongly limit the dislocation motion; therefore alloy strength and hardness are rather high while plasticity and toughness are rather low. It can be implied from Figures 7-9a and b that, for specimen aged at 400°C, brittle and trans-granular fractures are observed. For the specimen aged 4h at 550°C, the fracture surface profiles in Figure 7-9c and d show a very good toughness, which correspond to the elongation of 12%.

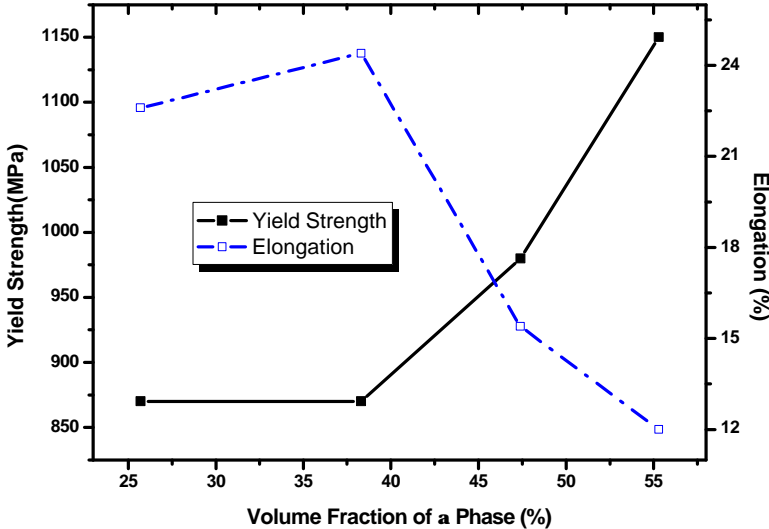


Figure 7-8 Variations of yield strength and elongation versus α phase volume fraction obtained after different aging temperatures.

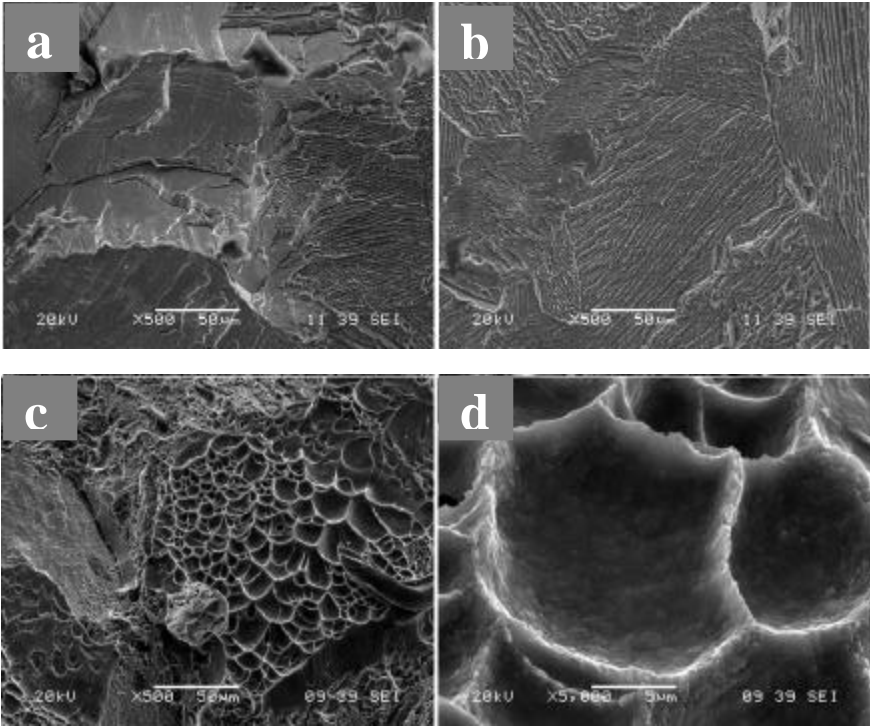


Figure 7-9 Fractured profiles of alloy after 400°C and 550°C aging
(a) 500°C - 400°C (b) 500°C - 400°C (c) 500°C - 550°C (d) 2000°C - 550°C

The results show that the best compromise for the mechanical properties concerning strength and ductility can be obtained for aging temperatures of 500~550°C. The volume fraction of α phase is maintained around 55%, after treatment at those temperatures, the microstructure is composed of α phase and β phase; wherein, α phase appears in acicular shape and distributed inside the β grain. Precipitates are parallel arranged, or with mutual-intercross in beta grain boundaries; meanwhile, the size of α phase is a little increased when increasing the aging temperature.

Anyway, additional work should be done on the relationship between microstructure and properties, in order to relate the volume fraction, size, distribution of precipitates, and strength and ductility.

VII.3. Summary

- 1) This chapter focuses on characterization at room temperature of mechanical properties of Ti-B19 specimens aged at different temperatures. The results obtain show that the strength of the alloy reaches the maximum value when the aging temperature is 450°C. Meanwhile, the ductility is rather poor. At the temperature above 500°C, as the aging temperature increases, the alloy strength decreases, but the elongation increases. The best compromise is obtained for aging temperature varying between 500-550°C. Further study suggests that, when the aging temperature is around 510~530°C, the best balance of the strength and ductility (the yield strength is about 1200MPa, and meanwhile the elongation keeps above 8%) can be obtained.
- 2) Aging in the range of 300-350°C, leads to a fine ω phase homogeneously distributed in the matrix. These precipitates increase the tensile strength of the alloy; but make the ductility worse.

3) When aging temperature is near 400-450°C, the alloy microstructure after aging is a mixture of α (or α'') phase and β phase. For these temperatures, the very thin size of α precipitates leads to a high tensile strength and a poor ductility. Mechanical characteristics relate tightly to the volume fraction, shape, distribution and size of the α phase, especially when the aging temperature is above 500°C. In general, when α transformation volume fraction is maintained at around 55%, the characteristics of the alloy are rather good and a good compromise is obtained.

CONCLUSIONS

The phase transformation kinetics, microstructure evolutions as well as the nucleation and growth conditions of metastable β titanium alloy Ti-B19 have been studied in the present work by several methods as in-situ electric resistivity measurements, synchrotron X-ray diffraction, SEM, TEM, etc. Primary conclusions are as follows:

1. The isothermal phase transformation kinetics and microstructure observations have been studied systemically in Ti-B19 alloy during aging at temperatures ranging from 300°C to 700°C. The results indicated that: at 300°C/20h aging treatment, only ω phase precipitated with a volume fraction of 27%; additional treatments at longer times allow to precise the sequence of metastable β phase decomposition that is $\beta \rightarrow \omega + \beta \rightarrow \omega + \beta + \alpha \rightarrow \alpha + \beta$. The increase in aging temperature to 350°C gives a direct transformation sequence $\beta \rightarrow \omega + \beta + \alpha \rightarrow \alpha + \beta$, and the formed ω and α volume fraction is of 5% and 13.5%, respectively. When the aging temperature is increased to 400°C and 450°C, the formation of a fine, acicular shape, α phase is identified with a volume fraction of 51% and 57% respectively; the decomposition sequence of the metastable β phase is $\beta \rightarrow \alpha + \beta$. The α forms at first within the β grains presenting a “tire” patterns with an angle of 60° between each other. For this treatment condition, the α formation may include two steps: for the first one corresponds to intragranular nucleation of precipitates on dislocation lines and growth; the second one includes intragranular nucleation and growth as well as nucleation at the β/β grain boundaries; diffusion controlled growth of acicular α phase plays an important role in the transformation process. For the aging at 500°C and 550°C, the transformation product is also α with a volume fraction of 57.7% and 55.3% respectively. For these temperatures, the nucleation occurs at

the β grain boundaries and within the β grains simultaneously and the grain boundary α phase forms in parallel acicular structure and grow into the β grain. As the isothermal aging temperature elevates to $600^{\circ}\text{C} \sim 700^{\circ}\text{C}$, we still observe the formation of α phase; the α nucleation sites are mainly the β grain boundaries, intragranular nucleation happens later. The volume fraction of α is 47%, 38% and 26% at 600°C , 650°C and 700°C respectively. The decrease in α phase amount is associated with the variations of equilibrium α phase amount with temperature. Meanwhile, the width of α precipitates is increased as aging temperature is increased. Anyway, the phase transformation kinetics have been analyzed using JMAK equation, and the values of Avrami index n , temperature constant K and the phase transformation activation energy E of Ti-B19 alloy have also been gained. Then the TTT diagram of Ti-B19 alloy in isothermal phase transformation have been established depending on the experimental data and calculated results respectively, and “nose temperature” is in the temperature range of $500\sim 550^{\circ}\text{C}$ due to the driving force of phase transformation and the diffusion rate of solute atoms that cooperate ideally.

2. The research results of the influence of heating rate on phase transformation behaviors show that the beta metastable decompose in Ti-B19 alloy during heating and isothermal aging is obviously dependent on the heating rate. For heating rate of 1°C/s and 10°C/s , the decomposition of the beta metastable phase occurs mainly at the aging temperature. For lower heating rate of 0.1°C/s , the ω_{iso} phase is formed at $300\sim 360^{\circ}\text{C}$; then the formation of α'' is observed at the detriment of ω_{iso} ; the amount of α'' increases strongly after 440°C . At 500°C , α'' evolves toward to forming α structure. However, the heating rate has no considerable influence on the final amount of α phase in the alloy after aging at 500°C for 4h, but it affects the kinetics of the phase transformation and sequences. At the heating rates of 10°C/s and 1°C/s , Avrami index value of JMAK functions is $n=2.17$, while it is $n = 0.67$ at the heating of 0.1°C/s . For the lower heating rate

(0.1°C/s), a complex transformation sequence is observed with the first formation of β phase that is uniformly distributed in the matrix and act as favorable nucleation sites for the formation of fine acicular α'' precipitates.

3. The research results of the effect of a pre-deformation on the phase transformation during aging in Ti-B19 alloy releases that the deformation degrees obviously influence the phase transformation behavior during heating and holding at different heating rates. For kinetics, a phase transformation kinetics are considerably increased, no incubation period is observed and the transformation time is shortened by over 90%. This is related to defects in the grain and at grain boundaries resulting from the pre-deformation and providing more favorable nucleation sites for precipitation of β or α . Meanwhile, the pre-deformation restrains the α phase transformation, i.e. after aging at 500°C for 4h, the α phase amount is lower as the deformation amount increases. Similarly, during heating and for a same heating rate, the amount of precipitated alpha phase is lower for the higher pre-deformation amount. This decrease in transformation amount is related to the existence of internal stress caused by room temperature deformation and/or to an increase in the deformation energy associated with the transformation.
4. Transformation during continuous cooling from the β phase temperature range in Ti-B19 alloy occurs by nucleation and growth with a preferential nucleation of α at the β grain boundaries. The critical cooling rate of α phase formation is about 1°C/s. By using Scheil superposition principle and JMAK functions, the phase transformation kinetics during continuous cooling has been analyzed for Ti-B19 alloy. In a first attempt, the following function has been proposed to describe the phase transformation kinetics:

$$f(t) = 1 - \exp \left\{ - K_0 \left(\int_0^t \exp \left(- \frac{E}{mR (1033 + C_v t)} \right) dt \right)^m \right\}$$

Wherein, when the cooling rate is smaller than 0.08°C/s, $m=1.3$. The equation allows describing good trends for the evolutions of transformation progress with time, but transformation temperature range is too high.

5. Relationships between mechanical properties and microstructure of Ti-B19 alloy have been obtained. It is shown that aging in the range of 300-350°C, leads to fine ω phase homogeneously distributed in the matrix resulting to an increase of tensile strength and meanwhile a decrease of the ductility. When aging temperature is higher than 400°C, the alloy microstructure after aging is a mixture of α (or α'') phase and β phase. Mechanical characteristics are tightly related to the volume fraction, the shape, the distribution and the size of the α precipitates. In general, when α transformation volume fraction is around 55%, a good compromise is obtained with the yield strength and elongation is more than 1200MPa and 8% respectively.

APPENDIX

Analysis of calculated phase transformation kinetics during continuous cooling

Using the following relation, developed in chapter 6 (equation 6-16), we have calculated the variations of phase transformation progress versus time calculated for Ti-B19 alloy during continuous cooling and for different cooling rates (0.012~1? /s). At first we have calculated the kinetics using a m value equal to 1.3 and E equal to 4.17415×10^5 J/mol.

$$f(t) = 1 - \exp \left\{ -K_0 \left(\int_0^t \exp \left(-\frac{E}{mR(1033 + C_v t)} \right) dt \right)^m \right\} \quad \text{A-1}$$

The calculated kinetics are given in Figure A-1. It can be observed that, for all cooling rates, transformation occurs at very early time. But the kinetics is strongly dependent on the cooling rate. For 0.1? /s, the end of the $b \rightarrow a + b$ phase transformation occurs after about 2,000s; but when the cooling rate is lowered to 0.03? /s, it is necessary to spend about 4,300s to finish the transformation.

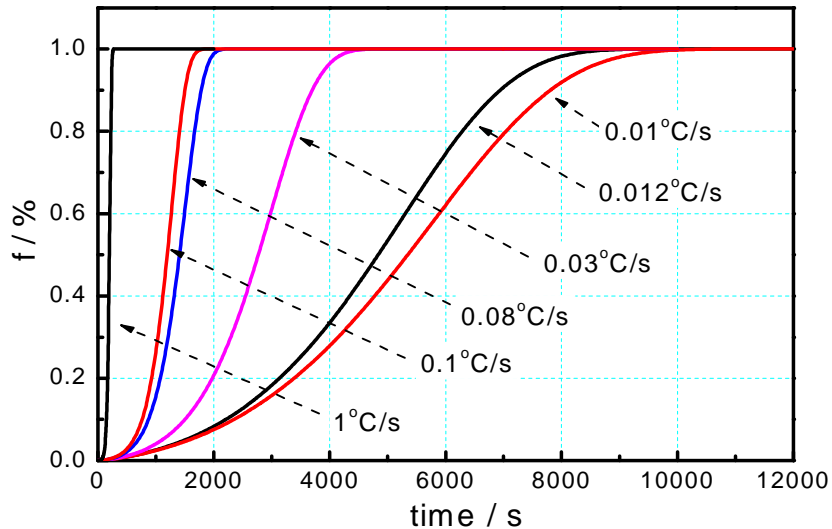


Figure A-1 Calculated kinetics during continuous cooling from 900? at different cooling rates.

We can further analyze the calculated results and test the sensitivity of the parameters used in the calculations.

Influence of the Avrami coefficient on the calculated transformation kinetics

Since $\mathbf{b} \rightarrow \mathbf{a} + \mathbf{b}$ phase transformation happens during continuous cooling from high-temperature β domain, nucleus formation will be favored on β grain boundaries; however, in the overall phase transformation process, nucleus formation takes place on different sites, such as β grain edge and spatial angle and defects. The m factor in Function 6-16 is depending on the activated nucleation sites as well as on the morphology of the precipitates. In the previous calculations, we considered a constant m value taken from experimental ones at 600-700°C. In order to analyze the effect of the m values, calculations have been realized for different m values. Figure A-2 shows the calculated transformation kinetics during continuous cooling at 0.03°C/s, 0.05°C /s and 0.07°C /s, and the m equal to 1, 2 and 3 respectively. It is observed that, the kinetics is considerably changed (Figure A-3). For the lower m values (1 and 2) (Figures A-3a and A-3b), differences are obtained for the three cooling rates of 0.03, 0.05 and 0.07°C/s. Those differences are the highest for $m = 1$; for example, the $\mathbf{b} \rightarrow \mathbf{a} + \mathbf{b}$ phase transformation is completed at 6,500s, 4,200s and 3,300s for respectively 0.03, 0.05 and 0.07°C/s cooling rates.

Increasing m values leads to decrease the effect of the cooling rate for the range of cooling rate investigated. Indeed, when $m = 3$ (Figure A-3c), the cooling rate has no influence on the transformation kinetics. In Figure A-3d we represent the phase transformation progress versus time for different m values and cooling rate of 0.03°C/s. The transformation is completed at 6,500s, 1,100s and 120s for Ti-B19 alloy when m value varies from 1, to 2 and 3. Thus increasing m values tend to decrease the transformation duration time, all other parameters being the same.

However, from microstructure observations, there is not a single mechanism for α nucleation and growth when $\mathbf{b} \rightarrow \mathbf{a} + \mathbf{b}$ phase transformation happens in Ti-B19 alloy during continuous cooling. In the previous calculations a single m value was considered. In fact, Avrami index m is

associated with the nucleation formation and the growth modes, m value relates to the prior index factor K_0 , the transition temperature T and the cooling rate C_v . The microstructure observations revealed changes in the nucleation sites (grain boundaries, intra granular sites) which activation varies as a function of the driving force, changes in the morphologies leading to different m values (Chapter 3).

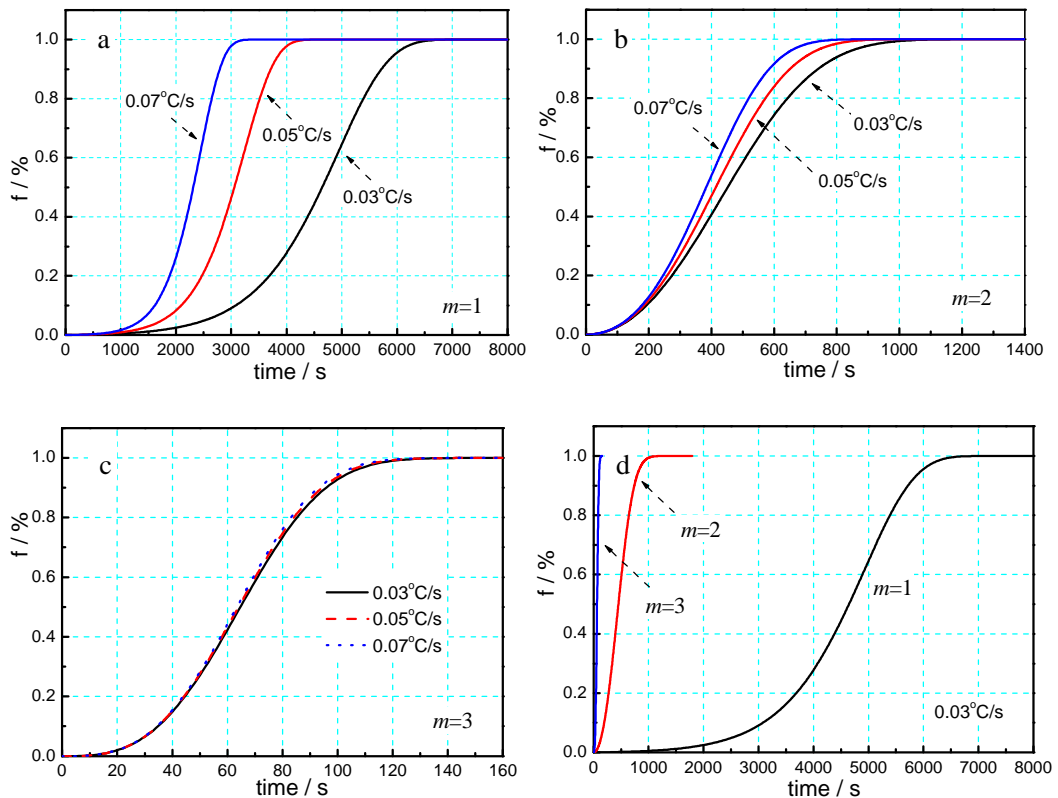


Figure A-2 Phase transformation kinetics curves for Ti-B19 alloy during continuous cooling when a phase nuclear at different location of b phase (a) $m = 1$, (b) $m = 2$, (c) $m = 3$, (d) $0.03? /s$.

Estimation of CCT diagram

CCT diagrams reflect the relationship among temperature, time and phase transformation of the alloy at different cooling rates; therefore, it can provide information for direct application value [88,102,107,109,110]. It is possible to use different methods as thermal analysis, resistivity etc, in order to determine the kinetics of α phase transformation of Ti alloy. Meanwhile, it is possible to

calculate kinetics, in order to gain the CCT curve. We used Formula (6-16) to establish the CCT curve of $b \rightarrow a + b$ phase transformation for Ti-B19 alloy in the continuous cooling process.

Experimental results as calculated ones have shown that m may vary with temperature. We have thus calculated transformation kinetics on cooling considering variable m values. For rather low cooling rate ($<0.08^\circ/\text{s}$), m value is taken as 1.3; for higher cooling rates ($>0.08^\circ/\text{s}$), we consider that m value varies with temperature and time.

The following relationship of m value against temperature and time has been considered:

$$m = 5.9775 - 0.00707T \quad \text{A-2}$$

$$m = -1.32581 + 0.00707C_v \cdot t$$

Introducing last formula in Formula (6-16), and taking into consideration the relationship between temperature T , cooling rate C_v and time t , we calculate new transformation kinetics for the different cooling rates (Figure A-3). It can be observed that the incubation period for the $b \rightarrow a + b$ phase transformation is considerably decreased.

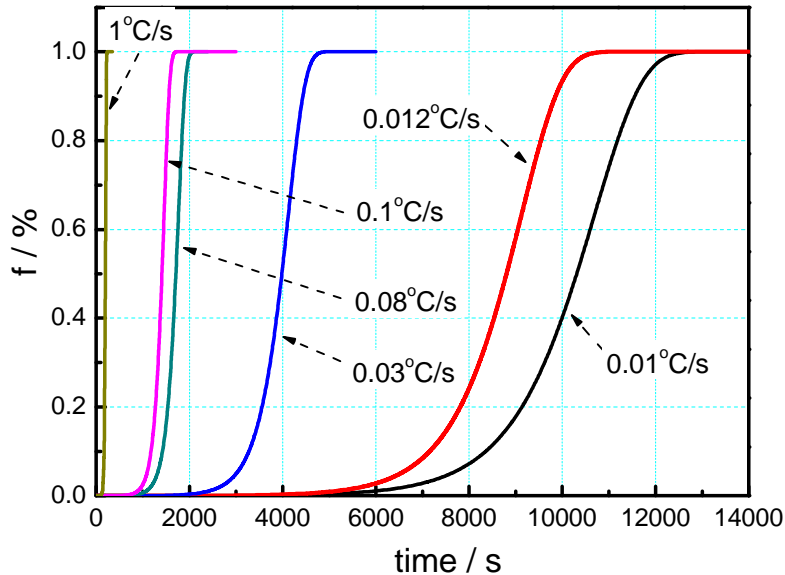


Figure A-3 Phase transformation kinetics for Ti-B19 alloy during continuous cooling from 900°C at different cooling rates (with m varying with temperature).

From these last calculated kinetics taking into account the variations of m with temperature and cooling rate, we get a CCT diagram shown Figure A-4, wherein, in rather low cooling rate

conditions, m value takes 1.3; in higher cooling rate condition, correction can be done to m value with Formula (A-2).

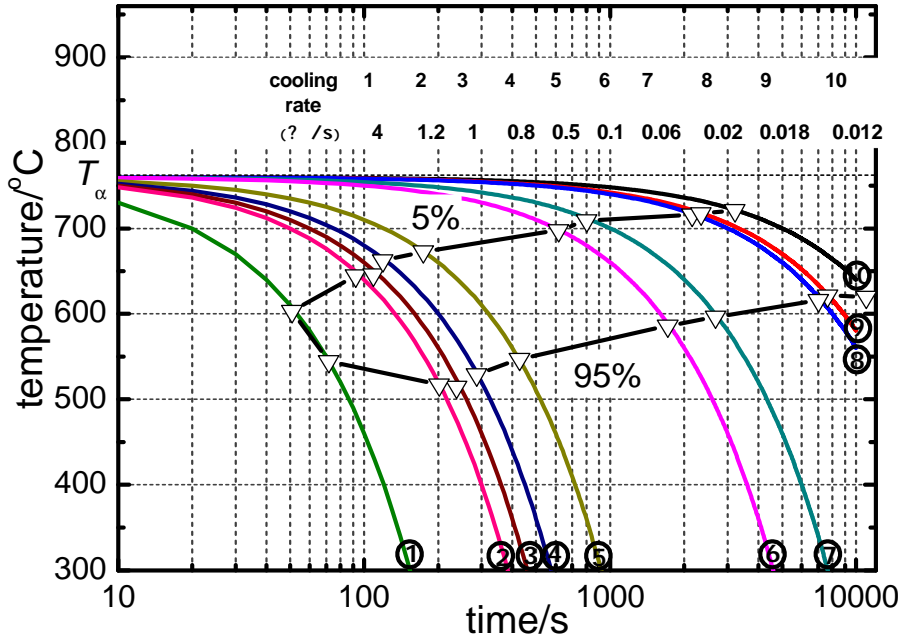


Figure A-4 Calculated CCT diagram of Ti-B19 alloy in continuous cooling process.

In all cases the transformation kinetics occurs at too high temperatures. Introduction of a variable m value does not allow a good prediction of the transformation temperature range. Therefore, the model should be further developed. One way is to consider separately the incubation time as it is done in the literature.

REFERENCES

- [1]. C.Lynes, M.Peters ed.. Zhenghua Cheng Trans. Titanium and titanium alloys. Beijing: Chemical Industry Publisher. 2005.
- [2]. Xiyang Zhang etc. ed. Titanium and its Application, Beijing, Chemical Industry Press. 2005
- [3]. Jinyou Wang, Zhiming Ge, Yanbang Zhou Ed. Titanium alloy for Aerospace. Shanghai, Science and Technology Publisher. 1985.7.
- [4]. Ludovic Hélicher, Contribution la modelisation des transformations de phases dans les alliages de titane—application a l’alliage β -CEZ, L’Institut National Polytechnique De Lorraine, 2004.
- [5]. Nonferrous metal and its heat treatment, Beijing, National defence Publisher.1981.8
- [6]. Boyer R., Welsch G., Collings E.W., Materials properties handbook: Titanium alloys, ASM International,1994.
- [7]. Jiuhong Qian. New titanium alloys developed for aerospace and its application[J]. Rear Metals. 2000, 24(3):218~223
- [8]. Robert Pederson. Microstructure and phase transformation of Ti-6Al-4V, licentiate thesis, Lulea University of technology, 2002.
- [9]. M.G. Glavicic and S.L. Semiatin, X-ray line-broadening investigation of deformation during hot rolling of Ti-6Al-4V with a colony-alpha microstructure Acta Materialia, Volume 54, Issue 20, December 2006, Pages 5337-5347
- [10]. D. Bhattacharyya, G.B. Viswanathan, S.C. Vogel, D.J. Williams, V. Venkatesh and H.L. Fraser, A study of the mechanism of α to β phase transformation by tracking texture evolution with temperature in Ti-6Al-4V using neutron diffraction Scripta Materialia, Volume 54, Issue 2, January 2006, Pages 231-236
- [11]. N. Stanford and P.S. Bate, Crystallographic variant selection in Ti-6Al-4V Acta Materialia, Volume 52, Issue 17, 4 October 2004, Pages 5215-5224
- [12]. M. G. Glavicic, P. A. Kobryn, T. R. Bieler and S. L. Semiatin, An automated method to determine the orientation of the high-temperature beta phase from measured EBSD data for the low-temperature alpha-phase in Ti-6Al-4V Materials Science and Engineering A,

Volume 351, Issues 1-2, 25 June 2003, Pages 258-264

- [13]. S. Malinov, W. Sha, Z. Guo, C. C. Tang and A. E. Long, Synchrotron X-ray diffraction study of the phase transformations in titanium alloys *Materials Characterization*, Volume 48, Issue 4, June 2002, Pages 279-295
- [14]. T. Seshacharyulu and B. Dutta, Influence of prior deformation rate on the mechanism of $\beta \rightarrow \alpha + \beta$ transformation in Ti-6Al-4V *Scripta Materialia*, Volume 46, Issue 9, 10 May 2002, Pages 673-678
- [15]. R. Ding, Z. X. Guo and A. Wilson, Microstructural evolution of a Ti-6Al-4V alloy during thermomechanical processing *Materials Science and Engineering A*, Volume 327, Issue 2, 30 April 2002, Pages 233-245
- [16]. C. Schuh and D. C. Dunand, Non-isothermal transformation-mismatch plasticity: modeling and experiments on Ti-6Al-4V *Acta Materialia*, Volume 49, Issue 2, Summer 2001, Pages 199-210
- [17]. F. Berberich, W. Matz, E. Richter, N. Schell, U. Kreißig and W. Möller, Structural mechanisms of the mechanical degradation of Ti-Al-V alloys: in situ study during annealing *Surface and Coatings Technology*, Volumes 128-129, 1 June 2000, Pages 450-454
- [18]. N. Gey, M. Humbert and H. Moustahfid, Study of the $\alpha \rightarrow \beta$ phase transformation of a Ti-6Al-4V sheet by means of texture change, *Scripta Materialia*, Volume 42, Issue 6, 28 February 2000, Pages 525-530
- [19]. W. Sha and Zhanli Guo, Phase evolution of Ti-6Al-4V during continuous heating, *Journal of Alloys and Compounds*, Volume 290, Issues 1-2, 30 August 1999, Pages L3-L7
- [20]. Zhu Zhang. Review of Beta titanium alloy [J]. *Rear Metals*, 1995, 19(4): 296~299
- [21]. R.R. Boyer. Aerospace application of beta titanium alloys [J]. *JOM*, 1994(7): 20~23
- [22]. Jianlin Wang. Development and Application of high strength beta titanium alloys [J]. *Research of Steel of Shanghai*, 2001(2): 25~33
- [23]. Jinsheng Yao, Lijian Zhang. The influence of heat treatment on phase transformation and properties in Ti-10V-2Fe-3Al [J]. *Shanghai Metals*, Vol. 3, 2000: 19-24
- [24]. Jeffrey R. Toran and Ronald R. Biederan, Phase transformation study of Ti-10V-2Fe-3Al, P. Lacombe, R. Tricot, and G. Beranger, *Sixth World Conference on Titanium*, 1988: 1491~1501
- [25]. A. Bhattacharjee, S. Bhargava, V. K. Varma, S. V. Kamat, A. K. Gogia, Effect of β grain size on
-

References

- stress induced martensitic transformation in β solution Ti-10-2-3 alloy, *Scripta Materialia* 53(2005): 195~200.
- [26]. Anhua Zhang. Martensite transformation in titanium alloys[J]. *Shanghai Nonferrous Metals*. Vol.4, 1999:196~ 199
- [27]. Tingjie Zhang. Research of phase transformation of titanium alloys by electron microscope (IV) ---- ω phase transformation in titanium alloys[J]. *Rear Metal Materials and Engineering*. Vol.5, 1989:77~82
- [28]. Tingjie Zhang. Research of phase transformation of titanium alloys by electron microscope (V) ----deposition of two kinds alpha phase during deposition of metastable beta phase in aging [J]. *Rear Metal Materials and Engineering*. Vol.6 1989:77~82
- [29]. Xinagming Tui, Guangjue Zhou, Yang Li. Microstructure and properties of Ti-811,Ti-6242 and Ti-17 alloys[J]. *Rear Metals*.1995,19(2):150~154.
- [30]. Tingjie Zhang. Research of phase transformation of titanium alloys by electron microscope (?) ---- Martensite transformation in titanium alloys [J]. *Rear Metal Materials and Engineering*. Vol.4,1989:71~78
- [31]. Thomas J. Headley and Henry J. Rack. Phase transformations in Ti-3Al-8V-6Cr-4Zr-4Mo[J]. *Met. Trans. A*, 10A (1979)909.
- [32]. O.M.Ivasishin, A.I.Ustino, V.S.Skorodzievshii, M.S.Kosenko, Yu.V.Matviychuk and F.I.Azamatova, Structural and compositional changes during isothermal annealing of α' -martensite in Ti-8wt.%Mo alloy, *Scripta Materialia*, Vol.37,No.6: 883~888.
- [33]. Jian Wang, Yu Wang, R. Schaublin, C. Abromeit and Rolf Gotthardt, The effect of point defects on the martensitic phase transformation, *Materials Science and Engineering: A*, Volumes 438-440, 25 November 2006, Pages 102-108
- [34]. Y. Mantani and M. Tajima, Phase transformation of quenched α' martensite by aging in Ti-Nb alloys, *Materials Science and Engineering: A*, Volumes 438-440, 25 November 2006, Pages 315-319
- [35]. D.H. Ping, C.Y. Cui, F.X. Yin and Y. Yamabe-Mitarai, TEM investigations on martensite in a Ti-Nb-based shape memory alloy, *Scripta Materialia*, Volume 54, Issue 7, April 2006, Pages 1305-1310
- [36]. A.V.Dobromyslov and V.A.Elkin. Martensitic transformation and metastable β phase in binary titanium alloys with d-metals of 4~6 periods[J]. *Scripta mater.* 44(2001) 905~910
- [37]. J.I.Qazi, B.Marquardt, L.F.Allard, H.J.Rack. Phase transformations in
-

- Ti-35Nb-7Zr-5Ta-(0.06-0.68)O alloys[J]. *Materials Science and Engineering*. C25 (2005), 389~397.
- [38]. J.I.Qazi, O.N.Senkov, J.Rahim, F.H.(Sam)Froes. Kinetics of martensite decomposition in Ti-6Al-4V-xH alloys[J]. *Materials Science and Engineering*. A359(2003), 137~149.
- [39]. A.M. Sandu, K. Tsuchiya, S. Yamamoto, Y. Todaka and M. Umemoto, Influence of isothermal ageing on mechanical behaviour in Ni-rich Ti-Zr-Ni shape memory alloy, *Scripta Materialia*, Volume 55, Issue 12, December 2006, Pages 1079-1082
- [40]. James M. Howe, Comparison of the atomic structure, composition, kinetics and mechanisms of interfacial motion in martensitic, bainitic, massive and precipitation face-centered cubic-hexagonal close-packed phase transformations, *Materials Science and Engineering: A*, Volumes 438-440, 25 November 2006, Pages 35-42
- [41]. F. Zimmermann and M. Humbert, Determination of the habit plane characteristics in the β - α' phase transformation induced by stress in Ti-5Al-2Sn-4Zr-4Mo-2Cr-1Fe, *Acta Materialia*, Volume 50, Issue 7, 19 April 2002, Pages 1735-1740
- [42]. S.Ankem, S.R.Aeagle. Heat treatment of metastable beta titanium alloys [A]. R.R.Boyer, H.W.Rosenberg *Beta Titanium in the 1980's* [C].Warrendale: PA, TMS-AIME, 1984,107~126
- [43]. Yasuya Ohmori, Toshitaka Ogo, Kiyomichi Nakai, Sengo Kobayashi. Effects of ω -phase on β to α, α'' transformations in a metastable β titanium alloy[J]. *Materials Science and Engineering*. A312 (2001), 182~188.
- [44]. A. Bénéteau, P. Weisbecker, G. Geandier, E.Aeby-Gautier, B. Appolaire. Austenitization and precipitate dissolution in high nitrogen steels: an in-situ high temperature X-ray synchrotron diffraction analysis using the rietveld method[J]. *Materials Science and Engineering A* 393 (2005) 63-70.
- [45]. Duerig TW, Terlinde GT, Williams JC. *Metall Trans A* 1980;11:1987.
- [46]. F.Prima, P.Vermaut, G.Textier, D.Ansel, T.Gloriant. Evidence of α -nanophase heterogeneous nucleation from ω particles in a β -metastable Ti-based alloy by high-resolution electron microscopy[J]. *Scripta materialia*. 54(2006) 645~648.
- [47]. C.G.Rhodes, J.C.Williams. The precipitation of α phase in metastable β titanium alloys[J]. *METALLURGICAL TRANSACTIONS A*. June 1975, 1975~2103
- [48]. E.Sukedai, Y.Kitano and A.Ohnishi, Investigation of initial structure of aged ω phase crystals in β titanium alloys using high resolution electron microscopy, *pergamon micron*
-

References

- 1997, Vol.28 No.4: 269~277
- [49]. T.W.Duerig,G.T.Terlinde,J.C.Willams. The β -phase reaction in titanium alloys [A]. H.Kimura,O.Izumi. Titanium'80 Science and Technology [C]. New York.AIME, 1980,1309~1316.
- [50]. L.Wagner, J.K.Gregory. Improvement of mechanical behavior in Ti-3Al-8V-6Cr-4Mo-4Zr by duplex aging [A]. D.Eylon,R.R.Boyer and D.A.Koss. Beta Titanium Alloy in the 1990's[C].Warrendale: Pennsylvania, TMS,1996.421~433.
- [51]. Guiqin Shen, Bin Xu, Yiqun Peng, Xingming Tui. Phase transformation of Ti-15Mo-2.7Nb-3Al-0.2Si[J]. Materials Engineering. Vol.3, 1999:21~ 23
- [52]. Shin-ya Komatsu, Masahiko Ikeda, Takashi Sugimoto, Kiyoshi Kamei, Osamu Maesaki and Masa-aki Kojima, Aging behaviour of Ti-15Mo-5Zr and Ti-15Mo-5Zr-3Al alloy up to 573 K, Materials Science and Engineering: A, Volume 213, Issues 1-2, 15 August 1996, Pages 61-65
- [53]. P.J.Bania. Ti-1100: A new high temperature titanium alloy [A]. P.Lacombe, R.Tricot, G.Beranger. Sixth world conference on titanium [C]. Les Ulis: Les editions de physique, 1988.825~830.
- [54]. Mengyi Hao, Jianming Cai, Juan Du. The effects of heat treatment of BT36 alloy on Microstructure and properties[J]. Transaction of Aero Materials. 2003,23(2):14~173
- [55]. M.Harper, RWilliams, G.B.Viswanathan, et al. The effect of heat treatment on the microstructure of Ti-5Al-5Mo-5V-3Cr-1Fe(Ti-555)[A]. G.Lutjering. J.Albrecht. Ti-2003 Science and Technology [C]. WILEY-VCH: DGM,2004.1559-1566.
- [56]. Ankem S, Green C A. Recent developments in microstructure/property relationships of beta titanium alloys. Zhou L, Eylon D, Lutjering G, Ouchi C. Titanium'98 Proceedings of Xi'an International Titanium Conference[C]. Beijing: International Academic Publishers, 1999.487~494.
- [57]. R.R.Boyer, G.Welsch, E.W.Collings. Materials properties handbook Titanium Alloys. USA:ASM Internatinal,1994,907.
- [58]. Qingru Wang, Jiming Ma, Qingling Zhang. Research on aging properties in Ti-15-3 alloy[J]. Transaction of Aero Materials.1998,18(1):7~14.
- [59]. R.K.Bird, T.A.Wallace, W.O.Brewer. Effect of heat treatment on microstructure, strength and toughness of EIMETAL-21S. I.Weiss.R.Srinivasan,P.J.Bania,D.Eylon,S.L.Semiatin. Advances in the science and technology of titanium alloy processing [C].Warrendale:
-

- Pennsylvania, TMS,1996.472~480.
- [60]. J.R.Wood, P.A.Russo. Heat treat of titanium alloys [A]. I.Weiss. R.Srinivasan, P.J.Bania, D.Eylon, S.L.Semiatin. Advances in the science and technology of titanium alloy processing [C].Warrendale: Pennsylvania, TMS,1996.421~433.
- [61]. Pengling Mao. Phase transformation and heat treatment criterion of alpha+beta alloys[J].Shanghai Research of Steel.1995(3):50~58
- [62]. G.C.Morgan, C.Hammmond. The aging characteristics of Ti-3Al-8V-6Cr-4Mo-4Zr (Ti-38644). H.Kimura, O.Izumi. Titanium'80 Science and Technology [C]. New York.AIME, 1980,1443~1451.
- [63]. G.H.Isaac,C.Hammmond. The formation of type 2a phase in Ti-3Al-8V-6Cr-4Zr-4Mo[A]. G.Lutjering, U.Zwichker, W.Bunk. Titanium Science and Technology [C]. Adenauerallee: Deutsche Gesellschaft fur Metallkunde e. V., 1995, 1605~1612.
- [64]. H.Fujii, H.G.Suzuki. Effect of solution-temperature conditions on aging response in Ti-15V-3Cr-3Sn-3Al [A]. D.Eylon,R.R.Boyer and D.A.Koss. Beta Titanium Alloy in the 1990's[C].Warrendale: TMS,1993.249~259.
- [65]. H.W.Rosenberg. Property scatter in beta titanium: some problems and solutions [A]. R.R.Boyer, H.W.Rosenberg Beta Titanium in the 1980's [C]. Warrendale: PA, TMS-AIME,1984.145~160.
- [66]. T.Suzuki, N.Niwa, K.Goto, et al. Effect of aging on the mechanical properties of beta titanium alloys of Ti-13V-11Cr-3Al, Ti-15V-3Cr-3Sn-3Al and Ti-3Al-8V-6Cr-4Mo-4Zr [A]. P.A.Blenkinsop, W.J.Evans H.M.Flower. Titanium'95 Science and Technology [C]. London: The Institute of Materials,1996.1294~1301.
- [67]. X. D. Zhang, P. Bonniwell, H. L. Fraser, W. A. Baeslack, III , D. J. Evans, T. Ginter, T. Bayha and B. Cornell, Effect of heat treatment and silicon addition on the microstructure development of Ti-6Al-2Cr-2Mo-2Sn-2Zr alloy, Materials Science and Engineering A, Volume 343, Issues 1-2, 25 February 2003, Pages 210-226
- [68]. C. Schuh and D. C. Dunand, Non-isothermal transformation-mismatch plasticity: modeling and experiments on Ti-6Al-4V, Acta Materialia, Volume 49, Issue 2, Summer 2001, Pages 199-210
- [69]. C. J. Butler and D. G. McCartney, An experimental study of phase transformations and a comparison with calculated phase equilibria in Ti-Al-Mn alloys, Acta Materialia, Volume 46, Issue 6, 23 March 1998, Pages 1875-1886
-

References

- [70]. T. Ahmed and H. J. Rack, Phase transformations during cooling in $\alpha+\beta$ titanium alloys, *Materials Science and Engineering A*, Volume 243, Issues 1-2, 15 March 1998, Pages 206-211
- [71]. T. Novoselova , S. Malinov , W. Sha and A. Zhecheva, High-temperature synchrotron X-ray diffraction study of phases in a gamma TiAl alloy, *Materials Science and Engineering A*, Volume 371, Issues 1-2, 25 April 2004, Pages 103-112
- [72]. S. Malinov, T. Novoselova and W. Sha, Experimental and modelling studies of the thermodynamics and kinetics of phase and structural transformations in a gamma TiAl-based alloy, *Materials Science and Engineering A*, Volume 386, Issues 1-2, 25 November 2004, Pages 344-353
- [73]. T. Makino, R. Chikaizumi, T. Nagaoka, T. Furuhashi and T. Makino, Microstructure development in a thermomechanically processed Ti-15-3 alloy, *Materials Science and Engineering: A*, Volume 213, Issues 1-2, 15 August 1996, Pages 51-60
- [74]. D. Bhattacharyya, G. B. Viswanathan, Robb Denkenberger, D. Furrer and Hamish L. Fraser, The role of crystallographic and geometrical relationships between α and β phases in an α/β titanium alloy, *Acta Materialia*, Volume 51, Issue 16, 15 September 2003, Pages 4679-4691
- [75]. P. Laheurte, A. Eberhardt and M.J. Philippe, Influence of the microstructure on the pseudoelasticity of a metastable beta titanium alloy, *Materials Science and Engineering A*, Volume 396, Issues 1-2, 15 April 2005, Pages 223-230
- [76]. O.M. Ivasishin, P.E. Markovsky, S.L. Semiatin and C.H. Ward, Aging response of coarse- and fine-grained β titanium alloys, *Materials Science and Engineering: A*, Volume 405, Issues 1-2, 25 September 2005, Pages 296-305
- [77]. Peterson Luiz Ferrandini, Flavia Farias Cardoso, Sandra Araujo Souza, Conrado Ramos Afonso and Rubens Caram, Aging response of the Ti-35Nb-7Zr-5Ta and Ti-35Nb-7Ta alloys, *Journal of Alloys and Compounds*, Corrected Proof, Available online , 4 August 2006
- [78]. J.W. Elmer, T.A. Palmer, S.S. Babu and E.D. Specht, In situ observations of lattice expansion and transformation rates of α and β phases in Ti-6Al-4V *Materials Science and Engineering A*, Volume 391, Issues 1-2, 25 January 2005, Pages 104-113
- [79]. T.Furuhashi, T.Maki, T.Makino. Microstructure control by thermomechanical processing in β -Ti-15-3 alloy[J]. *Journal of Materials Processing Technology*. 117(2001) 318~323.
-

- [80]. C.Angelier, S.Bein, J.Bechet. Building a continuous cooling transformation diagram of β -CEZ criterion Illography and electrical resistivity measurements[J]. METALLURGICAL AND MATERIALS TRANSACTIONS A. 28A(1997) 2467.
- [81]. Benoit Appolaire, Ludovic Hericher, Elisabeth Aeby-Gautier. Modeling of phase transformation kinetics in Ti alloys-Isothermal treatments[J]. *Acta materialia*. 53(2005) 3001~3011.
- [82]. Julien Da Costa Teixeira, Benoît Appolaire, Elisabeth Aeby-Gautier, Sabine Denis and Fabien Bruneseaux, Modeling of the effect of the β phase deformation on the α phase precipitation in near- β titanium alloys, *Acta Materialia*, Volume 54, Issue 16, September 2006, Pages 4261-4271.
- [83]. E. Laude, E. Gautier and S. Denis, Calculation of transformation kinetics of titanium alloys during continuous cooling-Application to the β -CEZ alloy, *Titanium'95:Science and Technology*, U.K. Birmingham, 1995.
- [84]. S.Malinov, P.Markovsky, W.Sha. Resistivity study and Computer modeling of the isothermal transformation kinetics of Ti-8Al-1Mo-1V alloy[J]. *Journal of Alloys and Compounds*. 333(2002) 122~132.
- [85]. S.Malinov, P.Markovsky, W.Sha, Z.Guo, Resistivity study and Computer modeling of the isothermal transformation kinetics of Ti-6Al-4V and Ti-6Al-2Sn-4Zr-2Mo-0.08Si alloy[J]. *Journal of Alloys and Compounds*. 314(2001) 181~192.
- [86]. Zuyao XU ed.. *Principle of phase transformation*. Beijing: Science Publisher.1990.
- [87]. Jimei Xiao ed. *Alloying phase and phase transformation (Second ed.)*, Beijing: Metallurgy industry Publisher.2004.
- [88]. Duan Feng ed.. *Physics of Metals, Vol.2 Phase Transformations*, Beijing: Science Publisher.1998.
- [89]. Duan Feng, Changxu Shi, Zhiguo Liu ed.. *Review of Materials Science*. Beijing: Chemical industry Publisher, Material Science and Engineering Punlisher.2002.
- [90]. Eric J.Mittemeijer and Ignacy A.Wierszyllowshi, The isothermal and nonisothermal kinetics of tempering iron-carbon and iron-nitrogen martensites and austenites, *Bd* 82(1991), H.6:421~429.
- [91]. Savko Malinov and Wei Sha, Modeling thermodynamics, kinetics, and phase transformation morphology while heat treating titanium alloys, *JOM*, September 2005: 42~45

References

- [92]. S. Malinov and W. Sha, Application of artificial neural networks for modelling correlations in titanium alloys, *Materials Science and Engineering A*, Volume 365, Issues 1-2, 25 January 2004, Pages 202-211
- [93]. Y.Wang, N.Ma, Q.Chen, F.Zhang, S.-L.Chen, and Y.A.Chang, Predicting phase equilibrium, phase transformation, and microstructure evolution in titanium alloys, *JOM*, September 2005:32~39.
- [94]. N.Saunders, Modeling of phase equilibrium in Ti-alloys, *Titanium'95:Science and Technology*, Bermingham, U.K. 1995:2167~2173.
- [95]. Julien DA COSTA TEIXEIRA, Etude experimentale et modelisation des eolutions microstructurales au cours des traitements thermiques post forgeage dans l'alliage de titane Ti17, Doctorat de L'Institut National Polytechnique De Lorraine, 2005.
- [96]. H.Chang, J.Chen, J.Deng, et al. Effect of heat treatment on room tensile properties and fracture toughness of a new near β titanium alloy-Ti-B19, *Proceeding of International Conference on Engineering and Technological Science 2000*, Advance materials Vol.1, Beijing: New world press, 2000, p410~412.
- [97]. H.Chang, J.Chen, L.Zhou. Microstructure and mechanical properties of a new near β titanium alloy-Ti-B19, *Ti-2003 Science and Technology*, Vol.3, Germany: 2003, p1575~1581.
- [98]. Shi Tian ed.. *Physical properties of Materials*. Beijing: Beihang University Publisher.2001.
- [99]. S.Malinov, W.Sha, P.Markovsky. Experimental study and computer modeling of the $b \rightarrow a + b$ phase transformation in $\beta 21s$ alloy at isothermal conditions. *Journal of Alloy and Compounds*, 348(2003) 110~118.
- [100]. S.Malinov, P.Markovsky, W.Sha. Resistivity study and computer modeling of the isothermal transformation kinetics of Ti-8Al-1Mo-1V alloy. *Journal of Alloy and Compounds*. 333(2002) 122~132.
- [101]. C.Angelier, S.Bein, and J.Bechet, Building a continuous cooling transformation diagram of β -CEZ alloy by metallography and electrical resistivity measurements, *Metall. Mat. Trans. A*, 1997, Volume 28A:2467~2475.
- [102]. Fabien Bruneseaux, Guillaume Geandier, Elisabeth Gautier, Benoit Appolaire, Moukrane Dehmas, Pascal Boulet. In situ characterization of the transformation sequences of Ti17 alloy by high energy X-ray diffraction: influence of the thermal path. Edited by M.Niinomi et al. *Ti-2007 Science and Technology*, Proceedings of the 11th World

- Conference on Titanium(JIMIC5), 3~7 June, 2007, Kyoto, Japan. Volume ?, P563~566.
- [103]. E. Aeby-Gautier, F. Bruneseaux, J. Da Costa Teixeira, B. Appolaire, G. Geandier, and S. Denis. Microstructural Formation in Ti Alloys: In-situ Characterization of Phase Transformation Kinetics. JOM, January 2007, P54~58
- [104]. Yuanyuan Luo. Phase transformation of Ti-B19 alloy during aging. Master Thesis, Northwestern Polytechnical University, 2006.
- [105]. Huabing Yang, Hui Chang, Jun Cheng, Hui Li. Isothermal phase transformation of near beta titanium alloy Ti-B19. Transaction of Metals, Vol.38, 2002, Supp. :S221~ S223
- [106]. Hui Chang, E.Gautier, F.Bruneseaux, Lian Zhou. Rear Metal Materials and Engineering. 2006, Vol.35, 11: 1695~ 1699
- [107]. ZuyaoXu ed.. Principles of Phase Transformation. Beijing: Science Publisher.2000.
- [108]. H.Chang, J.Chen, Aging response of new near beta titanium alloy Ti-B19, I.V.Gorynin and S.S.Ushkov, Titanium'99:Science and Technology, Russia: Central research institute of structure materials(CRISM) "Prometey",1999,557~562.
- [109]. J. Da Costa Teixeira, L. Hélicher, B. Appolaire, E. Aeby-Gautier, G. Cailletaud, S. Denis, N. Späth, Prediction of the kinetics of the phase transformations and the associated microstructure during continuous cooling in the Ti17,
- [110]. Eric J.Mittemeijer and Ignacy A.Wierszyllowshi, The isothermal and nonisothermal kinetics of tempering iron-carbon and iron-nitrogen martensites and austenites, Bd 82(1991), H.6:421~429.

RESUME

L'alliage Ti-B19 est un alliage de titane β métastable, mis au point et utilisé en Chine dont les propriétés (limite d'élasticité, charge de rupture, ténacité) sont fortement liées aux traitements thermiques utilisés pour obtenir les propriétés finales du matériau. En effet, les propriétés dépendent de la microstructure de l'alliage et celle-ci dépend vivement des paramètres de traitement et de la procédure de traitement thermique par les transformations de phases qui s'y produisent. Les différences de chemin thermique, de vitesse de chauffage et de refroidissement peuvent conduire à différentes natures de phases, à des différences de fraction volumique des phases en présence, de la forme, des dimensions et de la répartition spatiale des précipités, et en conséquence des différences de performance. L'optimisation des propriétés doit conduire à définir les conditions de formation des microstructures, donc la nature et les cinétiques de transformations de phases.

Le but du travail de thèse est d'étudier systématiquement les cinétiques de transformation de phase pour différents chemins thermiques, notamment au cours du chauffage, du refroidissement, de maintien isotherme ou celles après une pré-déformation plastique de la phase β - métastable. La cinétique de transformation est suivie in situ au cours des cycles thermiques par la résistivité électrique. La caractérisation des structures est menée par diffraction des rayons X, et celle des microstructures par des observations à différentes échelles comme la microscopie optique (OM), la microscopie électronique à balayage (MEB) et la microscopie électronique en transmission (MET). L'observation d'échantillons partiellement transformés a permis d'étudier les sites de germination et la croissance des phases, et l'évolution de l'arrangement spatial des précipités pendant la transformation en condition de transformation isotherme et non-isotherme. Nous avons établi un

diagramme TTT pour les transformations isothermes de l'alliage Ti-B19 et les cinétiques de transformation en refroidissement continu. Ces données expérimentales sont fondamentales pour analyser les microstructures de l'alliage TiB19, voire pour développer des outils numériques pour concevoir des alliages de titane, surtout des alliages à haute résistance.

Le contenu de cette thèse traite les points suivants : 1) L'étude par résistivité électrique in situ des cinétiques d'évolution des phases au cours du vieillissement, en condition isotherme (température variant de 300 à 700°C) pour l'alliage Ti-B19. La nature du changement de phase, l'évolution de l'organisation spatiale des précipités sont abordées, 2) l'influence de la vitesse de chauffage sur la cinétique de transformation de phase isotherme et sur l'arrangement spatial des précipités, 3) l'influence de la déformation à température ambiante de la phase bêta métastable sur la cinétique de transformation au vieillissement, 4) la cinétique de transformation de phase et l'organisation des précipités pour des transformations au refroidissement; 5) les relations entre les microstructures et les propriétés de traction.

La cinétique de transformation est analysée en utilisant le modèle de JMAK. Le diagramme TTT a été établi et la caractérisation des microstructures et structures a été menée par diffraction des rayons X, et par microscopies..

1. Pour étudier systématiquement la cinétique de transformation de phase de l'alliage Ti-B19, les conditions de germination et de croissance, nous avons choisi de réaliser des traitements isothermes dans le domaine de température de 300 à 700°C (une température d'essai tous les 50°C). La structure initiale de l'alliage est l'état bêta métastable, obtenu par une mise en solution dans le domaine bêta, à 900°C/10min suivi d'un refroidissement très rapide. La vitesse de chauffage pour le traitement de mise en solution est de 5? /s, celle de refroidissement est supérieure à 20°C/s. Le but est de contrôler la

dimension du grain β et d'éviter les transformations de phase. Pour l'étude de la transformation au vieillissement, la vitesse de chauffage est de 10°C/s , afin d'éviter la précipitation au cours du chauffage. Le temps de maintien est tel que la cinétique de transformation est complète. Après transformation, l'échantillon est refroidi rapidement afin d'éviter toute transformation ultérieure au maintien. Les résultats obtenus conduisent à des cinétiques isothermes de variations de résistivité électrique. Toutes les cinétiques ont été analysées, et les échantillons traités ont été caractérisés par différentes techniques de microscopie (MO/MEB//MET) et analysés par diffraction des rayons X. Pour préciser les conditions de transformation de phase isotherme, nous avons trempé des échantillons au cours des traitements isothermes à 400°C , 500°C et 600°C à différents temps de maintien choisis suivant la cinétique de transformation. Les points de trempé sont: pour 400°C , 1000s et 2000s ; pour 500°C , 1000s et 2000s, quant à 600°C , 2500s, 6000s et 10800s. Les résultats principaux sont les suivants :

- Après traitement isotherme à 300°C et pour le traitement considéré, la phase β est la seule phase formée avec une teneur d'environ 27% ; des études complémentaires pour des temps de maintien très longs ont montré que la séquence de transformation de la phase β métastable est: $b \rightarrow w + b \rightarrow w + b + a \rightarrow a + b$. Quand la température est de 350°C , la phase β et la phase a se forment dans l'alliage, les fraction volumique des phases β et a est respectivement de 5.4% et 13.5%. Pour cette température, la séquence de transformation de la phase β métastable est: $b \rightarrow w + b + a \rightarrow a + b$.
- Quand la température de transformation est de 400°C ou 450°C , on identifie après maintien la présence de phase α ; sa fraction volumique est

respectivement de 51% et 57%. La séquence de transformation de la phase β métastable est: $\beta \rightarrow \alpha + \beta$. Pour ce domaine de température, la phase α a une forme de fine aiguille, et elle apparaît tout d'abord à l'intérieur du grain β . Les aiguilles s'auto organisent (présentation comme des dessins de pneu) et ont un angle entre elles de 60° . La transformation de phase peut être divisée en deux séquences: au cours de la première il y a germination de phase α sur des lignes de dislocation et croissance sous la forme d'aiguille ; pour la deuxième il y a germination et croissance de phase α à l'intérieur de grain et aux bords de grain.

- Quand la température de maintien est de 500°C ou 550°C , la phase α se forme encore directement, germant et croissant simultanément à l'intérieur et aux bords des grains. La fraction volumique de phase α est de 57.7% et 55.3%. L'arrangement spatial de la phase α est sous la forme de veinure de pneu. Certains précipités grandissent le long de certaine "ligne" et l'angle entre les précipités α aciculaires est de 60° . Les précipités de phase α formée au voisinage des joints des grains se présente de manière parallèle le long du joint des grains β et croit vers l'intérieur du grain β .
 - Quand la température de maintien est de 600°C ou 700°C , la phase α se forme encore directement, mais le site de germination le plus favorable est le joint de grain β . La phase α se forme et croit à l'intérieur de grain lorsque la transformation progresse. Quand les températures de prescription sont de 600°C , 650°C et 700°C , la fraction volumique de phase α est respectivement de 47.4%, 38.3% et 25.7%, et la largeur de la phase α aciculaire augmente lorsque la température de maintien augmente.
 - En se basant sur le modèle de cinétique globale de transformation établi par Johnson-Mehl, Avrami et Kolmogorov, nous avons analysé les cinétiques de
-

transformation isotherme à partir de l'équation JMAK, permettant d'obtenir le coefficient d'Avrami n , la constante de température K et l'énergie d'activation E de la transformation. Avec les données expérimentales et celles issues des lois JMAK, nous avons établi le diagramme TTT de transformation de l'alliage Ti-B19, qui montre que la vitesse de changement de phase la plus rapide a lieu entre 500°C et 550°C. Dans cet intervalle de température, la force motrice de transformation de l'alliage est grande, et la vitesse de diffusion des solutés est encore assez grande pour conduire à une cinétique rapide.

2. La vitesse de chauffage jusqu'à la température de maintien est un facteur très important. Pour étudier l'influence de la vitesse de chauffage la cinétique de transformation de phase isotherme et la microstructure en résultant, nous avons utilisés trois différentes vitesses de chauffage. En utilisât le suivi des évolutions par résistivité électrique, nous avons déterminer les domaines de changements au cours du chauffage et au cours du maintien en température. Pour assurer la cohérence des essais, l'état initial était similaire à celui utilisé précédemment pour l'étude des transformations de phases en condition isotherme avec un chauffage jusqu'à la température de maintien à 10°C/s. Une seule température de maintien a été sélectionnée, celle de 500°C. La vitesse de chauffage de la température ambiante jusqu'à la température 500°C, est respectivement de 10°C/s, 1°C/s et 0.1°C/s ; le temps de maintien à 500°C est de 4 heures. Un refroidissement rapide est appliqué après le maintien pour éviter toute transformation, la vitesse de refroidissement est donc supérieure à 20°C/s. Pour la vitesse de chauffage de 0.1°C/s, des trempes interrompues au cours du chauffage ont été réalisées à 350°C, 450°C et 500°C, températures choisies en fonction des évolutions de résistivité mesurées. Ces échantillons ont été analysés par diffraction des rayons X et des observations microstructurales. Les principaux

résultats obtenus sont donnés ci-dessous:

La vitesse de chauffage influence largement la décomposition de la phase β métastable de l'alliage Ti-B19. Quand la vitesse de chauffage est élevée (1°C/s et 10°C/s), la décomposition de la phase β métastable se produit principalement au cours du maintien isotherme. Quand la vitesse de réchauffement est lente (0.1°C/s), la précipitation se produit au cours du chauffage. Les évolutions de résistivité permettent de définir quatre étapes, soit: la phase ω_{iso} se forme à la température de $300\sim 360^\circ\text{C}$; avec l'augmentation de température, la phase α'' (de structure orthorhombique) se forme au détriment de la phase ω_{iso} ; quand la température est supérieure à 440°C , beaucoup de phase α'' se forme; à la température de 500°C , la phase α'' commence à se transformer en phase α qui a une structure HCP (hexagonale pseudo compacte).

- La vitesse de chauffage influence faiblement la quantité finale de phase α dans l'alliage (après le maintien isotherme de $500^\circ\text{C}/4\text{h}$), mais modifie la cinétique de transformation et la séquence de transformation de phase de l'alliage. L'analyse des cinétiques de transformation isotherme avec les lois JMAK ($\ln(\ln(1/(1-f))) - \ln(t)$) conduit à un coefficient d'Avrami n égal à 2.17 pour les vitesses de 10°C/s et 1°C/s ; cet indice est de 0.67 quand la vitesse de chauffage est de 0.1°C/s .
- Si la vitesse de chauffage est faible, la séquence de changement de phase est plus compliquée; les précipités de phase ? se forment en premier, se répartissant régulièrement dans le grain. Ils sont métastables, et sont des sites favorables pour la formation des précipités aciculaires α qui se forment par la suite. Les précipités de phase ? disparaissent graduellement avec la formation et la croissance des précipités de phase α . Différents travaux ont porté sur la formation de phase de phase ? par MET et leur rôle sur la formation de α .

Pour ces études, les auteurs estiment que les précipités de phase ω sont des sites favorables de germination pour la phase α . Trois raisons sont principalement évoquées. La première est que la phase α se fait à une certaine distance de l'interface ω/β , zone enrichie en Aluminium, qui offre de bonnes conditions pour la formation de la phase α . Pour la deuxième, les auteurs pensent que la phase α se forme dans la phase ω/β , et croit vers les phases β et ω , consomme la phase ω . Pendant cette formation, des relations d'orientations sont maintenues entre les trois phases : $(\bar{1}\bar{1}00)_\omega // (10\bar{1}0)_\alpha // (211)_\beta$, $(\bar{1}\bar{1}20)_\omega // (0001)_\alpha // (0\bar{1}1)_\beta$, $(0001)_\omega // (\bar{1}2\bar{1}0)_\alpha // (\bar{1}11)_\beta$. La troisième raison est que la phase α se forme directement dans la phase ω [49], à ce moment la relation entre la phase α et la phase ω est comme ci-dessous : $(\bar{2}\bar{1}0)_\omega // (002)_\alpha$, $[001]_\omega // [110]_\alpha$. Nos résultats se conforment plutôt à la deuxième idée.

- La caractérisation de l'énergie d'activation de la transformation conduit à une valeur élevée ; cette valeur élevée peut être attribuée à la séquence de transformation qui se fait tout d'abord de la phase α métastable en phase α'' au lieu de la phase α ; α'' est une phase métastable, qui au cours du de chauffage et du maintien isotherme se décompose en phase β stable. Ce résultat n'est obtenu que pour la faible vitesse de chauffage, la phase α se formant premièrement, puis se forme la phase α'' à la position de la phase α , en finalement la phase α'' se transforme en phase α stable. En conséquence la microstructure est fortement modifiée (longueur et épaisseur plus faibles, et densité de précipités plus élevée).

3. Une pré - déformation plastique a une influence importante sur la cinétique de transformation isotherme. Comme la température de maintien isotherme, la vitesse de chauffage, la pré - déformation va modifier la cinétique de la phase de

transformation au cours du vieillissement isotherme. Pour étudier l'influence de la déformation plastique sur la cinétique isotherme de transformation et sur les mécanismes d'évolutions de la microstructure (germination et croissance), des échantillons d'alliage Ti-B19 ont été déformés à la température ambiante de 42% ou 53%, l'alliage étant à l'état β métastable (après traitement à 900°C/10min, trempés à 20°C/s). Puis les échantillons ont été chauffés à 500°C avec des vitesses variables de 10°C/s, 1°C/s et 0.1°C/s et maintenus à la température de 500°C pendant 4 heures. On a utilisé la résistivité pour suivre les évolutions dans l'alliage au cours du chauffage et du maintien, et on a observé la microstructure des échantillons. Les principales conclusions sont :

- Au cours du chauffage à 10°C/s, la résistivité évolue de manière monotone, comme pour les échantillons sans pré - déformation. Il n'y a pas de transformation en cours de chauffage. Quand la vitesse est 1°C/s et 0.1°C/s, les variations de résistivité présentent deux parties au cours du chauffage. Ce changement traduit une transformation de phase identifiée comme étant $\mathbf{b} \rightarrow \mathbf{a} + \mathbf{w}$. De plus, le taux pré - déformation a une influence sur la température de début de transformation.
 - Au cours du vieillissement isotherme à 500°C, la variation de résistivité est étroitement liée à la vitesse de chauffage. Pour les pré - déformations de 42% et 53% la variation de résistivité en cours de maintien est la plus élevée pour la vitesse de chauffage la plus rapide. La transformation se situe essentiellement en cours de maintien. Pour des vitesses de 1°C/s et 0.1°C/s, le changement de résistivité en cours de maintien sont similaires. Les évolutions sont plus compliquées car une partie de la transformation s'est effectuée au cours du chauffage.
 - Le taux de déformation a une influence importante sur la cinétique de
-

transformation au cours du maintien isotherme. La pré - déformation accélère considérablement la cinétique du changement de phase α ; la période d'incubation est diminuée comme la durée de la transformation qui est raccourcie de plus de 90%. L'observation des microstructures montre que la pré-déformation conduit à la déformation du grain β ; une augmentation du nombre de défauts intra granulaires est observée, et la taille des grains est diminuée (à priori macles de déformation). Ces défauts sont des nouveaux sites potentiels de nucléation de la phase de γ ou α , et conduisent à accélérer la cinétique du changement de la phase. Lorsque la vitesse de chauffage est de 1°C/s et 0.1°C/s , le changement de la phase se passe au cours du chauffage, la phase γ se présente sous forme granulaire et la phase de α se présente sous forme d'aiguille, les deux phases sont uniformément réparties dans le grain β .

- Si la pré - déformation conduit à une accélération de la cinétique de transformation, elle conduit aussi à réduire la fraction volumique de phase α formée, c'est-à-dire qu'après traitement de $500^\circ\text{C}/4$ heures, la quantité de phase α diminue avec le taux de déformation. En même temps, au cours du chauffage, et pour une même vitesse de chauffage, l'échantillon ayant été plus pré - déformé présente une plus faible quantité de phase α . La diminution de la quantité de phase α est liée aux contraintes internes générées au cours de la pré - déformation à température ambiante et/ou à une augmentation de l'énergie de déformation associée au changement de la phase.

4. Les conditions de transformation au cours de refroidissement continu depuis le domaine de la phase β (haute température) jusqu'à la température ambiante ont été étudiées pour différentes vitesses de refroidissement. Après chauffage à 900°C et maintien à la température pendant 10min, les échantillons ont été refroidis à des vitesses de refroidissement de 1°C/s , 0.2°C/s , 0.1°C/s , 0.06°C/s et 0.03°C/s . Les

cinétiques de transformation sont suivies résistivité électrique. Les microstructures sont observées à température ambiante, après refroidissement. Les principaux résultats sont les suivants:

- La transformation de phase $\beta \rightarrow \beta+\alpha$ se produit au cours du refroidissement continu. La germination de la phase α se fait préférentiellement aux joints de grain β . Lorsque la vitesse de refroidissement diminue, la transformation progresse principalement par croissance de la phase α qui a nucléé aux joints de grains. Pendant ce temps, de nouveaux précipités de phase α germent aux joints de grain β et à l'intérieur des grains, ce qui augmente la fraction volumique de phase α .
- Pour décrire la cinétique de transformation en condition de refroidissement continu, on a utilisé dans une première approche le modèle de JMAK pour décrire la cinétique en condition isotherme et le principe d'additivité de Scheil (sans séparer les périodes d'incubation et de transformation). Nous avons établi l'équation suivante pour la cinétique de transformation de phase au cours du refroidissement continu:

$$f(t) = 1 - \exp \left\{ - K_0 \left(\int_0^t \exp \left(- \frac{E}{mR (1033 + C_v t)} \right) dt \right)^m \right\}$$

Quand la vitesse de refroidissement est moins de 0.08°C/s , $m=1.3$; quand la vitesse de refroidissement est supérieure à 0.08°C/s , $m = -1.32581 + 0.00707C_v \cdot t$. Les résultats décrivent schématiquement les évolutions mesurées, mais les températures de transformation restent plus élevées que celles mesurées expérimentalement. Les résultats expérimentaux montrent que la vitesse de refroidissement critique au delà de laquelle il n'y a pas de formation de phase α est de 1°C/s .

5. Des caractérisations par traction ont été réalisées pour établir la relation entre les microstructures et les propriétés de l'alliage Ti-B19. Des essais ont été réalisés pour différents échantillons après vieillissement isotherme à des températures variant de 300 à 700°C. Les essais ont été réalisés sur une machine INSTRON 5581. Les principaux résultats sont les suivants :

- Pour des températures de maintien de 300°C et 350°C, la charge à rupture est élevée et l'allongement à rupture est faible (voire nul). Ce comportement est dû à la précipitation fine et uniforme de phase ω , répartie de manière homogène dans la matrice.
- Pour les températures de maintien de plus de 400°C, la microstructure est formée de phase α (ou α'') et β . Les propriétés mécaniques sont fonction de la fraction volumique, la forme, la répartition et dimension de la phase α . En particulier aux températures supérieures à 550°C, la fraction volumique de phase α décroît comme la charge à la rupture alors que l'allongement augmente. Quand la quantité de phase α est d'environ 55%, cet alliage a les performances optimales (charge à rupture/ allongement).

Mots clés: Alliage de titane β métastable, transformation de phases à l'état solide, cinétique de transformation de phase, microstructures, propriétés mécaniques.

AUTORISATION DE SOUTENANCE DE THESE
DU DOCTORAT DE L'INSTITUT NATIONAL
POLYTECHNIQUE DE LORRAINE

o0o

VU LES RAPPORTS ETABLIS PAR :

Monsieur Joël DOUIN, Directeur de Recherche, CEMES, Toulouse

**Monsieur Xianghong LIU, Professeur, Northwest Institute for Nonferrous Metals Resarch,
Shannxi, China**

Le Président de l'Institut National Polytechnique de Lorraine, autorise :

Monsieur CHANG Hui

à soutenir devant un jury de l'INSTITUT NATIONAL POLYTECHNIQUE DE LORRAINE,
une thèse intitulée :

"Phase transformations in the metastable Ti B19 alloy"

en vue de l'obtention du titre de :

DOCTEUR DE L'INSTITUT NATIONAL POLYTECHNIQUE DE LORRAINE

en "Sciences des Matériaux" Spécialité : « **Science et Ingénierie des Matériaux et
Métallurgie** »

Fait à Vandoeuvre, le 13 octobre 2006

Le Président de l'I.N.P.L.,

F. LAURENT

La Vice-Présidente
du Conseil d'Administration de l'INPL

Christine ROIZARD



NANCY BRABOIS
2, AVENUE DE LA
FORET-DE-HAYE
BOITE POSTALE 3
F - 54501
VANDOEUVRE CEDEX

Résumé

Les évolutions de microstructures du nouvel alliage chinois Ti B19 ont été étudiées au cours de divers traitements thermiques et des relations entre microstructures et propriétés mécaniques ont été établies. Les cinétiques de transformation isothermes ont été établies par des mesures de résistivité électrique. Les structures et microstructures ont été caractérisées par DRX synchrotron, Microscopies Optiques et Electroniques (MEB, MET). Les cinétiques de transformation et les caractéristiques microstructurales dépendent fortement de la température de vieillissement variant de 300°C à 700°C. Les cinétiques de transformation isothermes ont été obtenues, analysées (loi JMAK), et cet ensemble de résultats a conduit à l'établissement du diagramme TTT de l'alliage TiB19.

Enfin il a été montré que la vitesse de chauffage a une très forte influence sur les transformations mises en jeu, et qu'une pré déformation plastique accélère les cinétiques de transformation (introduction de nouveaux sites de germination). Enfin les cinétiques de transformation ont été caractérisées en refroidissement continu depuis le domaine monophasé bêta. Une première approche de la modélisation des cinétiques de transformation a été menée en utilisant la loi JMAK et le principe d'additivité de Scheil. Enfin les relations entre microstructures et propriétés sont discutés.

Mots clés : alliage de titane bêta métastable ; transformation de phases en phase solide ; transformation isotherme ; microstructures ; propriétés mécaniques.

Abstract

The phase transformations and microstructure evolutions has been characterized for different thermal treatments, and the relationships between final microstructures and properties have been investigated in the new metastable Ti-B19 alloy. The isothermal phase transformation kinetics and the influence of different heat treatment paths have been established by using in-situ electrical Resistivity. The structures have been determined by synchrotron X-Ray Diffraction and the microstructures were observed by SEM and TEM. The results show that phase transformation kinetics and microstructure characteristics are strongly dependent on the aging temperature (ranging from 300 to 700°C). The global isothermal phase transformation kinetics has been got and analyzed with JMAK equation, and the TTT diagram of Ti-B19 alloy has been established. We have also shown that the heating rate has remarkable influence on the isothermal phase transformation behaviors and the pre-deformation accelerates the transformation kinetics. The microstructure evolutions during cooling are obviously dependent on the cooling rates. A first attempt has been made to calculate the transformation kinetics during cooling using JMAK law and Scheil principle. Finally, the relationship between mechanical properties and microstructure has been discussed.

Keywords: metastable titanium alloy, solid phase transformation, isothermal transformation, microstructure, mechanical properties.